Finite Formulation with an Incentric Dual Mesh for Time-Harmonic Electromagnetics

By

Maryam Heshmatzadeh

A Thesis submitted to the Faculty of Graduate Studies of

the University of Manitoba

in partial fulfilment of the requirements of the degree of

Doctor of Philosophy

Department of Electrical and Computer Engineering

University of Manitoba

Winnipeg

THE UNIVERSITY OF MANITOBA

FACULTY OF GRADUATE STUDIES

*****

COPYRIGHT PERMISSION

Finite Formulation with an Incentric Dual Mesh for Time-Harmonic Electromagnetics

BY

Maryam Heshmatzadeh

A Thesis/Practicum submitted to the Faculty of Graduate Studies of The University of Manitoba in partial fulfillment of the requirement of the degree

Of

Doctor of Philosophy

ABSTRACT

A Finite Formulation technique, the Cell Method, is developed in the framework of an incentric dual mesh and applied to the general problem of guided wave structures. Cell Method is a numerical technique which uses a primal-dual mesh complex and global (integral) variables instead of field variables (densities). In the Cell Method, Maxwell's curl equations are exactly discretized as topological relations. Constitutive relations, on the other hand, are approximately discretized by the use of a proper dual mesh. The common choice for construction of the dual mesh is the barycentric scheme which produces non-diagonal constitutive matrices. A new time-harmonic finite formulation using a non-orthogonal dual mesh is presented which is based on choosing incenters of primal triangles as an alternative to barycentric dual points. In the incentric formulation, diagonal constitutive matrices are obtained which result in a symmetric positive definite eigenvalue problem in the first step (zero-order approximation).A minimization procedure is then utilized to take into account the non-orthogonality of the dual mesh and efficiently improve the accuracy of the zero-order solution. An eigenvalue system with symmetric positive definite constitutive matrices assures the stability and convergence of the solution while being computationally inexpensive.

In this thesis, the finite formulation for time-harmonic electromagnetic is described in detail. This is followed by a comprehensive theoretical explanation about the proposed incentric scheme. Several examples of electromagnetic problems including multi-scale geometries and inhomogeneous media are presented. Results of applying the proposed numerical technique are compared with the results obtained from a Finite Element Method. Analytical solutions are also used for comparison wherever possible.

Acknowledgement

I would like to express my sincere thanks, first and foremost, to my dear advisor, Professor **Greg Bridges**, for his clear thoughts, valuable guidance and advice, and his support and understanding through all stages of my PhD studies. Working with him was an exceptional experience and fruitful time period in my study life.

I really appreciate valuable comments from the members of my thesis committee: Dr. **David Chen** from Dalhousie University, Dr. **Sh. Lui** from the Department of Mathematics, University of Manitoba, and Dr. **I. R. Ciric,** from ECE Department, University of Manitoba. I thank them for accepting to be on the committee and reviewing and commenting on my thesis. Many thanks to **James Dietrich** who made the remote attendance of Dr. Chen in my Oral Exam possible.

It has been a pleasure to be a part of ECE Department for all these years. I thank all the staff and technical team members in ECE Department especially **Karin Kroeker** for her help and support during my studies. I would also like to thank all my friends in **SPM Lab** for being supportive whenever I needed them. Especial thanks to Dr. **Sandra Ingram**, for reviewing four chapters of my thesis on short notice and to **Graham** for reviewing one chapter.

I have been fortunate to make lots of good friends during my PhD studies. Many special thanks to Dr. **Zahra Moussavi** and Dr. **Sima Noghanian**, without whom I wouldn't even be able to move to Canada and pursuit my studies. A warm thank you goes to all my friends in ECE: **Tina Shoa, Arghavan Emami, Faeze** and **Majid, Azadeh, Alireza Foroozesh, Miodrag Kandic** and **Ali** and **Maria,** who submitted my thesis for

distribution while I was on a trip.

My heartfelt thanks go to all my teachers in different stages of my life. My dear mathematics teachers in high school: **Kobra Karvandi, Fereshteh Parsian, Rostam Keshmiri, Mr. Morteza Hasaninasab, Mr. Rostami, Mr. Naderi,** my Persian Literature teacher: Mr. **Shaban Alaaie** and my dear friends from high school: **Shahnam Noori** and **Nazita Gholamrezaie**.

My deep gratitude to my family before marriage: **My father**, **my mother** who stayed with me in cold Canada for one year and helped me by taking care of the kids, and my sisters: **Marjan** and **Fati** for their unconditional love, support and good wishes.

My warmest thanks and ultimate gratitude belongs to my present family:
my dear partner of life for 15 years, my husband **Hassan**, my kind son, **Emad**, my lovely daughter, **Saba**, and my newborn son, **Sadra,** whose existence was the courage for me to finish this study,
for their real love and patience in hours without me when I was with my thesis.

Maryam, Winnipeg, Dec. 2008

Dedication

In the memory of my father, ***Fereydoun Heshmatzadeh***

My dear father, Baba,

Here is my PhD thesis in electrical engineering, as you always wished. It is about Maxwell's Equations, which I saw for the first time, in your little black notebook.

Although it is of no use for you today, I give it to you, along with my tears, for

your wasted intelligence,

your dark days of regret

your endless nights in pain

and the most unforgettable...

your tragic death.

May your soul receive what you didn't receive in this world:

Peace and Happiness

Your Banoo, Maryam, Winnipeg, Canada, 2008.

Table of Contents

List of Tables

List of Figures

Chapter One

Chapter Two

Chapter Four

Chapter Five

Chapter Six

List of Symbols

V	A volume
S	A surface
L	A line
P	A point
V	Electric voltage (Volts)
Ψ	Electric flux (Coulombs)
F	Magnetic voltage (Amps)
Φ	Magnetic flux
Q	Electric charge (Coulomb)
ρ	Charge density (Coulomb/m^3)
$\boldsymbol{D}$	Electric flux density
$\boldsymbol{B}$	Magnetic Flux density
$\boldsymbol{E}$	Electric field intensity (Volts/m)
$\boldsymbol{H}$	Magnetic field intensity (Amps/m)
j	Square root of (-1)
ω	Angular frequency
$\boldsymbol{J}$	Surface current density (Amps/m^2)
D	Divergence incidence matrix
C	Curl incidence matrix
G	Gradient incidence matrix
R	Ratio matrix
CPL	Coupling matrix
Z	Impedance matrix
Y	Admittance matrix

Chapter 1- Introduction

1.1 Background

Observation of electromagnetic phenomena and consistent experimental results are the starting point for the formulation of "electromagnetic laws". As in the case of all fields of science, the results of real experiments are usually expressed in terms of measurable (global) variables (charge, magnetic and electric flux and current). While the physical law itself describes a unique relationship between global variables, there are different ways for expressing the law. In almost all fields of science and engineering, the dominant tool for formulating physical laws is differential calculus. The basis for differential calculus is performing a limiting process on spatial (x,y,z) and temporal (t) dimensions and producing infinitely small objects (dx, dy, dz, dt). Utilizing this procedure, the physical law is applied on infinitesimal objects and the result is the "differential expression of the physical law". The common use for differential calculus and the strong ties between physics and mathematical tools, however, make us believe that the differential expression *is* in fact the physical law itself. The following example explains the journey from a physical law to its differential expression. Consider the electric Gauss's law:

"The total electric flux leaving a closed surface is equal to the total electric charge enclosed by the surface."

The above physical law is exact for any closed surface, regardless of dimensions, material properties and the metric chosen. In differential calculus, however, we apply the

law on an infinitesimal volume as shown in Fig. 1-1.

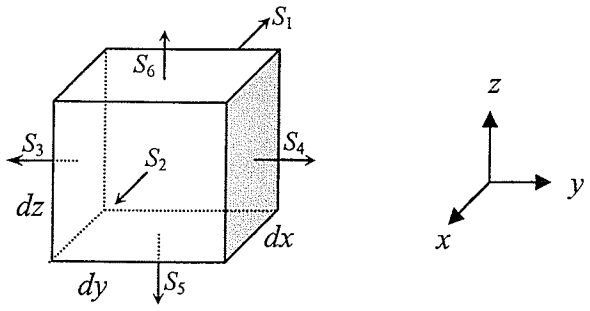

Figure 1-1: The infinitesimal volume, V, with dimensions dx, dy, dz is enclosed by surfaces S_1-S_6 and is used to derive the differential expression of Gauss's law.

By assuming the total charge inside the volume is $Q(V)$ and the total electric flux leaving (with respect to the volume) the surfaces of the volume is:

$$\Psi=\Psi(S_2)+\Psi(S_1)+\Psi(S_4)+\Psi(S_3)+\Psi(S_6)+\Psi(S_5),$$

where $\Psi(S)$ is the total electric flux leaving the surface, S.

We can now express the law in an exact form as $Q(V)=\Psi$. Introducing the field variable $\boldsymbol{D}=D_x\hat{a}_x+D_y\hat{a}_y+D_z\hat{a}_z$, electric flux density, for infinitesimal surface, dS, we have $\Psi(dS)=D_n|dS|$ where $|dS|$ is the area of surface dS and D_n is the normal (to the surface) component of $\boldsymbol{D}$. Therefore:

$$Q(V)=(D_{x+dx}\,dydz - D_x\,dydz)+(D_{y+dy}\,dxdz - D_y\,dxdz)+(D_{z+dz}\,dxdy - D_z\,dxdy).$$

Dividing both sides by $|V|=dxdydz$ gives

$$Q/|V| \stackrel{\Delta}{=} \rho=dD_x/dx+dD_y/dy+dD_z/dz$$

where ρ is the electric charge density. The familiar expression in the right hand side of the above definition is in fact divergence operator, $\nabla\cdot\boldsymbol{D}$.

In this journey, we departed from physically meaningful global variables (total charge,

Q, and total electric flux, Ψ) and used field variables (charge density, ρ, and electric flux density, ***D***) instead. We also lost the geometrical objects associated with the global variables (volume for charge and surface for electric flux) and instead obtained functions defined on every spatial point. The advantage of using differential calculus is presumably the "accuracy" of an exact solution function, $f(x,y,z,t)$. It is yet to be investigated and determined how necessary and worthy this journey is in reality when an exact analytical solution does not exist. Even when an analytical solution exists, the accuracy of the obtained solution is restricted since calculations need to be truncated at some point. Fortunately, there are also other approaches developed for solving physical problems.

The practical answer to the significant problem of solving differential equations with no analytical solution is "Numerical Techniques". In these techniques, the spatial (and/or temporal) domain is divided to many small (non-infinitesimal) elements (Fig. 1-2). The linear system of algebraic equations obtained from discretization of domain is then solved for a finite number of unknowns.

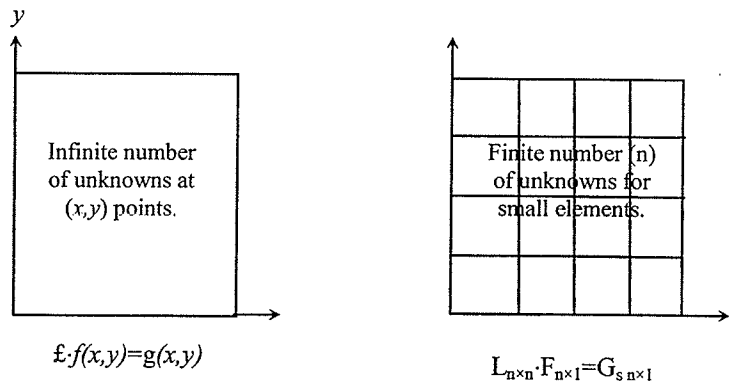

Figure 1-2: Left: Differential representation of a 2-D physical problem. Differential operator, £, unknown solution function, f, and the source function, g_s, are all defined on infinite number of points (x,y). Right: Numerical representation of the same problem. Matrix operator, L, unknown column vector, F, and the source vector, G_s in a matrix relation.

Experimental laws and relations in a physical field often result into one final equation to be solved. Numerical techniques are developed to find an accurate approximation to the solution of this (often differential) equation which is called the "fundamental equation". A question might now arise: is a differential formulation the best basis for starting a numerical technique? Finite Formulation or Finite Integration Techniques (FIT) are a successful NO answer to the above question. Starting from Maxwell's equations in their differential form is the basis for differential-based numerical methods such as Finite-Difference-Time-Domain (FDTD), Finite Element Method (FEM) and Transmission Line Matrix (TLM). Finite Volumes also uses differential equations in a conservative form. Starting from the integral or finite form of Maxwell's equations is the basis for Finite Integration Techniques (FIT) and the Cell Method.

Cell Method is a numerical technique based on exact discretization of physical laws and on using global (integral) variables. While the field variables are a result of performing a limiting process and defined at every point of the spatial domain, global variables are defined and measurable on their corresponding geometrical elements. For example, when describing "current", it is completely necessary to relate the concept to a "surface" through which the current passes.

Cell Method is categorized as a Finite Integration Technique with respect to its use of global variables. Some attractive features of a Finite Formulation as compared with a differential formulation are its simple basis, separation of topological relations and material and metric dependent (constitutive) relations, natural continuity of global variables over material discontinuities and less spurious solutions.

Fig. 1-3 expresses a basic comparison between Finite Formulation and differential

formulation in [1] where the important bases for the Cell Method are stated as follows:

- Physical laws are topological relations and can be applied directly and exactly on any discrete domain by using proper global variables.
- Material and metric dependent relations, constitutive relations, can be approximated over the discrete domain.
- Discretization of constitutive relations can benefit from the use of a dual mesh either explicitly (e.g. in the Cell Method and FIT) or implicitly (e.g. in Finite Elements or Finite Volumes methods).

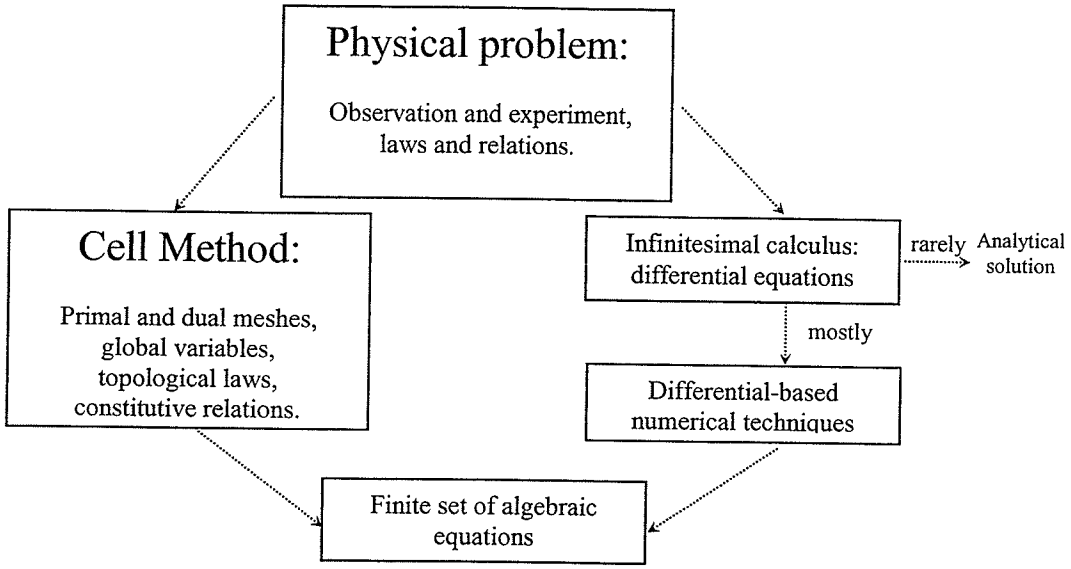

Figure 1-3: Cell Method as a direct path from the physical problem to the final discrete matrix equation.

An important fact should be mentioned here: discretization of constitutive relations is the only place that approximations are applied in all numerical techniques [1-3]. Practical differences between numerical techniques arise from the way that these relations are approximated and constitutive matrices are built. This fact is clearer in the Cell Method as topological and constitutive relations are distinguished by their different nature.

The objective of this thesis is to:

- Explain the theory and attractive features of the Cell Method by utilizing the method in modeling some applied electromagnetic problems
- Investigate the role and importance of having a dual mesh and the relation between the dual mesh and interpolation or so called shape functions
- Propose a new scheme (Incentric Cell Method) for construction of the dual mesh emphasizing its advantages over the existing schemes
- Report the results of applying the new scheme on some real complex guided wave structures
- Compare the results of the proposed scheme with the results obtained from other well known numerical schemes to show its effectiveness

1.2 Review

The term "Cell Method", as referring to a computational technique to solve physical problems, was first originated in Tonti's publications on the use of direct discrete formulation in electromagnetics [1,2]. The concept, however, was based on a long time study of similarities between physical laws in different fields of science (see references to Tonti's earlier publications from 1972 in [1,2]) which resulted in a functional classification of physical variables and definition of two kinds of orientations (inner and outer) for physical variables as given in [1,2]. The similar idea of applying algebraic topology to the analysis of other techniques, such as Finite Element Method, FEM, and Finite Volume Method, FVM, was addressed by Mattiussi [3]. Bossavit's research on a discrete Hodge operator and reinterpretation of FEM [4,5] also reveals the same concept

of different numerical treatments for topological relations and constitutive relations. Finite Integration Techniques, FIT, although not under the same name, was introduced by Weiland for solving Maxwell's equations as early as 1977 [6]. His more recent publication, including all details about using Finite Integration Technique in time-domain for structured grids [7], is usually considered as the original reference for FIT in electromagnetics. The results of applying FIT to a wide range of electromagnetics problems including S-parameters computations and time-domain applications validates FIT and its accompanying code named MAFIA [7]. Schuhmann and Weiland introduced Finite Integration Technique on non-orthogonal grids with triangular fillings [8] and its application to eigenvalue problems later [9]. Volume 32 of *PIER, Progress In Electromagnetics Research, Monograph Series on "electromagnetism and geometry"*, includes many papers on discrete electromagnetics, Finite Formulation, and geometry and topology related considerations in computational electromagnetics.

When Tonti first presented Finite Formulation or the Cell Method [1], many similarities with FIT put the Cell Method under FIT category of numerical techniques. Bossavit uses the term, Yee-Like-Schemes, as referring to a category of numerical techniques in which two meshes, dual to each other, are used to solve Maxwell's equations [10,11]. The concepts and methodology of the Cell Method have been also compared with, or explained in the context of, some other less familiar techniques such as Domain-Integrated Field Relations approach [12] where it is concluded that the main difference between the two techniques is the approach taken in the modeling of the constitutive relations. Repetto and Trevisan have used the term "Global Formulation" as referring to the same concept as Finite Formulation [13]. Comparisons between the

results obtained from a Finite Formulation and a Finite Element commercial code are given in [13] for two magnetostatic examples.

The majority of the literature on the Cell Method concerns:

- The concept and fundamental theory
- Numerical issues: stability, accuracy, convergence and numerical expense
- Comparisons with other numerical techniques
- Variations and hybrid algorithms
- Applications

The essence of the "Cell Method" is to provide a direct discretization of field laws without requiring a differential framework. Based on the frontier publications on Finite Formulation and the Cell Method technique [1-3, 12, 14], the computational procedure can be summarized in the following steps:

- Discretization of the spatial domain (primal mesh)
- Definition of global variables on oriented primal geometrical objects
- Applying the proper physical laws directly on the finite cells in the primal mesh
- Construction of the dual mesh and definition of the global variables on the oriented dual geometrical objects
- Applying the proper physical laws directly on the finite cells in the dual mesh
- Discretization of constitutive relations as the link between primal and dual variables
- Solving the final set of algebraic equations

Although the Cell Method is categorized as a Finite Integration Technique, it does not

employ the integral of field variables as it is done in FIT. Instead, the Cell Method uses global variables which are measurable physical quantities. The attempt to avoid the use of field variables sometimes fails because constitutive relations are often stated in a point-wise form compatible with differential formulation. It is also important to note that in all numerical techniques and *only* in the discretization of the constitutive relations, we use approximations (interpolation or shape functions, even uniform ones) either explicitly or implicitly. In our recent work [15] we discuss the finite framework for discretization of constitutive relations. The premise is that constitutive relations are usually obtained based on experimental data and measurements on global variables and hence can be expressed in a finite framework.

While the first publications on the Cell Method [1-12] mostly consider fundamental concepts and the philosophy of the Cell Method, later works addressed important computational issues such as the construction of proper constitutive matrices which guarantee consistency, convergence and stability of the technique.

As was mentioned earlier, the Cell Method utilizes a primal-dual mesh framework. The explicit use of a dual mesh enables one to properly define electromagnetic variables on their corresponding geometrical objects. It also defines a robust geometrical base for interpolation and averaging schemes. Characteristics of the dual mesh are directly employed in the construction of the constitutive matrices, therefore, a good knowledge about the construction of the dual mesh seems necessary. In almost all related publications, a barycentric dual mesh is considered. Delaunay-Voronoi, as an orthogonal primal-dual mesh complex is a good choice with the advantage of producing diagonal constitutive matrices, however, it is not always possible to achieve a Delaunay-Voronoi

tessellation especially in complex geometries and inhomogeneous media [16].

The most challenging issue in all numerical techniques is building proper discrete constitutive matrices, discrete Hodge operators, [4,5]. The order of accuracy in a numerical technique, convergence, stability and consistency issues depend solely on the properties of the constitutive matrices. It is *only* in the process of discretizing constitutive relations that we need to apply approximations and interpolation schemes. A major portion of research on the Cell Method has been carried out so far on the properties of the constitutive matrices derived from different dual mesh construction schemes used and different approaches to derive proper constitutive matrices. It has been proved that a sufficient condition for a computational scheme to be consistent is to have symmetric positive definite constitutive matrices [17-19]. Microcell Interpolation Scheme, MIS, for building constitutive matrices on a barycentric subdivision was proposed by Marrone [6] soon after the first publications on the Cell Method [1,2]. Constitutive matrices derived by MIS, in general, are non-diagonal and asymmetric. The results of applying MIS to solve a resonant cavity problem show good agreement with an FDTD solver [6]. Later on, a new consistent way to build symmetric constitutive matrices for 2-D grids called symmetrized MIS, SMIS, was proposed by Marrone [20]. The results reported in [20] show better accuracy in comparison with MIS when applied to the 2-D Laplace equation and a 2-D circular cavity. In a further theoretical study on the properties of constitutive matrices [21], Marrone investigated constitutive matrices for electrostatic and magnetostatic cases and stated that these properties can be used to provide an alternative sufficient condition for the stability of a generalized hybrid FDTD algorithm. Two generalized hybrid algorithms based on the Cell Method formulation were presented by Marrone and Mitra

for 2-D [22] and 3-D [23] multiscale problems. The two algorithms were validated by providing numerical examples and were compared in terms of accuracy and computational efficiency.

The barycentric subdivision, as the most common choice for the construction of the dual mesh in Finite Formulation, has been extensively studied. Bossavit discusses Whitney Forms (node elements, edge elements and face elements) along with some concepts of differential forms in [10]. Microcell Interpolation Scheme, MIS, has been used for the construction of the constitutive matrices with FIT [19] and the Cell Method formulation [20-25]. Other general approaches to build constitutive matrices for a barycentric dual mesh have been also proposed, investigated and applied to some electromagnetic problems [26-31]. In [26], different shapes of primal cells, oblique parallelepipeds or oblique triangular prisms, are considered with a barycenteric subdivision. Novel discretization of constitutive relations has been deduced and symmetric positive definite constitutive matrices are obtained. The proof of symmetric positive definiteness is given. Numerical examples in the frequency-domain show an expected $O(h^2)$ error behavior. Comparisons between the results obtained from the proposed scheme and the analytical solutions (or the results obtained from MicroWave Studio) show good agreement.

The finite set of algebraic equations resulting from Cell Method formulation has been compared, in different ways, to that obtained from other numerical techniques, FEM in particular. It has been proved that the final coefficient matrices are the same for The Cell Method with a barycentric subdivision [1,3,17,21,27] or a Voronoi dual mesh [15,17], and FEM with linear shape functions. The source vector (RHS vector), however, can be

different depending on the discretization of source functions.

Another major portion of research on the Cell Method is the application of the Cell Method to different electromagnetic problems. Trevisan and other researchers have used the Cell Method formulation in different electrostatic [32,33], magnetostatic [34], 2-D and 3-D Eddy-Current problems [35-37]. In [32] two kinds of primal cells, triangular and quadrilateral, are used to calculate the capacitance of a simple 2-D geometry. The results are close to each other and to those obtained from FEM. A Delaunay-Voronoi cell complex has been used in [33] to implement finite formulation for the computation of the electric potential in a 2-D electrostatic problem. A barycentric dual mesh has been considered in [34] and the problem of a ferromagnetic sphere in a uniform field is solved. The results show good agreement with the analytical solution.

While there is a considerable number of publications on the application of the Cell Method in electrostatics, magnetostatics and time-domain problems, frequency-domain problems are studied only in a few publications. Marrone applied the Cell Method formulation to the analysis of 2-D photonic crystals [24] and compared the results to those obtained from FEM. The comparisons show very good agreement. Application of Finite Integration Technique to solving 3-D resonator problems and comparisons given in [26] also validates the formulation in the frequency-domain. Marrone, Grassi and Mitra, have used the Cell Method with MIS for calculation of the propagation constant of inhomogeneous filled waveguides [38] where less accuracy for the barycentric Cell Method, compared with FEM, is reported.

Application of the Cell Method to a wide range of electromagnetic problems and comparisons with other numerical techniques, demonstrates the abilities of the Cell

Method in accurately modeling electromgnetics problems with complex geometries, inhomogeneous and anisotropic media in both time and frequency domain .

Recent related research on the Cell Method includes extensions of the meshless approach on Cell Method [39], implementation of different open boundary conditions such as Perfectly Matched Layer, PML, [30], boundary integral formulation [40] , and surface impedance boundary conditions [41]. It is concluded in [40] that the proposed procedure for implementation of the boundary integral formulation in Cell Method converges to the exact solution (of the discussed example) even for coarse meshes. It is also shown in [41] that very little computational effort is needed to find a very good approximation of simple Surface Impedance Boundary Conditions, SIBCs, and that such approximation is easily fitted into existing Cell Method codes.

The review of the research carried out about finite formulation suggests that this framework is an easy to implement, effective and robust alternative to differential framework.

1.3 Contribution and outline

In the new world of computational power and super fast computers, and in the era of complicated applications requiring electromagnetic analysis, it is quite reasonable to choose numerical techniques over analytical approaches because we often have to (as analytical solutions do not exist for the majority of realistic problems).

Differential-based numerical techniques use a framework which is based on a limiting process and point-wise approaches. A reasonable, attractive and natural choice to avoid the unnecessary limiting process would be a Finite Formulation. In Chapter Two of this

thesis, we explain Finite Formulation and compare it in detail with the Differential Formulation using an electrostatic example.

Cell Method formulation for general 3-D time-harmonic electromagnetics is given in Chapter Three. The discussion is then narrowed to the case of waveguide structures with an extruded 2-D primal mesh. The final eigenvalue problem is derived for this case. In the last section of Chapter Three we investigate the role of the dual mesh in the construction of constitutive matrices. Two common choices for the dual mesh on a primal triangulation, Voronoi dual mesh and the barycentric dual mesh are introduced along with their characteristics, advantages and weaknesses. An interesting discussion is carried out on the accuracy issue and how the order of accuracy is determined in the Cell Method through discretization of constitutive relations. We also discuss and answer the question: where is the dual mesh in other numerical techniques, e.g. Finite Element and Finite Volume, and what is the relation between shape functions and the dual mesh?

Since there are only two schemes mainly used for the construction of a dual mesh, Chapter Three leaves one with the question: Are there any other schemes available for the construction of a dual mesh? To have a positive answer to this question, we have proposed a new dual mesh construction scheme, Incentric Cell Method. The attempt in this scheme is to retain the orthogonality of the primal-dual complex as in the case of an orthogonal dual mesh while making it possible for arbitrary primal triangulation including possible obtuse triangles. The proposed scheme is explained in complete detail including simplified schemes for Transverse Electric, TE, Transverse Magnetic, TM, and Hybrid cases in Chapter Four of this thesis.

Waveguide structures are a very common configuration in electromagnetics. The

analysis of these structures is both interesting and useful because of their wide range of application in common systems and circuits. Waveguide structures are a good choice for applying and examining a new numerical scheme as the analysis can be carried out in a simplified 2-D extruded geometry.

A common issue in the analysis of unbounded problems in electromagnetics, e.g. microstrip transmission lines, is the treatment of open boundaries. Chapter Five of this thesis discusses the treatment of boundary conditions, particularly transverse open boundaries, in the Incentric scheme .We introduce an adaptive mesh open boundary to truncate the computational domain. An asymmetric coplanar waveguide is considered as a numerical example to validate the adaptive mesh open boundary condition.

In Chapter Six, a variety of complex waveguide structures are examined. We present the results of applying Incentric Cell Method scheme and comparisons are made with a FEM solver, Comsol Multiphysics. The results are also compared to the available analytical solutions, empirical formulations or the reported results of applying other numerical schemes, e.g. barycentric subdivision, whenever possible. Explanations are given on the results obtained from applying the Incentric scheme.

Results of applying the Incentric Cell Method to the problems in Chapter Six and comparisons with other numerical techniques and analytical solutions validate the accuracy and effectiveness of the proposed scheme. It is concluded that this scheme can be effectively applied to complex multi-scale problems in electromagnetics. Chapter Seven concludes the thesis and discusses some open areas of research on the related topics.

Chapter 2- Finite Formulation versus Differential Equations

Physical laws are the result of consistent observations and experiments. The great similarity between physical laws in different physical fields is an important fact supporting the idea: **discovering a physical law requires finding, defining and fitting proper physical variables to a topological relation which by itself does not involve any specific physical quantity.** Due to the historical evolution of physics and mathematics, topological relations have been expressed in a differential-integral form (e.g. Stokes and Divergence theorems), however, they can be expressed directly and exactly in a finite framework [1-7]. For a brief description of finite topological relations consider Fig. 2-1 and the following notation and definitions for directed three dimensional geometrical objects:

1- V_γ is an arbitrary volume in the spatial domain and its boundary is a closed surface, S: $\partial(V_\gamma) = S$, $\partial(S) = 0$. We can define a direction for V_γ arbitrarily as being either a source (outward to its closed surface) or a sink.

2- S_β is an arbitrary surface in the spatial domain and its boundary is a closed line, L: $\partial(S_\beta) = L$, $\partial(L) = 0$. We can define a direction for S_β arbitrarily along its closed boundary.

3- L_α is an arbitrary line in the spatial domain and its boundary is a set of two directed points, P: $\partial(L_\alpha) = P$, $\partial(P) = 0$. We can define a direction for L_α arbitrarily from one boundary point to the other.

4- P_i is an arbitrary point in the spatial domain and we can define a positive direction for P_i arbitrarily as being either a sink or a source.

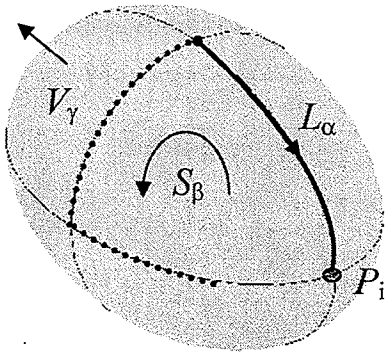

Figure 2-1: Geometrical objects and their closed boundaries.

Now we define the following generic global variables as *linear* functions operating on the geometrical objects: K (V_γ) on volumes, Φ (S_β) on surfaces, V (L_α) on lines and ϕ (P_i) on points. The linearity property, $F(aX_i+bX_j)=aF(X_i)+bF(X_j)$, where F is a global variable defined on the geometrical object X, and a and b are scalars, allows us to add global variables on the corresponding geometrical objects and define topological relations.

2.1 Topological relations

Topological relations linearly (e.g. up to a scaling factor) relate the global variable on any geometrical object (except points) to the global variable defined on its boundary as

$$V(L_\alpha) = a_G\, \phi(\partial L_\alpha), \tag{2-1.a}$$

$$\Phi(S_\beta) = a_C\, V(\partial S_\beta), \tag{2-1.b}$$

$$K(V_\gamma) = a_D\, \Phi(\partial V_\gamma), \tag{2-1.c}$$

where a_G, a_C, and a_D are scaling factors. To illustrate the three relations in (2-1), consider

the following examples.

2.1.1 Gradient relation

Given the global variable on points as shown in Fig. 2-2, we can define the global variable on lines as in (2-1.a) with a_G=-1:

$$V(L_1) = -(-\phi(P_1) + \phi(P_3))$$
$$V(L_2) = -(-\phi(P_1) + \phi(P_2))$$
$$V(L_3) = -(\phi(P_2) - \phi(P_3))$$

or $\overline{V} = -G \cdot \overline{\phi}$, (2-2.a)

where '·' denotes matrix multiplication and $\overline{V}$ and $\overline{\phi}$ are column vectors. Matrix G is the finite equivalent of the gradient operator and represents the topological relation between directed points and lines as

$$G_{\alpha i} = \begin{cases} 0 & \text{; if point i is not a face of line } \alpha. \\ 1 & \text{; if point i is a face of line } \alpha \text{ with the same direction.} \\ -1 & \text{; if point i is a face of line } \alpha \text{ with the opposite direction.} \end{cases},$$

where a "face" for a line is any of its boundary points.

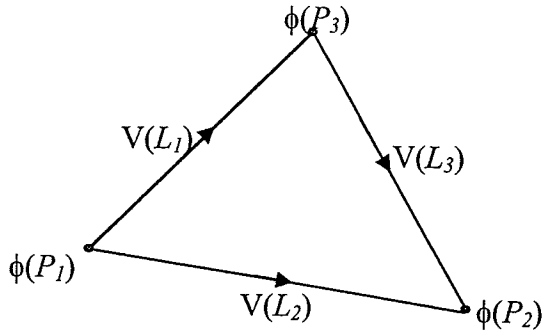

Figure 2-2: Topological relation between lines and points.

2.1.2 Curl relation

Given the global variable on lines as shown in Fig. 2-3, we can define the global variable on surfaces as in (2-1.b) with a_C=1:

$$\Phi(S_1) = V(L_2) - V(L_3) + V(L_5)$$
$$\Phi(S_2) = -V(L_1) - V(L_4) - V(L_5)$$

or $\overline{\Phi} = C \cdot \overline{V}$, (2-2.b)

where $\overline{\Phi}$ is a column vector. Matrix C is the finite equivalent of the curl operator and represents the topological relation between directed surfaces and lines as

$$C_{\beta\alpha} = \begin{cases} 0 & \text{; if line } \alpha \text{ is not a face of surface } \beta. \\ 1 & \text{; if line } \alpha \text{ is a face of surface } \beta \text{ with the same direction.} \\ -1 & \text{; if line } \alpha \text{ is a face of surface } \beta \text{ with the opposite direction.} \end{cases},$$

where a "face" for a surface is any of its boundary lines.

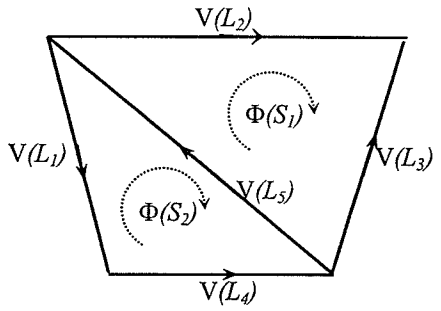

Figure 2-3: Topological relation between surfaces and lines.

As an exercise, we can start from the values on the points in Fig. 2-2 and obtain the finite equivalent of the vector analysis identity $(\nabla \times (\nabla \phi) \equiv 0)$ as

$$\overline{V} = -G \cdot \overline{\phi}\ ,\ \overline{\Phi} = C \cdot \overline{V} \Rightarrow \overline{\Phi} = -C \cdot (G \cdot \overline{\phi}) = 0,\ C \cdot G \equiv 0.$$

2.1.3 Divergence relation

Given the global variable on surfaces as shown in Fig. 2-4, we can define the global variable on volumes as in (2-1.c) with a_D=1:

$$K(V_1)=\Phi(S_1)+\Phi(S_2)-\Phi(S_3)+\Phi(S_4)$$

$$\text{or } \overline{K} = D \cdot \overline{\Phi}\ , \qquad (2\text{-}2.c)$$

where $\overline{K}$ is a column vector. Matrix D is the finite equivalent of the divergence operator and represents the topological relation between directed volumes and surfaces as

$$D_{\gamma\beta}=\begin{cases} 0 & \text{; if surface } \beta \text{ is not a face of volume } \gamma \\ 1 & \text{; if surface } \beta \text{ is a face of volume } \gamma \text{ with the same direction.} \\ -1 & \text{; if surface } \beta \text{ is a face of volume } \gamma \text{ with the opposite direction.} \end{cases} ,$$

where a "face" for a volume is any of its boundary surfaces.

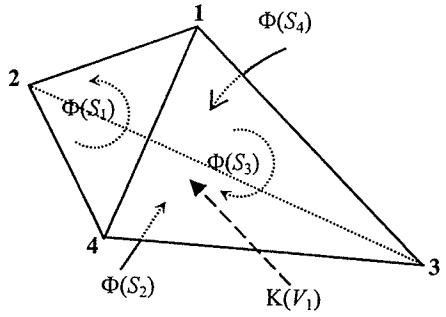

Figure 2-4: Topological relation for volumes and surfaces. The surfaces are arbitrarily directed as: $S_1(1,2,4)$,$S_2(2,3,4)$,$S_3(1,3,4)$,$S_4(1,3,2)$. The volume is directed as a source.

As an exercise, we can start from some values on the lines in Fig. 2-4 and obtain the finite equivalent of the vector analysis identity ($\nabla \cdot (\nabla \times \mathbf{A}) \equiv 0$) as

$$\overline{\Phi} = C \cdot \overline{V} \ , \overline{K} = D \cdot \overline{\Phi} \Rightarrow \overline{K} = D \cdot (C \cdot \overline{V}) = 0, \ D \cdot C \equiv 0.$$

Relations 2-1.a, 2-1.b, 2-1.c, are the finite equivalents of the "Fundamental Integration Theorem", "Stokes Theorem", and "Divergence Theorem", specified by the incidence matrices, G, C, D, respectively. They do not contain any material and metric information. To solve a physical problem, in addition to topological relations, we also need "physical links" between variables which contain medium and metric information. These links are usually called "constitutive relations" [3].

2.2 Constitutive relations

Having the spatial domain divided into a (primal) mesh consisting of geometrical objects, proper global variables can be defined and topological relations stated. To use global primal variables to describe a real physical system requires defining a set of "dual" variables and forming a physical-based relation between primal and dual variables. For example, the variables defined on surfaces (fluxes) are related to the variables defined on dual lines (voltages). This relation is where all material and metric-dependent information appear. To formulate constitutive relations, we need to define a dual mesh. The minimal requirement to construct a dual mesh is:

For any primal (dual) volume, V_γ ($\tilde{V}_i$), there is one and only one dual (primal) point, $\tilde{P}_\gamma$ (P_i). For any primal (dual) surface, S_β ($\tilde{S}_\alpha$), there is one and only one dual (primal) line, $\tilde{L}_\beta$ (L_α).

The correspondence between primal and dual variables can be described as

$$\tilde{P}_\gamma \leftrightarrow V_\gamma \ , \tilde{L}_\beta \leftrightarrow S_\beta \ , \ \tilde{S}_\alpha \leftrightarrow L_\alpha \ , \ \tilde{V}_i \leftrightarrow P_i$$

The dual geometrical objects for the primal mesh in Fig. 2-1 are shown in Fig. 2-5.

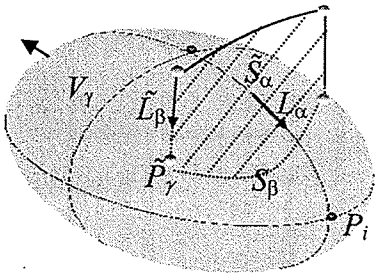

Figure 2-5: Dual geometrical objects for primal geometrical objects in Fig. 1. The dual volume for the primal point (P_i) is not shown.

With the given definition for duality, it is easy to show the following relations between incidence matrices for primal and dual meshes:

$$\tilde{G} = -D^t \quad , \quad \tilde{C} = C^t \quad , \quad \tilde{D} = -G^t \quad ,$$

where superscript t denotes the transpose operator and $\tilde{G}$, $\tilde{C}$ and $\tilde{D}$ are Gradient, Curl and Divergence incidence matrices for the dual mesh. The same topological relations as (2-2) are also valid for the dual geometrical objects as

$$\overline{F} = \tilde{G} \cdot \overline{N}, \tag{2-3.a}$$

$$\overline{\Psi} = \tilde{C} \cdot \overline{F}, \tag{2-3.b}$$

$$\overline{Q} = \tilde{D} \cdot \overline{\Psi}, \tag{2-3.c}$$

where $\overline{N}, \overline{F}, \overline{\Psi}, \overline{Q}$ are the column vectors containing the global variables defined on the dual points, lines, surfaces and volumes, respectively.

With definition of eight global variables on primal and dual geometrical objects and six topological relations (2-2, 2-3) we still need two more relations to be able to solve for

any global variable.

The link between the variables for the primal lines and the variables for the dual surfaces (and vice-versa) embody the physical system they are used to describe, and are called constitutive relations.

Constitutive equations can be *approximately* expressed as a mapping from the space of V to the space of Ψ, and from the space of F to the space of Φ as

$$\begin{aligned} \overline{\Psi}(\widetilde{S}) &= \mathrm{M}_{\varepsilon}\overline{\mathrm{V}}(L), \\ \overline{\Phi}(S) &= \mathrm{M}_{\mu}\overline{\mathrm{F}}(\widetilde{L}), \end{aligned} \tag{2-4}$$

where M_{ε} and M_{μ} are constitutive matrices.

In contrast to the exact and physically independent nature of topological relations, constitutive relations (and therefore constitutive matrices) are dependent on the physical properties of the media, construction of the dual mesh, metric and directions chosen. In a physical link between global variables (as scalar numbers) all the above information are included in the constitutive matrices. The results of experiment and measurement on a defined physical system must be fit in the finite matrix forms of (2-4). In (2-4), global variables defined on surfaces (fluxes) are considered as scalar numbers with an implicit direction given to them as the normal to the surface. It is based on the physical concept of "passing through a surface" which automatically includes only the normal component of a directional flow. The above concept is mathematically expressed using field variables (e.g. magnetic flux density) as the inner product of a flow and the normal to the surface (e.g. $\iint \boldsymbol{B} \cdot \mathrm{ds}$).

Specific choices for the dual mesh might result in simple mapping functions from the

primal variables to the dual variables. For example, if the physical link is a relation between fluxes (which implicitly means normal flux) through the primal surfaces and voltages on the dual lines in an isotropic linear media, an orthogonal dual mesh (if possible) results in diagonal constitutive matrices. For a non-orthogonal dual mesh, knowing the value of the flux through a primal surface is not enough to obtain the voltage on the dual line and an averaging procedure is needed using the neighbor fluxes. The resulting constitutive matrix is therefore non-diagonal.

To understand how we can apply the discussed finite framework to solve a real physical problem, we study the electrostatic case as an example in the following section.

2.3 Example: Electrostatic laws

Electrostatic laws are the statement of relations between global electromagnetic quantities when $\partial / \partial t \rightarrow 0$ and are known as: Faraday's law, Gauss's law and the electric constitutive relation. We now study these laws in both finite and differential frameworks.

2.3.1 Faraday's law

In its general time dependent form, Faraday's law is a curl relation, (2-1.b), and relates the value of changes (in time) in magnetic flux, Φ, for a surface, S, to the value of the electric voltage, V, on the boundary of the surface, ∂S. Since the time variation of magnetic flux is zero in electrostatics; the electrostatic Faraday's law states:

"The electric voltage for any closed line is zero."

Finite formulation:

Using global variables on the primal geometrical objects, Faraday's law in electrostatics is

$$\Phi(S_\beta) = V(L) = 0 \; ; \quad L = \partial S_\beta \, . \tag{2-5}$$

By defining a global variable on primal points (electric potential, ϕ) it is guaranteed that the value of Φ is zero for all surfaces. This yields the equivalent gradient form of Faraday's law as $\overline{V} = -G \cdot \overline{\phi}$. The minus sign is the scaling factor in Equation (2-1.a) due to experimental convention. Fig. 2-6 illustrates Faraday's Law.

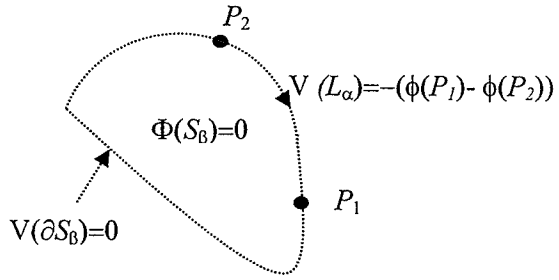

Figure 2-6: Faraday's law for the surface, S_β, enclosed by the line, ∂S_β .

Differential formulation:

Differential equations are the result of performing a limiting process on global variables and using field variables. Based on the defined global variables in (2-1), we can obtain electric field intensity, in a specific direction, α, as

$$E_\alpha \underset{L_\alpha \to 0}{\overset{\Delta}{=}} \lim \frac{V(L_\alpha)}{L_\alpha} \quad . \tag{2-6}$$

If a potential function, ϕ, is defined on the points, as shown in Fig. 2-6, then (2-6) can be rewritten as

$$E_\alpha \triangleq \lim_{L_\alpha \to 0} \frac{V(L_\alpha)}{L_\alpha} = \lim_{P_1 \to P_2} \frac{-(\phi(P_1) - \phi(P_2))}{|P_1 - P_2|} = -\nabla_\alpha \phi \tag{2-7}$$

which results in the definition of gradient operator, ∇, and differential expression of Faraday's law as $\boldsymbol{E} = -\nabla\phi$.

2.3.2 Gauss's law

Gauss's law is a balance or divergence relation, Equation (2-3.c), and relates the value of the charge, Q, in a volume, $\tilde{V}_i$, to the value of the electric flux, Ψ, passing through the boundary of the volume, $\partial\tilde{V}_i$. The electrostatic Gauss's law states:

"The electric flux leaving a closed surface is equal to the electric charge in the volume enclosed by the surface."

Finite formulation:

Using global variables on the dual geometrical objects, Gauss's law is written as:

$$Q(\tilde{V}_i) = \Psi(\tilde{S}) \;\; ; \;\; \tilde{S} = \partial\tilde{V}_i, \tag{2-8}$$

or in its equivalent matrix form

$$\overline{Q} = \tilde{D} \cdot \overline{\Psi}. \tag{2-9}$$

The scaling factor is equal to one in (2-3.c) due to experimental convention. Fig. 2-7 illustrates Gauss's law.

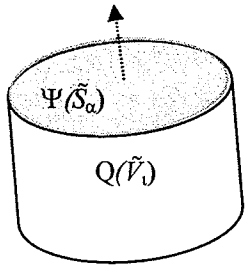

Figure 2-7: Gauss's law for a volume, $\tilde{V}_i$, enclosed by the surface, $\partial\tilde{V}_i$ states that: $Q(\tilde{V}_i)=\Psi(\partial\tilde{V}_i)$.

Differential formulation:

Performing a limiting process on the defined global variables in (2-8), we obtain electric charge density and electric flux density, respectively, as

$$\rho_i \overset{\Delta}{=} \lim_{\tilde{V}_i \to 0} \frac{Q(\tilde{V}_i)}{\tilde{V}_i} \ , \ D_\alpha \overset{\Delta}{=} \lim_{\tilde{S}_\alpha \to 0} \frac{\Psi(\tilde{S}_\alpha)}{\tilde{S}_\alpha} \ , \tag{2-10}$$

which, referring to the example in Chapter One, on Page 2, results in the differential (and/or integral) form of Gauss's law:

$$\rho = \nabla \cdot \boldsymbol{D} \ \Leftrightarrow \oiint_{\partial \tilde{V}} \boldsymbol{D} \cdot d\boldsymbol{s} = \iiint_{\tilde{V}} \rho dv \ , \tag{2-11}$$

where $\nabla \cdot$ is the divergence operator.

2.3.3 Constitutive relation

The electrostatic constitutive relation is a physical relation between the electric voltage and the electric flux in a physical medium. For simple isotropic linear media [42], this relation is described by a constant number, ε, relating the electric flux density to the electric field intensity at a point. Perhaps the most important problem in the finite expression of constitutive relations is that these relations are available using point-wise constants, e.g. ε and μ. Since constitutive relations are found experimentally and involve global variables, finite formulation is also a valid expression of these relations.

Finite formulation:

The electric constitutive relation can be approximated directly (not uniquely) as

$$\boldsymbol{\Psi}(\tilde{S}_\alpha) = \boldsymbol{M}_\varepsilon(\alpha,\alpha) \cdot \boldsymbol{V}(L_\alpha) , \tag{2-12}$$

where M_ε is a matrix factor to be found experimentally. This factor depends on material properties, geometrical primal-dual relation and the metric chosen. For an orthogonal primal-dual relation, as shown in Fig. 2-8, and in a simple analogy with the concept of the electrostatic capacitance, (2-12) can be rewritten as:

$$\frac{\Psi(\tilde{S}_\alpha)}{|\tilde{S}_\alpha|} = \underbrace{M_\varepsilon(\alpha,\alpha)\cdot\frac{|L_\alpha|}{|\tilde{S}_\alpha|}}_{\varepsilon}\cdot\frac{V(L_\alpha)}{|L_\alpha|}\ ,\ M_\varepsilon(\alpha,\alpha)=\varepsilon\cdot\frac{|\tilde{S}_\alpha|}{|L_\alpha|}\quad ,\quad \frac{\Psi(\tilde{S}_\alpha)}{|\tilde{S}_\alpha|}=\varepsilon\cdot\frac{V(L_\alpha)}{|L_\alpha|} \tag{2-13}$$

where ε, electric permittivity, is a constant solely dependent on the material's electric properties. It can be seen that M_ε depends on both material properties (through ε) and metric and primal-dual mesh relation (through the term $\frac{|\tilde{S}_\alpha|}{|L_\alpha|}$). $|A|$ refers to the length, area or volume of the geometrical object, A.

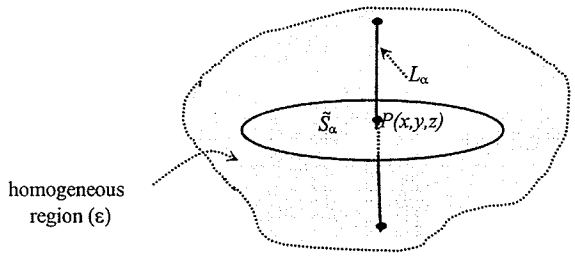

Figure 2-8: Electric constitutive relation for a homogeneous region.

Differential formulation:

Performing a limiting process on (2-13) and using definitions (2-6) for $\boldsymbol{E}$, and (2-10) for $\boldsymbol{D}$, the differential form of the electrostatic constitutive relation becomes:

$$\boldsymbol{D}\,(x,y,z)=\varepsilon\boldsymbol{E}(x,y,z) \tag{2-14}$$

where ε is the permittivity of the infinitesimal volume around the point $P(x,y,z)$ as in Fig. 2-8.

2.3.4 Poisson's equation

Using global variables and finite formulation, (2-2.a, 2-9, 2-12), we obtain the finite from of Poisson's equation as

$$G^t \cdot M_\varepsilon \cdot G \cdot \overline{\phi} = \overline{Q} \ . \tag{2-15}$$

The differential expression of electrostatic laws (2-7, 2-11, 2-14) results in the familiar form of Poisson's equation as

$$\nabla \cdot \varepsilon \nabla \phi = -\rho \, . \tag{2-16}$$

The finite form of Poisson's equation, (2-15), is applicable to a discrete spatial domain directly and results in a set of algebraic equations. In cases with no exact analytic solution (almost all cases), however, numerical techniques are needed to solve the differential form (2-16) which, after the appropriate discretization, also lead to a set of algebraic equations.

Differential equations are, with no doubt, very powerful tools for analyzing and solving physical problems. It should be noted that the discussion in this thesis is not about the usefulness of differential equations. The discussion here is about the necessity of using differential equations while we often have to use numerical techniques for solving real physical problems. It is reasonable to consider the effectiveness of a discrete framework when using numerical techniques.

Chapter 3- Finite Formulation for Time-Harmonic Electromagnetics

Finite formulation of physical laws leads us to a computational framework which does not require the use of differential calculus. A finite formulation can be generally applied in both time-domain and frequency-domain analysis of inhomogeneous electromagnetic problems with irregular geometries. In this chapter a finite formulation technique, the Cell Method, is explained and applied to formulate a general 3-D source-free inhomogeneous problem in the frequency-domain (time-harmonic). To establish the finite framework we shall define and address:

1-Time-harmonic global variables and topological relations for the primal mesh

2-Time-harmonic global variables and topological relations for the dual mesh

3-Finite form of constitutive relations, the link between primal and dual variables

The third issue, without doubt, is the most important and challenging aspect of all numerical techniques including finite formulation [1-7,10-12].

Practical problems in electromagnetics can be categorized in main classes such as: antennas and radiation, scattering, EM imaging and detection techniques, and transmission lines and guided wave structures. Guided wave structures are specifically considered in this thesis because of the wide range of applications and instructive purposes. In the numerical analysis of a guided wave structure, the 2-D cross section is discretized and a 2-D extruded mesh is used to simplify the 3D formulations. Complete Cell Method formulations are given for this class of problems which result in an eigenvalue equation.

In the last section of this chapter, construction of a dual mesh is discussed in detail. We also briefly explain how the explicit construction of a dual mesh in the Cell Method is related to the implicit use of a dual mesh through shape functions or interpolation functions in other numerical techniques.

3.1 General time-harmonic electromagnetics

Maxwell's equations are a set of four topological and material-independent laws (Faraday's law, Maxwell-Ampère's law, Gauss's electric law and Gauss's magnetic law) governing the behavior of electromagnetic waves. Maxwell's equations are usually expressed as a set of differential or integral equations in the time-domain or frequency-domain.

In frequency-domain (time-harmonic) analysis, we assume that the variation in time for any electromagnetic variable, $\boldsymbol{F}$, obeys the exponential relation: $\boldsymbol{F}(x,y,z,t)=\boldsymbol{F}_s(x,y,z)\cdot e^{j\omega t}$ where $\boldsymbol{F}_s$ is the spatial component of the variable, $\boldsymbol{F}$. This assumption results in time-harmonic Maxwell's equations and the familiar differential and integral expressions are

$$\begin{aligned} &\nabla\times\boldsymbol{E}=-j\omega\boldsymbol{B},\\ &\nabla\times\boldsymbol{H}=j\omega\boldsymbol{D}+\boldsymbol{J},\\ &\nabla\cdot\boldsymbol{B}=0,\\ &\nabla\cdot\boldsymbol{D}=\rho \end{aligned} \qquad (3\text{-}1)$$

or

$$\begin{aligned} &\oint_{L=\partial S}\mathrm{E}\cdot\mathrm{dl}=-\mathrm{j}\omega\iint_{S}\mathrm{B}\cdot\mathrm{ds},\\ &\oint_{L=\partial S}\mathrm{H}\cdot\mathrm{dl}=\mathrm{j}\omega\iint_{S}\mathrm{D}\cdot\mathrm{ds}+\iint_{S}\mathrm{J}\cdot\mathrm{ds},\\ &\oiint_{S=\partial V}\mathrm{B}\cdot\mathrm{ds}=0,\\ &\oiint_{S=\partial V}\mathrm{D}\cdot\mathrm{ds}=\iiint_{V}\rho\cdot\mathrm{dv}, \end{aligned} \qquad (3\text{-}2)$$

respectively, where $\boldsymbol{E}$ is the electric field intensity, ω is the angular frequency=$2\pi f$, j is $\sqrt{-1}$, $\boldsymbol{B}$ is the magnetic flux density, $\boldsymbol{H}$ is the magnetic field intensity, $\boldsymbol{D}$ is the electric

flux density, $\boldsymbol{J}$ is the electric current density and ρ is the electric charge density. When ω is not zero and along with current continuity enforcement (conservation of charge) the first two equations in (3-1) or (3-2) known as Maxwell's curl equations, automatically result in the last two equations (Maxwell's divergence equations) and hence we only consider the first two equations in (3-1) or (3-2) as the fundamental time-harmonic electromagnetic laws.

Maxwell's curl equations are mathematical expressions of topological relations between electromagnetic global variables as

Faraday's law

The electric voltage measured for any closed line is proportional to the change (in time) of the total magnetic flux passing through the surface enclosed by the line.

The scaling factor for this proportionality is found, by experiment and measurement, to be $(-\partial/\partial t)$ in general and $(-j\omega)$ in the time-harmonic case.

Maxwell-Ampère's law

The magnetic voltage measured for any closed line is proportional to the change (in time) of the total electric flux passing through the surface (including the conduction flux) enclosed by the line.

The scaling factor for this proportionality is found, by experiment and measurement, to be $(\partial/\partial t)$ in general and $(j\omega)$ in the time-harmonic case.

It is apparent from the above expressions that the only geometrical objects we need in order to apply Maxwell's curl equations on a spatial domain are primal and dual lines and surfaces. The lines and surfaces, however, should be members of a meaningful complete primal-dual relation as was defined in Chapter Two.

The first step to start a numerical procedure is discretization of the spatial domain (see an example of mesh-less approaches in [43]). In mathematics, discretization concerns the process of transferring continuous models and equations into discrete counterparts. This process is usually carried out as a first step toward making them suitable for numerical evaluation and implementation on digital computers. Different standard mesh generating programs are available and can be used to divide the spatial domain into small elements. The mesh can be either regular, same cell size and shape everywhere, or irregular with different cell size and cell shape. The advantage of having an irregular mesh is greatly appreciated in multi-scale problems when there are regions with very fine details as well as in problems with curved boundaries.

Triangular 2-D meshes and tetrahedral 3-D meshes are the most common form of spatial discretization. The unit cells in these meshes have the least possible number of sides and are called simplex [10]. For a 3-D tetrahedral mesh, a simplex consists of a volume (tetrahedron), four surfaces (triangles), six lines and four points as shown in Fig. 3-1.

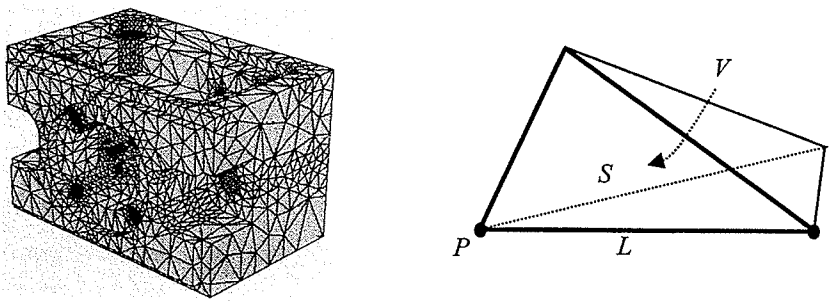

Figure 3-1: A 3-D irregular (tetrahedral) mesh and a tetrahedral unit cell (a 3-D simplex).

Referring to Fig. 2-1, all geometrical objects in a 3-D mesh (points, lines, surfaces and volumes) are oriented as

1- Points (P_i) are considered as "sink".

2- Lines (L_α) are oriented arbitrarily.

3- Surfaces (S_β) are oriented arbitrarily.

4- Volumes (V_γ) are oriented as "source" (i.e. their surfaces' outwards).

Following the definitions given in Chapter Two, we can readily build the incidence matrices (G, C, D) for the primal mesh. These matrices are utilized in the exact finite expression of Maxwell's equations.

3.1.1 Primal global variables and topological relations

To apply Faraday's law on primal mesh, we define the following primal global variables:

1- Electric voltage, V, is defined on primal lines and, based on the familiar differential-integral point of view, can be expressed as

$$\mathrm{V}(L) = \int_L \boldsymbol{E} \cdot dl \ , \text{(volt)}, \tag{3-3}$$

where L represents any primal line.

2- Magnetic flux, Φ, is defined on primal surfaces and, based on the familiar differential-integral point of view, can be expressed as

$$\Phi(S) = \iint_S \boldsymbol{B} \cdot ds \, , \text{(volt·second)}, \tag{3-4}$$

where S represents any primal surface.

Using these global variables, V and Φ, and the definition of curl incidence matrix, C (see equation. 2-2.b), we are able to write the exact finite form of Faraday's law as a topological relation

$$C \cdot \overline{V} = -j\omega\overline{\Phi} \tag{3-5}$$

where $\overline{V}$ is the column vector consisting of electric voltages defined on all primal lines and $\overline{\Phi}$ is the column vector consisting of magnetic fluxes defined on all primal surfaces.

3.1.2 Dual global variables and topological relations

For any given primal mesh, a dual mesh can be constructed to fulfill the minimum requirements mentioned in Chapter Two (see section 2.2). The center of each primal volume is a dual point. The choice of a "center" for primal volumes or surfaces is determined by the chosen dual mesh construction scheme. The last section of this chapter concerns the construction of the dual mesh, its effect on the accuracy of the scheme, and its relation to the shape functions used in Finite Element Method [44]. Dual lines connect dual points in adjacent primal volumes through their common surface and in general do *not* need to be one-piece straight lines. Fig. 3-2 depicts dual geometrical objects for the simplex in Fig. 3-1.

To apply Maxwell-Ampère's law on the dual mesh, we define the following dual global variables:

1- Magnetic voltage, F, is defined on dual lines and, based on the familiar differential-integral point of view, can be expressed as

$$F(\tilde{L}) = \int_{\tilde{L}} \boldsymbol{H} \cdot d\boldsymbol{l} \text{ , (ampere),} \tag{3-6}$$

where $\tilde{L}$ represents any dual line.

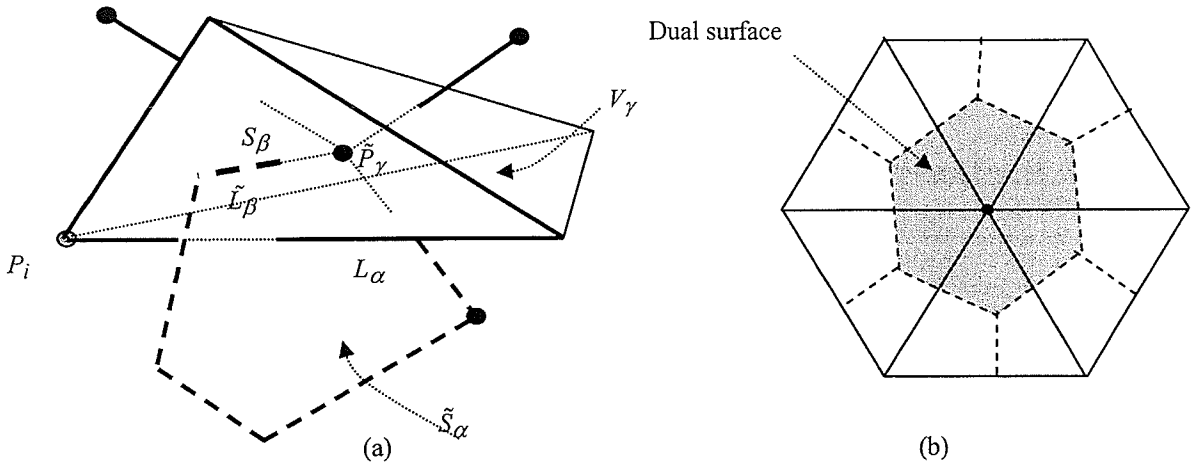

Figure 3-2: a) Dual geometrical objects for the 3-D simplex in Fig. 3-1, b) Dual surface for a primal point in a 2-D mesh.

2- Electric flux, Ψ, is defined on dual surfaces and, based on the familiar differential integral point of view, can be expressed as

$$\Psi(\tilde{S}) = \iint_{\tilde{S}} \boldsymbol{D} \cdot d\boldsymbol{s}\,, \text{ (ampere·second)}, \tag{3-7}$$

where $\tilde{S}$ represents any dual surface.

Using these global variables and the definition of dual curl incidence matrix, $\tilde{C}=C^t$, (see section 2.2) we are able to write the exact finite form of Maxwell-Ampère's law as a topological relation

$$\tilde{C} \cdot \overline{F} = j\omega \overline{\Psi} \tag{3-8}$$

where $\overline{F}$ is the column vector consisting of magnetic voltages defined on all dual lines and $\overline{\Psi}$ is the column vector consisting of electric fluxes defined on all dual surfaces.

The two matrix equations, (3-5) and (3-8), are the exact finite form of Faraday's law and Maxwell-Ampère's law, respectively. They do not depend on material properties or the metric chosen. To be able to solve for any unknown variable we need *physical* links

between global variables defined on the primal and dual meshes. These links are called "constitutive relations".

3.1.3 Constitutive relations

Based on the discussion in Chapter Two, in a very general form, we express the finite form of the electric and magnetic constitutive relations, respectively, as

$$\overline{\Psi} = M_\varepsilon \cdot \overline{V} \quad , \quad \overline{\Phi} = M_\mu \cdot \overline{F} \tag{3-9}$$

where M_ε and M_μ are square matrices dependent on the material properties and metric and geometrical information. Fig. 3-3 illustrates how the global variables (for time-harmonic electromagnetics) defined on primal and dual meshes are related thorough topological (curl) relations and constitutive relations.

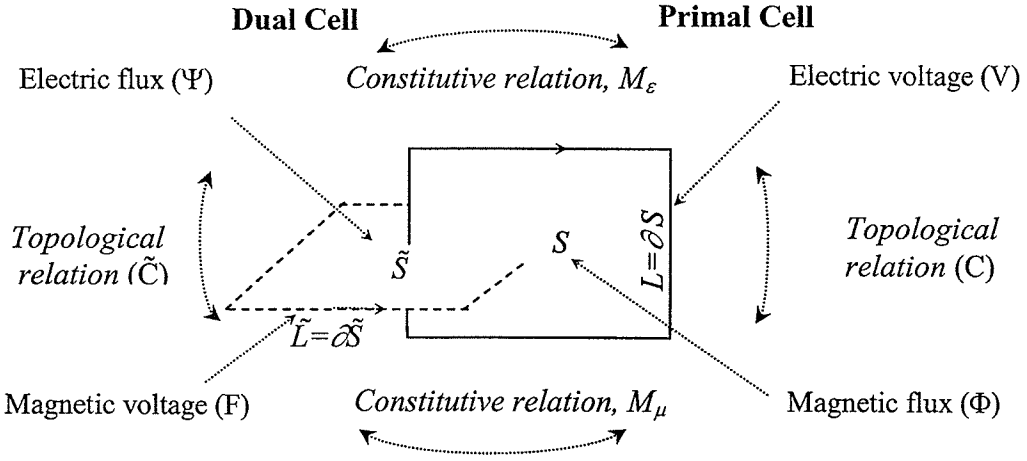

Figure 3-3: Global variables (for time-harmonic EM) defined on primal and dual meshes are related thorough topological relations (on the same mesh) and constitutive relations (on different meshes).

Substituting (3-9) in (3-5) and (3-8) results in the finite form of the wave equation for a general 3-D problem as

$$M_\varepsilon^{-1}\tilde{C}M_\mu^{-1}CV = \omega^2 V \qquad (3\text{-}10)$$

It is apparent from (3-10) that, in general, inverses of M_ε and M_μ are required in the computational procedure. This raises a concern in the efficiency of the numerical technique. These matrices should also satisfy some necessary conditions in order to ensure the stability and convergence of the time-domain schemes [7,11,17,20-23]. Diagonal constitutive matrices are the most convenient choice to ensure all computational requirements for a consistent and efficient numerical technique.

3.2 Finite formulation for guided wave structures

Guided wave structures refer to a category of electromagnetic problems where wave propagation in a specific direction is supported by the geometry and specifications of the problem. Examples of this category are waveguide and multiconductor transmission line configurations. In a guided wave problem, the transverse cross section is perpendicular to the direction of propagation and is invariant with respect to the direction of propagation. Consider the transverse cross section of a wave guide structure as an arbitrary 2-D surface in the x-y plane. Variation of all electromagnetic variables with respect to z is assumed as $e^{-\gamma z}$ and $\boldsymbol{F}(x,y,z)=\boldsymbol{F}_t(x,y)\, e^{-\gamma z}$, where $\boldsymbol{F}$ represents an arbitrary electromagnetic variable and $\boldsymbol{F}_t$ is its transverse component. Fig. 3-4 shows the 2-D cross section of the primal mesh and an extruded triangle. A dual volume (an extruded dual surface) for a primal point in a triangular mesh is shown in Fig. 3-5. The relation between primal and

dual geometrical objects and incidence matrices are simplified for a guided wave structure as:

$$\tilde{L}_\alpha \leftrightarrow L_\alpha \quad , \quad \tilde{S}_i \leftrightarrow P_i \quad , \quad \tilde{\mathrm{C}} = \mathrm{G}^{\mathrm{t}} \quad , \quad \tilde{\mathrm{G}} = \mathrm{C} \tag{3-11}$$

where G and C are incidence matrices for the 2-D primal mesh.

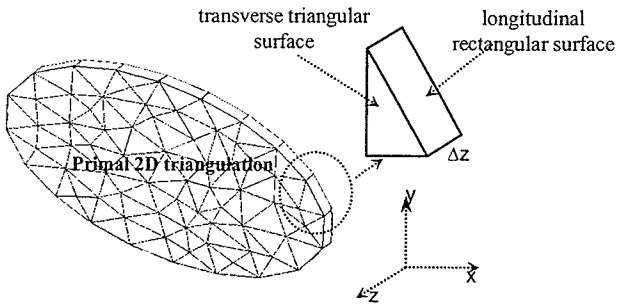

Figure 3-4: The general 2-D geometry for wave propagation problem and a unit extruded cell showing the transverse and longitudinal surfaces.

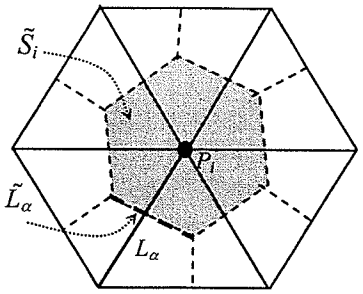

Figure 3-5: A dual line, $\tilde{L}_\alpha$ (for the primal line, L_α) and a dual surface, $\tilde{S}_i$ (for the primal point, P_i) in the 2-D cross section of a guided wave structure.

The key to obtaining the final eigenvalue equation for a waveguide structure is to apply topological laws on transverse triangles and longitudinal rectangles (as shown in Fig. 3-4) *separately*.

Application of Faraday's law (3-3) on primal transverse and longitudinal surfaces results in two equations as

$$CV_t^p = -j\omega\Phi_z^p \qquad \text{; for transverse surfaces,} \tag{3-12.a}$$

$$\gamma V_t^p + G\boldsymbol{E}_z^p = -j\omega\Phi_t^p \quad \text{; for longitudinal surfaces,} \tag{3-12.b}$$

where superscript p refers to the primal mesh and subscripts t or z, refers to transverse or longitudinal components, respectively. $\boldsymbol{E}_z^p$ is the longitudinal component of the electric field defined on primal points.

In the same manner, application of Maxwell-Ampere's law (3-4) on dual transverse and longitudinal surfaces results in two equations as

$$G^t F_t^d = j\omega\Psi_z^d \qquad \text{for transverse surfaces} \tag{3-13.a}$$

$$\gamma F_t^d + C^t \boldsymbol{H}_z^d = -j\omega\Psi_t^d \quad \text{for longitudinal surfaces,} \tag{3-13.b}$$

where superscript d refers to the dual mesh and subscripts t or z, refers to transverse or longitudinal components, respectively. $\boldsymbol{H}_z^d$ is the longitudinal component of the magnetic field defined on dual points. Some important points in deriving (3-12) and (3-13) are noted:

1- The final equations are independent of Δz and $\boldsymbol{E}_z^p$, $\boldsymbol{H}_z^d$ are therefore field variables (V/m and A/m, respectively). This is the result of our use of $e^{-\gamma z}$ function and elimination of Δz in the formulation

2- G is the gradient incidence matrix for the 2-D primal mesh

3- C is the curl incidence matrix for the 2-D primal mesh

4- We have used the approximation $1 - e^{-\gamma\Delta z} \approx \gamma\Delta z$

Figure 3-6 demonstrates in detail how different components in (3-12) and (3-13) are obtained.

For the 2-D case, constitutive relations can be rewritten as

$\Phi_t^p = M_{\varepsilon t} F_t^d$; electric constitutive relation in transverse direction, (3-14.a)

$\Phi_z^p = M_{\varepsilon z} \boldsymbol{H}_z^d$; electric constitutive relation in longitudinal direction, (3-14.b)

$\Psi_t^d = M_{\mu t} V_t^p$; magnetic constitutive relation in transverse direction, (3-14.c)

$\Psi_z^d = M_{\mu z} \boldsymbol{H}_z^p$; magnetic constitutive relation in longitudinal direction. (3-14.d)

Substituting (3-14) in (3-12) and (3-13) and eliminating the longitudinal field components, $\boldsymbol{E}_z^p$, $\boldsymbol{H}_z^d$, we obtain the final finite eigenvalue problem for the guided wave structure as

$$(\gamma^2 - (Z_t Y_t + Z_t C^t Z_z^{-1} C + G Y_z^{-1} G^t Y_t)) V_t^p = 0, \quad (3\text{-}15.a)$$

for primal electric voltages or

$$(\gamma^2 - (Y_t Z_t + C^t Z_z^{-1} C Z_t + Y_t G Y_z^{-1} G^t)) F_t^d = 0, \quad (3\text{-}15.b)$$

for dual magnetic voltages. In (3-15), $Y_t = j\omega M_{\varepsilon t}$ and $Z_t = j\omega M_{\mu t}$, are transverse admittance and impedance matrices, respectively and $Y_z = j\omega M_{\varepsilon z}$ and $Z_z = j\omega M_{\mu z}$, are longitudinal admittance and impedance matrices, respectively.

The first term in the inner bracket in the LHS of (3-15) is related to the transverse fields, the second term to the z component of the magnetic field, and the third term to the z component of the electric field. Therefore, in the case of a Transverse Magnetic (TM) problem the second term, and in the case of a Transverse Electric (TE) problem the third term, will not exist in the final eigenvalue equation. It is noted that only the longitudinal impedance and admittance matrices are inverted.

In the following sections and chapters of this thesis, the waveguide structure case with an invariant 2-D cross section perpendicular to the direction of propagation, z, and a triangular primal mesh is considered.

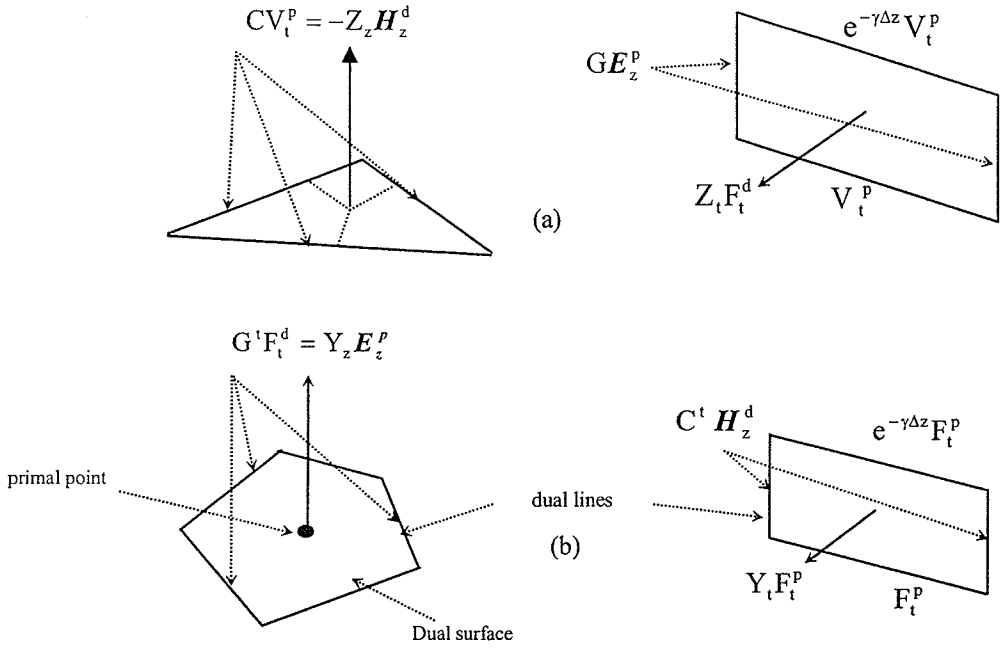

Figure 3-6: Surfaces used to derive: a) (3-12) for primal surfaces, b) (3-13) for dual surfaces.

3.3 Dual mesh and constitutive relations and matrices

The importance of constitutive relations as material and metric dependent relations has been extensively discussed in the literature. A major complexity in discretization of these relations is their conventionally specified continuous (point-wise) form, $\boldsymbol{D}=\varepsilon\boldsymbol{E}$ and $\boldsymbol{B}=\mu\boldsymbol{H}$, which is compatible with the differential expression of Maxwell's equations. For any physical material (excluding vacuum) these relations, however, are usually obtained based on experiment and measurements involving global variables. To appreciate the importance of the constitutive relations, it seems necessary to have a more detailed discussion on how construction of a dual mesh in FIT and the Cell Method helps in the construction of constitutive matrices.

The role of a dual mesh in the Cell Method can be summarized in the following important characteristics:

1- The dual mesh defines the "center" for each primal element

2- The dual mesh defines the relation between primal and dual lines (in an extruded mesh)

3- The geometrical properties of the dual mesh are used to average the constitutive relations when adjacent primal surfaces have different material properties

4- Using the primal-dual framework and definition of the incidence matrices (G, C, D) is convenient when assembling the coefficient matrices as well as in interpolation schemes

5- The actual existence of the dual mesh makes the computational procedure more reliable in terms of accuracy and stability

6- The primal-dual framework enables one to separately consider topological and constitutive relations. This is especially attractive when we need to squeeze, expand or scale the geometry of a problem while keeping the topology unchanged

It is assumed in this thesis that the *primal* mesh triangulation is always based on considering material discontinuities. Therefore any primal volume (extruded surface) is filled with one and only one specified material (ε,μ,σ) while the dual volumes (extruded surfaces) may consist of different materials.

The orthogonal dual mesh and the barycentric dual mesh, as the most common choices for a dual mesh, are described in the following sections.

3.3.1 Orthogonal and barycentric dual mesh

In an orthogonal primal-dual cell complex, dual lines are orthogonal to primal surfaces and vice-versa. Consider the primal surface in Fig. 3-7 and the orthogonal and non-orthogonal dual lines. The global variable defined on the primal surface is the (magnetic) "flux" passing through it. This flux implicitly includes only the perpendicular (to the surface) component and is independent of the tangential component of the (magnetic) field. The global variable, magnetic voltage, for the orthogonal dual line is also dependent solely on the orthogonal (to the surface, tangential to the line) component and therefore can be related uniquely to the (magnetic) flux in a scalar relation. For any non-orthogonal dual line the (magnetic) voltage is dependent on the tangential (to the surface) component of the field while the (magnetic) flux is not. Therefore, for a non-orthogonal dual line, a well-conditioned scalar relation (diagonal matrix) can not be found between primal and dual global variables. To approximate the value of the (magnetic) voltage for the non-orthogonal dual line, we need to use information about the neighbor primal (magnetic) fluxes, which results in a non-diagonal matrix relation.

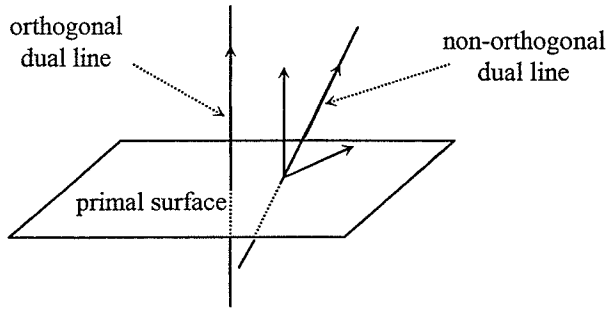

Figure 3-7: A primal surface and the orthogonal and non-orthogonal dual lines.

Examples of orthogonal 2-D dual meshes are a regular rectangular mesh and Delaunay-Voronoi triangulation as shown in Fig 3-8. In a 2-D Delaunay-Voronoi triangulation, each dual point is the circumcenter of the primal triangle and each dual line is the orthogonal bisector of a primal line.

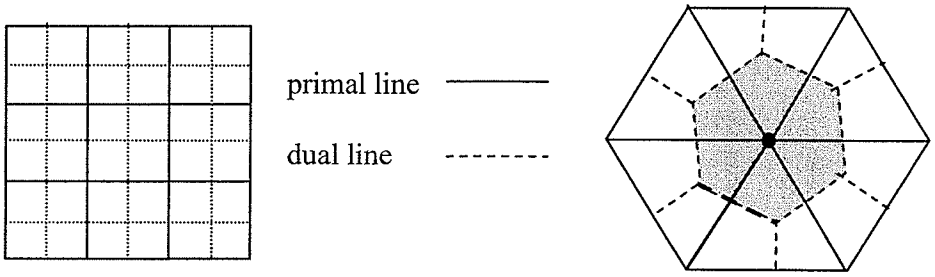

Figure 3-8: a) 2-D regular primal-dual mesh b) Delaunay-Voronoi triangulation.

A rectangular regular grid, as shown in Fig. 3-8, is not a good choice for multiscale problems or curved geometries since the grid size can not be adjusted to match fine details. In an irregular mesh, on the other hand, the size of cells can change to provide the proper resolution in different regions.

While an irregular mesh in general can consist of cells with different shapes and sizes, 2-D triangular and 3-D tetrahedral meshes are especially interesting since they are simplicial meshes [10]. Delaunay-Voronoi triangulation, is a good choice as an orthogonal dual mesh in multi-scale problems, but it is not always possible (especially in 3-D case) to build the Voronoi dual mesh since the circumcenter of an obtuse triangle (tetrahedron) is not inside the triangle (tetrahedron). A Delaunay-Voronoi tessellation can not guarantee the exact reconstruction of physical boundaries inside inhomogeneous media [16]. In the case of other arbitrarily chosen dual points, the orthogonality property

is not guaranteed and special averaging and interpolation techniques would then be necessary to build non-diagonal constitutive matrices.

As an example of a non-orthogonal dual mesh, a barycentric dual mesh is considered. In a barycentric dual mesh, each dual point is the barycenter (centroid) of the primal surface (volume) and dual lines are two-piece lines connecting adjacent dual points passing through the barycenter of primal lines (surfaces) as shown in Fig. 3-9. A barycentric dual mesh has unique attractive characteristics in interpolation and averaging schemes which will be mentioned later. Barycentric subdivision is a common choice in FIT where Whitney forms (node elements, edge elements and face elements [5,10,11]) are used in interpolation schemes. The Microcell Interpolation Scheme, MIS [6,17] has been used with the Cell Method formulation for construction of non-diagonal constitutive matrices in a barycentric subdivision.

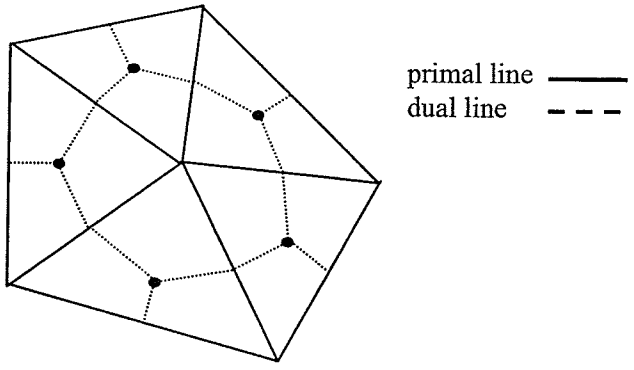

Figure 3-9: A 2-D barycentric dual mesh.

3.3.2 Order of accuracy and shape functions

In a real physical problem the constitutive characteristics of a physical medium are often considered "continuous" and expressed in a point-wise format in spatial

dimensions. We assume that a homogeneous physical media is continuous in comparison with the resolution of the spatial discretization, even in the case of a very fine mesh.

While discretization of the spatial domain does not affect topological laws, the discrete constitutive relations, which depend on the material and geometrical objects, are affected by the approximations used in the discretization process. "shape function" is the familiar name for these approximations as used in Finite Element Method, FEM.

The spatial accuracy issue arises from the fact that, in the discretization of a spatial domain, an infinite number of unknowns associated with each cell are replaced by a finite number of unknowns or Degrees of Freedom (DoF). The behavior of the solution function *inside* each cell is approximated based on DoF. For example, if we represent each cell by one unknown, a uniform (zero-order) shape function is obtained as the approximation to the solution inside each cell. Consider the 1-D example of Fig. 3-10. For the continuous function on the left, different DoF result in different approximations to the unknown function.

Zero-order shape functions are a low-accuracy, low-cost choice but they do not satisfy the continuity of the function on two adjacent elements. Higher-order shape functions require much more computation, memory and time, and significantly increase the complexity of the numerical procedure.

Constitutive relations are the only components in a discrete framework affected by discretization. Although constitutive relations are often obtained based on experiments and measurements, the result of these measurements on global variables is considered a "material property" (e.g. permittivity) with a continuous nature.

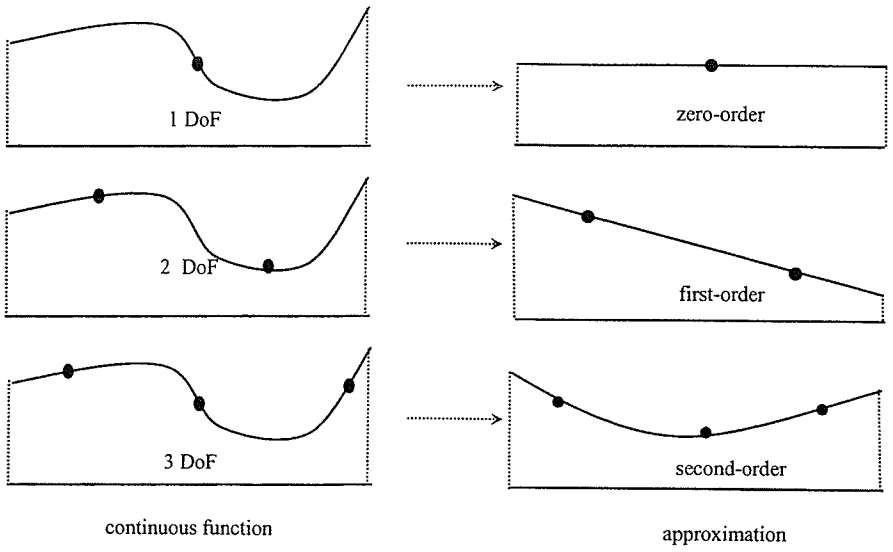

Figure 3-10: DoF and the order of accuracy.

As mentioned previously, a triangle is a simplex in 2-D space. This means that, as a closed curve defining a surface, it has the minimum number of sides (straight lines). The value of an unknown function can be linearly approximated *inside* the triangle based on the values of the function on the vertices of the triangle. Fig. 3-11 indicates the linear interpolation function for a triangle. The linear approximation can not be uniquely defined for surfaces with more than three sides.

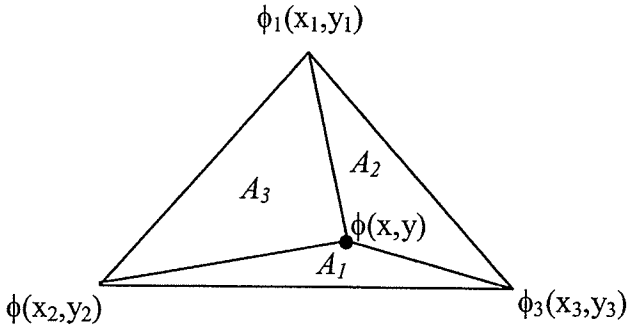

Figure 3-11 A linear shape function defined inside a triangle.

Referring to Fig. 3-11, the unknown function, $\phi(x,y)$, is linearly approximated as

$$\begin{aligned}\phi(x,y) &\cong \frac{A_1\phi(x_1,y_1)+A_2\phi(x_2,y_2)+A_3\phi(x_3,y_3)}{A} \\ &= \phi_1\alpha_1+\phi_2\alpha_2+\phi_3\alpha_3,\end{aligned} \tag{3-16}$$

where (x,y) is any point inside the triangle , $A=A_1+A_2+A_3$ is the area of the triangle and α_i are the shape functions.

Integration of a linear approximation over the triangle results in an attractive property of the barycentric dual mesh as follows;

$$\iint_A \phi(x,y)ds = \frac{\phi_1+\phi_2+\phi_3}{3}A = \phi_M A, \tag{3-17}$$

where M is the barycenter of the triangle. This implies that, for a linear shape function, the primal constitutive matrix in the z direction ($M_{\mu z}$ in 3-14.d) will be diagonal as

$$\Phi(S) = \iint_{S_\beta} \boldsymbol{B}(x,y)ds = \iint_{S_\beta} \mu \boldsymbol{H}_z ds = \mu \left|S_\beta\right| \boldsymbol{H}_z^d(\tilde{P}_\beta = M_\beta) \tag{3-18}$$

$$M_{\mu z}(\beta,\beta) = \frac{\Phi(S_\beta)}{H_z(\tilde{P}_\beta)} = \mu S_\beta \ , \tag{3-19}$$

where M_β is the barycenter of the primal surface, S_β. This however does not hold for the dual constitutive matrix in the z direction ($M_{\varepsilon z}$). This matrix has to be constructed using a zero-order approximation.

It is important to note that the numerical order of accuracy in the finite formulation directly reveals itself in the construction of the constitutive matrices. It should also be noted that employing a linear shape function for z component of the fields, implies a uniform approximation for the *transverse* variables over their corresponding geometrical objects.

3.4 Finite Formulation, Finite Element and Finite Volume

Many different types of numerical techniques are available to provide accurate approximations to the solution of physical problems. Although the results obtained using different numerical techniques can be similar or even exactly the same, each technique has its own attractive features or drawbacks which should be considered when choosing the proper technique to solve a specific problem. Numerical techniques, in general, have similarities and differences in the approach taken to model a physical problem.

In this section we

1- Compare Finite Formulation with Finite Element Method and Finite Volume Method in modeling a homogenous Helmholtz problem

2- Investigate the implicit use of a dual mesh in FEM and FVM

3- Explain why we prefer a Finite Formulation for modeling electromagnetic problems

Finite Element Method (FEM) and Finite Volume Method (FVM) were first introduced and applied in Computational Fluid Dynamics, CFD. Applications of these techniques in electrical engineering began later in the 1960s for FEM [45] and 1990s for FVM [46].

As it was mentioned earlier, Finite Formulation utilizes a discrete framework which is not based on a differential formulation. FEM and FVM, however, are considered differential-based techniques and do not explicitly employ a dual mesh. The word "Finite" in FEM and FVM refers to the finite elements in the *spatial* discrete domain. In FEM and FVM, topological relations are not distinguished from constitutive relations and the fact that discretization *only* affects the constitutive relations is not straightforward to

understand. Comparisons between Finite Formulation and other techniques, FEM in particular, have been made as early as the beginning of Finite Formulation itself [1, 3, 5, 11, 15].

Numerical techniques such as FDTD and Finite Integration Techniques, FIT, which benefit from a primal-dual framework, owe their noticeable success in Computational Electromagnetics to the duality concept hidden in the governing electromagnetic relations. In our comparison between the Finite Formulation technique and other "finite" techniques, FEM and FVM, we consider the role of a dual mesh in Finite Formulation and how it is implicitly constructed and used in FEM and FVM with linear shape functions. We use the example of the solution to the homogeneous Helmholtz wave equation, $\nabla^2\psi + k_z^2\psi = 0$, $(k_z^2 = -\gamma^2)$, for a rectangular waveguide geometry.

3.4.1 Helmholtz equation, Finite formulation

The finite form of Helmholtz wave equation for a waveguide geometry was derived in section 3-2 as in (3-15) and can be rewritten as

$$(C_{FF} + k_z^2 I)V_t^p = 0, \tag{3-20}$$

where $C_{FF} = Z_t Y_t + Z_t C^t Z_z^{-1} C + G Y_z^{-1} G^t Y_t$, $k_z^2 = -\gamma^2$ and V_t^p is the array of DoF for the primal edges. In C_{FF} , the G and C matrices are material and metric independent matrices defined only by the topology of the primal mesh. These matrices remain unchanged when the geometry is scaled or when the material or frequency change. k_z^2 is found from (3-20) as the eigenvalue of (- C_{FF}).

Geometrical characteristics of the dual mesh and the assumptions about the order of accuracy were utilized directly in the construction of Y and Z matrices in (3-20). For an orthogonal dual mesh and first order accurate longitudinal components, all Z and Y matrices in (3-20) are diagonal and consequently symmetric positive definite matrices which guarantees the consistency, convergence and stability of the scheme[10,17,20,21]. In the case of a non-orthogonal dual mesh or higher order of accuracy, the Y and Z matrices are not diagonal in general and different approaches are used to make alternative diagonal or symmetric positive definite Y and Z matrices or otherwise prove the consistency of the scheme [17,20, 23, 29].

3.4.2 Helmholtz equation, Finite Element Method

In the Finite Element Method, the homogeneous Helmholtz wave equation, $\nabla^2\psi + k_z^2\psi = 0$, is solved by minimizing a functional, $\boldsymbol{F}$. It is shown in [44] that solutions of Helmholtz wave equation render stationary the functional

$$\boldsymbol{F}(U) = \frac{1}{2}[\iiint_{\Omega} \nabla U \cdot \nabla U \cdot d\Omega - k_z^2 \iiint_{\Omega} U^2 \cdot d\Omega] \,, \tag{3-21}$$

provided the U functions are continuous within the problem region. The functional $\boldsymbol{F}$ in (3-21) attains its minimum (stationary point) at $U_0=\psi$ which is the solution of the Helmholtz wave equation.

To minimize (3-21), the spatial domain, Ω, is divided into many finite elements. The solution function is then approximated over each element in terms of the unknown values of the solution at the vertices of the elements (or more points as in higher order schemes).

We consider the components of the functional in (3-21) for a 2-D triangular element as shown in Fig. 3-11:

$$\begin{aligned} &U = \phi_1\alpha_1 + \phi_2\alpha_2 + \phi_3\alpha_3, \\ &\nabla U = \phi_1\nabla\alpha_1 + \phi_2\nabla\alpha_2 + \phi_3\nabla\alpha_3, \\ &\boldsymbol{F}(U) = (1/2)[\Phi_e^t \cdot S \cdot \Phi_e - k_z^2 \cdot \Phi_e^t \cdot T \cdot \Phi_e], \end{aligned} \tag{3-22}$$

where S_e, the element stiffness matrix, T_e, the element mass matrix, and Φ_e, the array of DoF on nodes, are defined as

$$S_{e,ij} = \int_{A_e} \nabla\alpha_i \cdot \nabla\alpha_j \, ds \,, \quad T_{e,ij} = \int_{A_e} \alpha_i \cdot \alpha_j \, ds \quad , \quad \Phi_e{}^t = [\phi_1 \;\; \phi_2 \;\; \phi_3]. \tag{3-23}$$

Here A_e refers to the area of the triangle. Minimization of the value of the functional (in terms of ϕ's which are free to vary) over the whole region and assembling all element matrices together, result in the following matrix equation:

$$S\Phi - k_z^2 T\Phi = 0. \tag{3-24}$$

Equation (3-24) can be rewritten as an eigenvalue equation as

$$(T^{-1}S - k_z^2 I)\Phi = 0 \quad . \tag{3-25}$$

This equation can be compared to (3-20) for the Finite Formulation.

We have proved [15] that for linear shape functions the matrices, S and T, which are dependent on the shape functions chosen, implicitly define dual lines as perpendicular bisectors and the dual points as barycenters. It is also important to note that the inverse of T matrix in (3-25) represents the dual surfaces around primal points in the finite formulation. The finite equivalent of the Cartesian Laplacian operator, ∇^2 ,(C_{FF}), is also equivalent to the stiffness matrix in FEM when linear shape functions are used. For a complete geometrical proof see [15].

As a conclusion it can be stated that shape functions are needed in both FEM and Finite Formulation. Dual mesh exists implicitly in FEM at least for first order shape functions, and it is defined by the integral of shape functions or their derivatives over the triangles. Having an explicit dual mesh, as in finite formulation, however, is beneficial regarding the points mentioned in the beginning of section 3-3.

3.4.3 Helmholtz equation, Finite-Volume Method

Finite Volume Method was originated in Computational Fluid Dynamics (CFD). In CFD, the governing equations are often expressed in a conservative (balance or divergence) form. The concept of control volumes was used in CFD instead of infinitesimal volumes in order to apply the balance equation.

Finite Volume Method did not receive attention in computational electromagnetics until 1990 [46]. Frequency-domain Finite Volume Method has received even less attention and has not been widely used in computational electromagnetics. Finite volumes does not offer a primal-dual framework and shape functions are not explicitly employed. The technique, however, is extensively based on averaging and interpolation schemes.

For time-harmonic electromagnetics, Maxwell's curl equations, which naturally involve lines and surfaces, need to be converted to a divergence form using volumes and surfaces. The six Cartesian components of E and H fields are lumped together in a vector form as: $\bar{U} = (E_x\ E_y\ E_z\ H_x\ H_y\ H_z)$ and Maxwell's curl equations are rewritten in a compact divergence form as [47]

$$j\omega\bar{U} + \nabla \cdot (M^{-1} \cdot \boldsymbol{G}(\bar{U})) = 0\ , \tag{3-26}$$

where the term, $\nabla \cdot \boldsymbol{G}(\bar{U})$, corresponds to the curl of $\boldsymbol{E}$ and $\boldsymbol{H}$ in the curl equations (3-1)

and M is a diagonal matrix specifying the material parameters. Integration of (3-26) over prisms with triangular bases (S_β) and height Δz, results in

$$j\omega\vec{U}_\beta = \frac{-1}{|S_\beta|}\left[\left(\sum_{\alpha=1}^{3} M^{-1}F(\vec{n}_\alpha)\vec{U}_\alpha|L_\alpha|\right) + \gamma M^{-1}F(\vec{a}_z)\vec{U}_\beta|S_\beta|\right], \tag{3-27}$$

where $\vec{U}_\beta$ is the collocated field vector computed at the barycenter of triangle β and $F(\vec{n}_\alpha)\vec{U}_\alpha = \boldsymbol{G}(\vec{U}_\alpha)\vec{n}_\alpha$. $\vec{U}_\alpha$ is the collocated field vector computed at the barycenter of the edge α of triangle β. This vector is interpolated using the value of U in the two adjacent triangles sharing the edge α as indicated in Fig. 3-12. It is important to note that the fluxes in the RHS of (3-27) are not independent variables, DoF, as is the case in the Finite Formulation (where fluxes associated to the faces are independent variables).

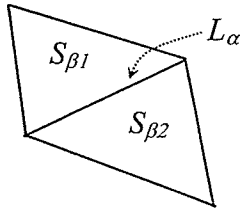

$$\vec{U}_\alpha = \frac{1}{2}(\vec{U}_{\beta 1} + \vec{U}_{\beta 2})$$

Figure 3-12 Interpolation of the field vector for the edge α shared between two triangles $\beta 1$ and $\beta 2$.

The field vector $\vec{U}$, in general, has six independent components which should be calculated for each triangle. The FVM works better for time-domain schemes where the field components are updated in each time step. Although the FVM does not use shape functions, interpolation of the field vector, U, for calculating the flux on faces as in Fig. 3-12, is a poor approximation and can be improved by using more accurate interpolation schemes (or shape functions). The FV scheme described here implicitly defines a barycentric dual mesh with orthogonal dual lines (used to calculate fluxes).

Chapter 4- Incentric Cell Method

The explicit use of a dual mesh is one of the important features of the Cell Method formulation. Two different dual mesh construction schemes, Delaunay-Voronoi tessellation as an orthogonal dual mesh and barycentric dual mesh as a non-orthogonal dual mesh, were introduced in the previous chapter. In this chapter, we propose a new dual mesh construction scheme for an arbitrary triangular primal mesh which can be used for solving two dimensional electromagnetic problems and guided wave structures. This dual mesh construction scheme can be extended to three dimensional tetrahedral meshes.

As discussed in Chapter Three, a good choice for construction of the dual mesh is a Voronoi dual mesh, which uses the circumcenter of the primal elements as dual points. This choice maintains the orthogonality between primal and dual geometrical objects but also imposes an additional condition on the primal mesh. The circumcenter for any obtuse triangle falls outside the triangle making it impossible to have a well-defined dual mesh.

The existence of a Delaunay-Voronoi tessellation for an arbitrary inhomogeneous region is not guaranteed [16]. The interior boundaries of the region, in general, do not coincide with the edges of Delaunay triangles or Voronoi polygons. Even for a homogenous 2-D region, building a Delaunay-Voronoi tessellation, with no obtuse triangles, is not an easy task. In multiscale problems when the size of cells changes drastically over the region, obtuse triangles can not be avoided in most common mesh generation algorithms. Table 4-1 reports the percentage of obtuse triangles in some of the examples studied in Chapters Five and Six. The meshes are obtained using FEMLAB (COMSOL, [48]) mesh generator. Even for triangles with angles close to 90°,

the circumcenter is very close to the longest side, as shown in Fig. 4-1, and is not a good choice for a "center" in interpolation schemes.

Table 4-1: Percentage of obtuse triangles in different geometries described in Chapter Six.

Geometry	Waveguide	CPW	ACPW	Buried cable	Microstrip
Percentage of Obtuse triangles	7	12	12	15	10

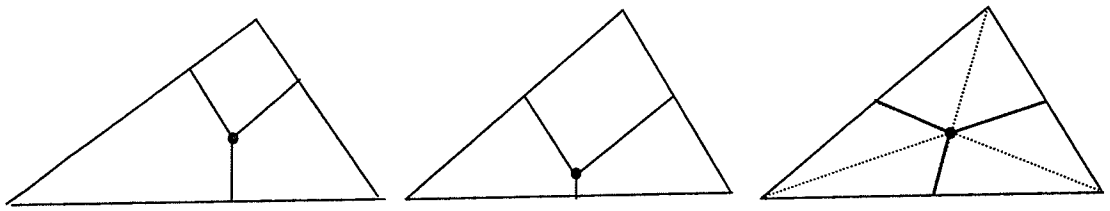

(a) (b) (c)

Figure 4-1: a) Incenter, b) circumcenter and c) barycenter for a triangle.

The barycenter of a triangle is always inside the triangle and also features interesting properties such as dividing the area of the triangle into three equal parts as shown in Fig. 4-1. The barycentric dual mesh has been used with the Finite Formulation using Whitney forms [10,11,13] or with the Microcell Interpolation Scheme, MIS [17,21-24] and produces non-diagonal constitutive matrices.

An Incentric dual mesh construction scheme is an attempt to achieve the advantages of an orthogonal dual mesh while making it possible to use any kind of triangular primal mesh, including obtuse triangles. This scheme is introduced and explained in detail in this chapter.

4.1 Geometrical objects

We consider a two-dimensional triangular primal mesh as shown in Fig. 4-2, with *np* primal points, P_i, *nl* primal (straight) lines, L_α, and *ns* primal surfaces (triangles), S_β. The dual mesh consists of *ns* dual points, $\tilde{P}_\beta$, *nl* dual lines, $\tilde{L}_\alpha$ and *np* dual surfaces, $\tilde{S}_i$.

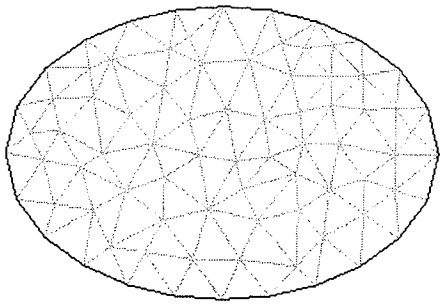

Figure 4-2: A 2-D triangular mesh

Primal geometrical objects do not depend on the choice for the dual mesh and remain the same as already explained. Dual geometrical objects, however, are introduced for the Incentric scheme as follows.

4.1.1 Dual points

In the incentric dual mesh construction scheme, we use the incenter of primal triangles as dual points. The three angle bisectors of a triangle meet in one point called the incenter. It is the center of the incircle, the circle inscribed in the triangle as shown in Fig. 4-3. The reasons for this choice are:

- The incenter of any triangle is always inside the triangle.
- The perpendicular lines drawn from the incenter to the sides are completely inside the triangle.
- The distances from the incenter to the sides are equal.

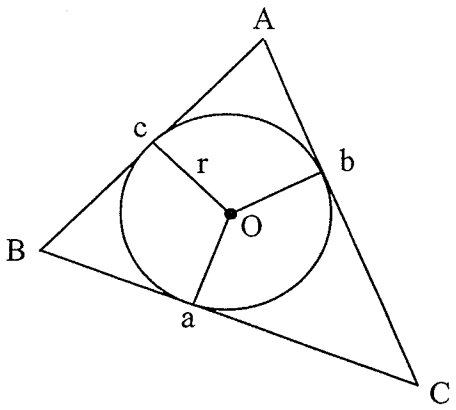

Figure 4-3: The incenter of a triangle, O. The radius of the incircle is $r=2S/(a+b+c)$ where S is the area of the triangle.

4.1.2 Dual lines

In a Voronoi dual mesh, dual lines simply connect the dual points for two adjacent triangles. In a barycentric dual mesh, dual lines are not straight lines but two-piece lines consisting of the shorter parts of the medians in two adjacent triangles.

Incenteric dual lines, in general, consist of three pieces, two orthogonal components and one tangential component as shown in Fig. 4-4. An important parameter in the incentric scheme is the length ratio of the tangential portion of the dual line to the primal line.

We define the diagonal "Ratio Matrix" as

$$R(\alpha,\alpha)=\frac{|L'_\alpha|}{|L_\alpha|}, \quad \alpha=1:nl, \tag{4-1}$$

where nl is the number of primal (or dual) lines and L_α and L'_α are indicated in Fig. 4-4. Mesh generating algorithms usually avoid having "bad" triangles in the mesh and maintain the triangles as close as possible to an equilateral triangle which results in a Ratio Matrix with a

small norm. This diagonal matrix appears in the final eigenvalue equation and as shown later plays an important role in the incentric scheme.

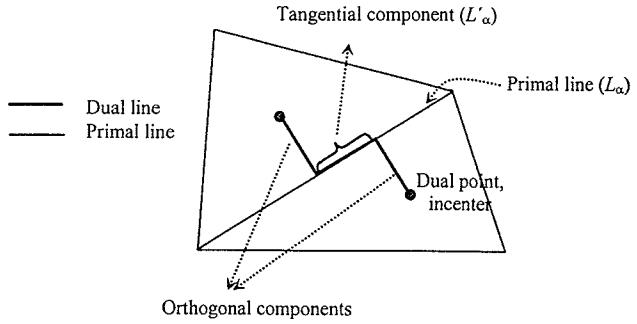

Figure 4-4: In the incentric scheme, dual lines consist of three components: the tangential component is a portion of the corresponding primal line and two orthogonal components are orthogonal to the corresponding primal line.

4.1.3 Dual surfaces

Dual surfaces are the areas enclosed by intersecting dual lines and surrounding a primal point. Fig. 4-5 illustrates a dual surface in an incentric dual mesh. We now introduce another important matrix, S_{PD}, related to primal and dual surfaces as

$$S_{PD}(\beta,i) = S_\beta \cap \tilde{S}_i; \quad \text{for} \quad \beta=1{:}ns, \quad \text{and } i=1{:}np, \tag{4-2}$$

which indicates the portion of the primal surface, S_β, shared by the dual surface, $\tilde{S}_i$ as shown in Fig. 4-5. This matrix is used in the incentric scheme in the interpolation of the z components of EM variables.

From the definition of the incentric dual lines and surfaces it is deduced that the global variables defined on transverse dual lines and longitudinal (extruded) dual surfaces need to be corrected for the "unwanted tangential component".

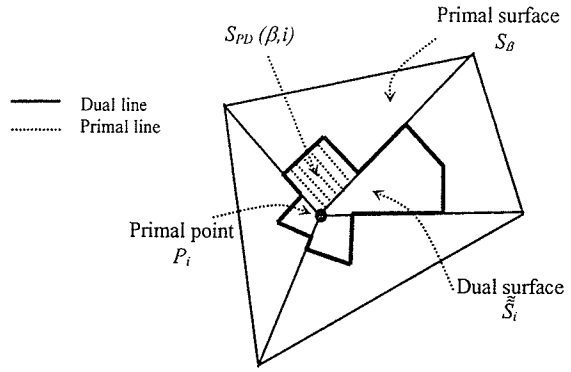

Figure 4-5: An incentric dual surface and S_{PD} matrix elements.

4.2 Incentric formulation

The general time-harmonic formulation for waveguide structures was given in Chapter Three, (3-12) to (3-15). In the incentric scheme with the geometrical objects defined as in section 4.1, special considerations are required for the proper treatment of the tangential component of the dual lines. The global variables defined on the tangential component do not exist in the general formulation (3-12, 3-13). In order to take into account the effect of the global variables defined on the tangential part of dual lines, we introduce a set of two dual formulations as follows.

In the *V-formulation*, electric voltage is defined on the primal lines $(\mathrm{V}_t^p, \boldsymbol{E}_z^p)$ and magnetic flux is defined on the primal surfaces (Φ_t^p, Φ_z^p). This set of variables was previously defined and used in the general formulation given in section 3-2, (3-12) to (3-15).

In the *F-formulation*, we switch the global variables defined on the primal and dual geometrical objects. Magnetic voltage is now defined on the primal lines $(F_t^p, \boldsymbol{H}_z^p)$ and electric flux is defined on the primal surfaces (Ψ_t^p, Ψ_z^p).

In comparison with the equations given in Chapter Three, primal equations in V-formulation remain exactly the same as in (3-12) because the primal geometrical objects have not changed.

Primal equation in F-formulation can be also written in the same manner as in (3-12). Equations for the dual variables, (3-13), however, need to be modified to include the tangential components in both formulations.

Based on the assumption of linear shape functions for z components (which imply a uniform approximation for the transverse variables), the global variables associated with the tangential parts are proportional to the same variable defined in the dual formulation. The coefficient for this proportionality is the coupling, *CPL(α,α)*, as indicated in Fig. 4-6.

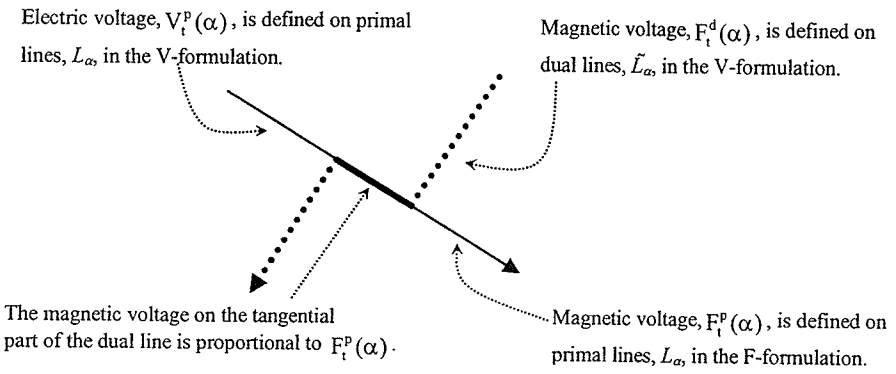

Figure 4-6: The coupling between dual variables in V-formulation and the corresponding primal variables in F-formulation is taken into account through the coupling matrix, *CPL*. Magnetic voltage defined on the tangential part of the dual line, L_α, is proportional to $F_t^p(\alpha)$ as $CPL(\alpha,\alpha)\times F_t^p(\alpha)$.

The coupling is related to the Ratio Matrix, (4-1), as

$$CPL(\alpha,\alpha)=\begin{cases} R(\alpha,\alpha)\ ; \text{case1} \\ -R(\alpha,\alpha); \text{case2} \end{cases} . \tag{4-3}$$

Here, case 1 is the case when going in the direction of the dual line, the tangential part is in the same direction as the primal line. Case 2 is the case when going in the direction of the dual line, the tangential part is in the opposite direction of the primal line. In Fig. 4-6 case 2 is depicted where *CPL(α,α)=-R(α,α)*.

Recalling (3-12) and modifying (3-13) to include the coupling, V-formulation for an incentric dual mesh can be written as

$$
\begin{aligned}
&\mathrm{CV}_t^p = -\mathrm{Z}_{z1}\boldsymbol{H}_z^d \\
&\gamma \mathrm{V}_t^p + \mathrm{GE}_z^p = -\mathrm{Z}_{t1}\mathrm{F}_t^d \\
&\mathrm{G}^t(\mathrm{F}_t^d + \mathrm{CPL}\cdot\mathrm{F}_t^p) = \mathrm{Y}_{z1}\boldsymbol{E}_z^p \\
&-\gamma(\mathrm{F}_t^d + \mathrm{CPL}\cdot\mathrm{F}_t^p) + \mathrm{C}^t\mathrm{H}_z^d = \mathrm{Y}_{t1}\mathrm{V}_t^p - \mathrm{CPL}\cdot\mathrm{Y}_{t2}\mathrm{V}_t^d
\end{aligned}
\qquad (4\text{-}4)
$$

where the numbers one and two in the subscripts refer to the V- or F- formulation, respectively.

F-formulation is obtained from (4-4) by changing all Z matrices to –Y, changing all F variables to V, $\boldsymbol{H}$ variables to $\boldsymbol{E}$ and vice versa. The numbers in the subscripts change as 1↔2. F-formulation is then written as

$$
\begin{aligned}
&\mathrm{CF}_t^p = \mathrm{Y}_{z2}\boldsymbol{E}_z^d \\
&\gamma \mathrm{F}_t^p + \mathrm{GH}_z^p = \mathrm{Y}_{t2}\mathrm{V}_t^d \\
&\mathrm{G}^t(\mathrm{V}_t^d + \mathrm{CPL}\cdot\mathrm{V}_t^p) = -\mathrm{Z}_{z2}\boldsymbol{H}_z^p \\
&-\gamma(\mathrm{V}_t^d + \mathrm{CPL}\cdot\mathrm{V}_t^p) + \mathrm{C}^t\mathrm{E}_z^d = -\mathrm{Z}_{t2}\mathrm{F}_t^p + \mathrm{CPL}\cdot\mathrm{Z}_{t1}\mathrm{F}_t^d
\end{aligned}
\qquad (4\text{-}5)
$$

Different variables and components in (4-4), except those related to the tangential parts, were depicted in Fig. 3-6. Fig. 4-7, in a similar manner, depicts different components in the primal and dual equations, (4-4).

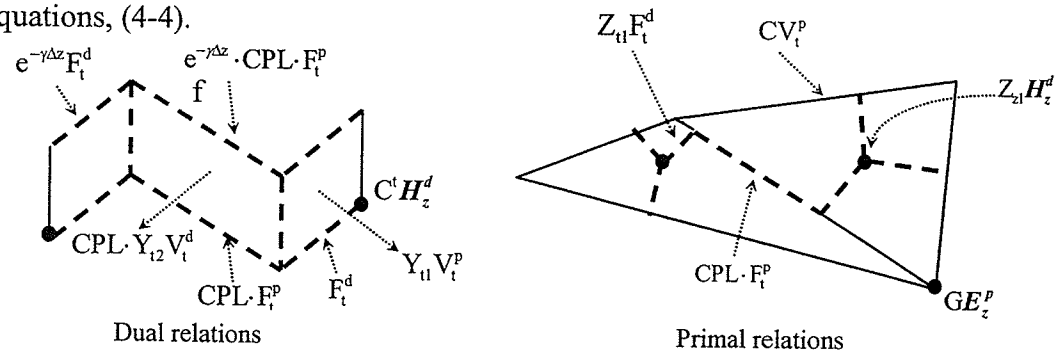

Figure 4-7: Different components and geometrical objects used in equations (4-4).

Using the second equation in (4-5), we can simplify the last equation in (4-4) as

$$
\begin{aligned}
&\gamma \mathrm{F}_t^p + \mathrm{G}\boldsymbol{H}_z^p = \mathrm{Y}_{t2}\mathrm{V}_t^d \;\rightarrow \mathrm{CPL}\cdot(\gamma \mathrm{F}_t^p + \mathrm{G}\boldsymbol{H}_z^p) = \mathrm{CPL}\cdot\mathrm{Y}_{t2}\mathrm{V}_t^d \\
&-\gamma \mathrm{F}_t^d + \mathrm{C}^t\boldsymbol{H}_z^d + \mathrm{CPL}\cdot\mathrm{G}\cdot\boldsymbol{H}_z^p = \mathrm{Y}_{t1}\mathrm{V}_t^p
\end{aligned}
\qquad (4\text{-}6)
$$

Similarly, using the second equation in (4-4), we can simplify the last equation in (4-5) as

$$\begin{aligned} &\gamma V_t^p + GE_z^p = -Z_{t1}F_t^d \;\rightarrow CPL\cdot(\gamma V_t^p + GE_z^p) = -CPL\cdot Z_{t1}F_t^d \\ &-\gamma V_t^d + C^t E_z^d + CPL\cdot G\cdot E_z^p = -Z_{t2}F_t^p \end{aligned} \quad . \tag{4-7}$$

The simplified V-formulation is then written as

$$\begin{aligned} &CV_t^p = -Z_{z1}\boldsymbol{H}_z^d \\ &\gamma V_t^p + G\boldsymbol{E}_z^p = -Z_{t1}F_t^d \\ &G^t(F_t^d + CPL\cdot F_t^p) = Y_{z1}\boldsymbol{E}_z^p \\ &-\gamma F_t^d + C^t\boldsymbol{H}_z^d + CPL\cdot G\cdot\boldsymbol{H}_z^p = Y_{t1}V_t^p \end{aligned} \quad , \tag{4-8}$$

and in a similar manner, the simplified F-formulation is written as

$$\begin{aligned} &CF_t^p = Y_{z2}\boldsymbol{E}_z^d \\ &\gamma F_t^p + G\boldsymbol{H}_z^p = Y_{t2}V_t^d \\ &G^t(V_t^d + CPL\cdot V_t^p) = -Z_{z2}\boldsymbol{H}_z^p \\ &-\gamma V_t^d + C^t\boldsymbol{E}_z^d + CPL\cdot G\cdot\boldsymbol{E}_z^p = -Z_{t2}F_t^p \end{aligned} \quad . \tag{4-9}$$

The CPL matrix, represents the effect of the coupling between variables in one formulation into the other formulation. After some manipulations, (4-8) and (4-9) result in the following final V- and F-formulations, respectively:

$$\left(\gamma^2 - (Y_{t1}\cdot Z_{t1} + C^t Z_{z1}^{-1} C\cdot Z_{t1} + Y_{t1}\cdot G Y_{z1}^{-1} G^t)\right) F_t^d = \gamma.CPL.G.\boldsymbol{H}_z^p + Y_{t1}.G.Y_{z1}^{-1}.G^t.CPL.F_t^p, \tag{4-10}$$

$$\left(\gamma^2 - (Z_{t2}\cdot Y_{t2} + C^t Y_{z2}^{-1} C\cdot Y_{t2} + Z_{t2}\cdot G Z_{z2}^{-1} G^t)\right) V_t^d = \gamma.CPL.G.\boldsymbol{E}_z^p + Z_{t2}.G.Z_{z2}^{-1}.G^t.CPL.V_t^p. \tag{4-11}$$

A few important points should be noted in (4-10) and (4-11). The left hand side in both equations is in the form of a normal eigenvalue problem as in (3-15). The CPL matrix appears only in the left hand side of the equations. In a zero-order approximation this matrix (and consequently the left hand sides of (4-10) and (4-11)) is considered zero which results in the following zero-order V0- and F0- formulations :

$$(\gamma^2 - Y_{t1}Z_{t1} - Y_{t1}GY_{z1}^{-1}G^t - C^tZ_{z1}^{-1}CZ_{t1})F_t^d = 0 \quad , \tag{4-12}$$

$$(\gamma^2 - Z_{t2}Y_{t2} - Z_{t2}GZ_{z2}^{-1}G^t - C^tY_{z2}^{-1}CY_{t2})V_t^d = 0 \, , \tag{4-13}$$

respectively. Close results are expected for the propagation constant, γ, obtained from (4-12) and (4-13). We also expect that the field distribution obtained from the two formulations agree well up to a scaling factor. These expectations are verified through examples and results given in Chapter Six. Equations (4-10) and (4-11) can be further simplified in the case of Transverse Electric (TE) or Transverse Magnetic (TM) propagation, respectively as explained in section 4.4. It is noted that all Z and Y matrices in the L.H.S of (4-12) and (4-13) are diagonal and therefore the eigenvalue problems are in the convenient form involving symmetric positive definite constitutive matrices which guarantees stability and convergence of the scheme[10,17,20,21].

In the next section construction of Z and Y matrices in (4-10) to (4-13) are explained.

4.3 Constitutive matrices and interpolation functions

In the Cell Method, DoF are global variables assigned to edges and faces in the primal and dual meshes. This guarantees the continuity boundary condition at the interface of different material since there is only one number assigned to a line (the tangential voltage) or a surface (the normal flux). Constitutive matrices are built based on this natural continuity of tangential voltages and normal fluxes in the Cell Method formulation. In the construction of the transverse constitutive matrices, Z_{t1}, Y_{t1}, Z_{t2}, Y_{t2}, we consider a uniform field distribution (zero-order approximation) over primal or dual lines. Referring to Fig. 4-8, transverse constitutive matrices are defined as follows.

$$F^d(\alpha)=\frac{|\tilde{L}_{1\alpha}|}{\mu_1}\cdot\frac{\Phi^p(\alpha)}{|L_\alpha|}+\frac{|\tilde{L}_{2\alpha}|}{\mu_2}\cdot\frac{\Phi^p(\alpha)}{|L_\alpha|}\quad,\quad Z_{t1}(\alpha,\alpha)=j\omega|L_\alpha|\left(\frac{|\tilde{L}_{1\alpha}|}{\mu_1}+\frac{|\tilde{L}_{2\alpha}|}{\mu_2}\right)^{-1},$$

$$\frac{V^d(\alpha)}{j\omega}=\frac{|\tilde{L}_{1\alpha}|}{\sigma_1+j\omega\varepsilon_1}\cdot\frac{\Psi^p(\alpha)}{|L_\alpha|}+\frac{|\tilde{L}_{2\alpha}|}{\sigma_2+j\omega\varepsilon_2}\cdot\frac{\Psi^p(\alpha)}{|L_\alpha|},\qquad (4\text{-}14)$$

$$Y_{t2}(\alpha,\alpha)=|L_\alpha|\left(\frac{|\tilde{L}_{1\alpha}|}{\sigma_1+j\omega\varepsilon_1}+\frac{|\tilde{L}_{2\alpha}|}{\sigma_2+j\omega\varepsilon_2}\right)^{-1},$$

$$Z_{t2}(\alpha,\alpha)=j\omega\frac{\mu_1|\tilde{L}_{1\alpha}|+\mu_2|\tilde{L}_{2\alpha}|}{|L_\alpha|}\quad,\quad Y_{t1}(\alpha,\alpha)=\frac{(\sigma_1+j\omega\varepsilon_1)\cdot|\tilde{L}_{1\alpha}|+(\sigma_2+j\omega\varepsilon_2)\cdot|\tilde{L}_{2\alpha}|}{|L_\alpha|}.$$

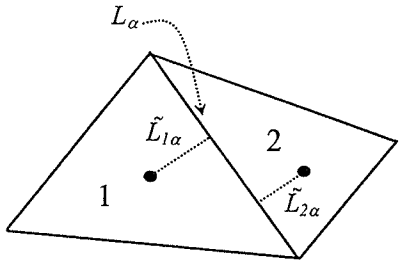

Figure 4-8: A primal line, L_α, is located on the interface of two different materials. Construction of the constitutive matrices in the Cell Method is based on the natural continuity of the tangential voltages and normal fluxes at the interface of the two materials, 1 and 2.

For constitutive matrices in the z direction, we consider a first-order (linear) approximation for z components of the fields over triangular elements. Based on (3-19), if the barycenter is considered, this assumption results in diagonal primal constitutive matrices in the z direction for Z_{z1} and Y_{z2}. In order to maintain the simplicity of the procedure, we ignore the distance between the incenter and the barycenter in the construction of these matrices. This assumption is validated through investigation of different triangles. The reason for choosing the incenter is that the perpendicular lines from the incenter to the sides of a triangle are always inside the triangle making it possible to have the incentric dual mesh for any arbitrary primal triangulation. Z_{z1} and Y_{z2} are then obtained as

$$Z_{z1}(\beta) = j\omega\mu_\beta |S_\beta| \quad , \quad Y_{z2}(\beta) = (\sigma_\beta + j\omega\varepsilon_\beta)\cdot |S_\beta| \tag{4-15}$$

For the dual constitutive matrices in the z direction, however, a linear interpolation function cannot be defined as the dual surfaces are polygons having more than three vertices. A linear interpolation over primal triangles also results in non-diagonal dual constitutive matrices in the z direction. A uniform approximation over dual surfaces results in diagonal dual constitutive matrices in z-direction as

$$\begin{aligned} Y_{z1}(i) &= \sum_{\beta\in\Omega} (\sigma_\beta + j\omega\varepsilon_\beta)\cdot S_{PD}(\beta,i) \quad , \quad \Omega = \{\text{primal surfaces sharing node i}\} \\ Z_{z2}(i) &= \sum_{\beta\in\Omega} (j\omega\mu_\beta)\cdot S_{PD}(\beta,i) \quad , \quad \Omega = \{\text{primal surfaces sharing node i}\} \end{aligned} \tag{4-16}$$

where S_{PD} was defined as in (4-2).

We shall now introduce two other interpolation functions that have been utilized in the incentric scheme. When the z components of the fields, $\boldsymbol{E}_z$ or $\boldsymbol{H}_z$, are obtained (either for the primal points or for the dual points), from (4-10) and (4-11), the value of the variables for any point in the 2-D region can be approximated using appropriate interpolation functions. We can approximate the value of the z components of the fields at the dual points in terms of the values at the primal points based on a simple linear approximation as

$$\overline{\boldsymbol{E}}_z^d = T_{dp}\overline{\boldsymbol{E}}_z^p, \quad \overline{\boldsymbol{H}}_z^d = T_{dp}\overline{\boldsymbol{H}}_z^p, \quad T_{dp} = \frac{1}{3}|C||G| \ , \tag{4-17}$$

where $\overline{\boldsymbol{E}}_z^d, \overline{\boldsymbol{H}}_z^d$ are column vectors containing all $\boldsymbol{E}_z$ and $\boldsymbol{H}_z$ components on the dual points and $\overline{\boldsymbol{E}}_z^p, \overline{\boldsymbol{H}}_z^p$ are column vectors containing all $\boldsymbol{E}_z$ and $\boldsymbol{H}_z$ components on the primal points. T_{dp} represents a simple linear interpolation of the fields ($\overline{\boldsymbol{E}}_z, \overline{\boldsymbol{H}}_z$) on three vertices of each primal triangle to obtain a value for the fields on the corresponding dual point. T_{dp} is expressed in terms of the curl matrix, C, and the gradient matrix, G, defined in Chapter Two.

In a same manner, we approximate the value of the fields at each primal point based on an equal weighting interpolation between all dual points surrounding the primal point. This interpolation can be written as

$$\overline{\boldsymbol{E}}_z^p = \mathrm{T}_{\mathrm{pd}}\overline{\boldsymbol{E}}_z^d \ , \qquad \overline{\boldsymbol{H}}_z^p = \mathrm{T}_{\mathrm{pd}}\overline{\boldsymbol{H}}_z^d \qquad , \quad \mathrm{T}_{\mathrm{pd}} = \mathrm{sign}(S_{PD}{}^{\mathrm{t}}) \ . \tag{4-18}$$

Note that equations (4-17) and (4-18) also resemble a local approximate pseudo-inversion, $(\mathrm{T}_{\mathrm{pd}})^{-1} \approx \mathrm{T}_{\mathrm{dp}}$, $(\mathrm{T}_{\mathrm{dp}})^{-1} \approx \mathrm{T}_{\mathrm{pd}}$. This approximation has been validated in different examples by reconstruction of $\boldsymbol{E}_z$ and $\boldsymbol{H}_z$ vectors.

4.4 Transverse Electric, Transverse Magnetic and Hybrid Formulations

In this section we propose a scheme to solve the coupled V- and F-formulations, (4-10) and (4-11) in the case of TE ($\boldsymbol{E}_z$=0), TM ($\boldsymbol{H}_z$=0) and hybrid (when both $\boldsymbol{E}_z$ and $\boldsymbol{H}_z$ exist) modes. Note that all terms containing the matrix Y_z are related to the z component of the electric field and will be deleted in the case of TE propagation. In the very same manner, all terms containing the matrix Z_z are related to the z component of the magnetic field and will be deleted in the case of TM propagation. Recalling (4-10) and considering the facts mentioned above, the simplified V-formulation for the TE case is written as

$$\left(\gamma^2 - (\mathrm{Y}_{\mathrm{t1}} \cdot \mathrm{Z}_{\mathrm{t1}} + \mathrm{C}^{\mathrm{t}}\mathrm{Z}_{\mathrm{z1}}^{-1}\mathrm{C} \cdot \mathrm{Z}_{\mathrm{t1}})\right) \mathrm{F}_{\mathrm{t}}^{\mathrm{d}} = \gamma.\mathrm{CPL.G}.\boldsymbol{H}_z^p \tag{4-19}$$

and the simplified F-formulation for the TM case is written as

$$\left(\gamma^2 - (\mathrm{Z}_{\mathrm{t2}} \cdot \mathrm{Y}_{\mathrm{t2}} + \mathrm{C}^{\mathrm{t}}\mathrm{Y}_{\mathrm{z2}}^{-1}\mathrm{C} \cdot \mathrm{Y}_{\mathrm{t2}})\right) \mathrm{V}_{\mathrm{t}}^{\mathrm{d}} = \gamma.\mathrm{CPL.G}.\boldsymbol{E}_z^p \ . \tag{4-20}$$

We now explain the procedure for solving TE case, (4-19). The procedure for solving TM case, (4-20) is carried out in the very same manner.

In the case of TE modes, (4-19) is first solved as a normal eigenvalue problem with CPL=0. The zero-order eigenvalue obtained as above is called, γ_0. In order to take into account the non-zero right hand side of (4-19), we use the interpolation relation (4-18) and the first two equations in (4-8) with $\boldsymbol{E}_z^p=0$ as follows:

$$\begin{aligned}
&\gamma \mathrm{CPL.G.}\boldsymbol{H}_z^p = \gamma \mathrm{CPL.G}\cdot \mathrm{T_{pd}}\cdot \boldsymbol{H}_z^d \\
&\boldsymbol{H}_z^d = -\mathrm{z_{zl}^{-1}CV_t^p} = (\frac{1}{\gamma})\mathrm{z_{zl}^{-1}CZ_{tl}F_t^d} \\
&\gamma \mathrm{CPL.G.}\boldsymbol{H}_z^p = \underbrace{\mathrm{CPL}\cdot \mathrm{G}\cdot \mathrm{T_{pd}}\cdot \mathrm{z_{zl}^{-1}}\cdot \mathrm{C}\cdot \mathrm{Z_{tl}}}_{\Delta 1}\cdot \mathrm{F_t^d}
\end{aligned} \qquad (4\text{-}21)$$

The right hand side of (4-19) is now written in terms of the eigenfunction $\mathrm{F_t^d}$. In order to maintain simplicity and advantages of solving the eigenvalue problem for diagonal constitutive matrices (in the LHS of (4-19)), we use a minimization procedure to modify the propagation constant γ_0 as (V1-formulation)

$$\begin{aligned}
&\text{Minimize}\left|\Delta 1\cdot \mathrm{F_t^d} - \Delta\gamma^2\cdot \mathrm{F_t^d}\right| \ , \ \ \Delta 1\cdot \mathrm{F_t^d} \approx \Delta\gamma^2\cdot \mathrm{F_t^d} \\
&[\gamma^2 - (\mathrm{Y_{tl}Z_{tl}} + \mathrm{C^tZ_{zl}^{-1}CZ_{tl}})]\cdot \mathrm{F_t^d} = \Delta\gamma^2\cdot \mathrm{F_t^d} \\
&[\underbrace{(\gamma^2 - \Delta\gamma^2)}_{\gamma^2_{new}} - (\mathrm{Z_{tl}Y_{tl}} + \mathrm{Z_{tl}C^tZ_{zl}^{-1}C})]\cdot \mathrm{F_t^d} = 0
\end{aligned} \qquad (4\text{-}22)$$

The same procedure (F1-formulation) can be applied to (4-20) in the case of TM modes to improve the accuracy of the zero-order solution (4-13). The results of applying this scheme are given in Chapter Six, examples 6.1 and 6.2 (for V1-formiulation) and 6.3 (for F1-formulation).

In a full wave (Hybrid) analysis of electromagnetic problems, we consider both transverse and longitudinal components of electric and magnetic voltages and fluxes. In this case, the two coupled equations, (4-10) and (4-11) should be solved together. Since the reported results in Chapter Six show that the propagation constant, γ, obtained from (4-12) and (4-13) agree well,

the results from one of these equations can be used to estimated the R.H.S. of the other equation and modify the zero-order solution. This procedure is explained in Fig. 4-9.

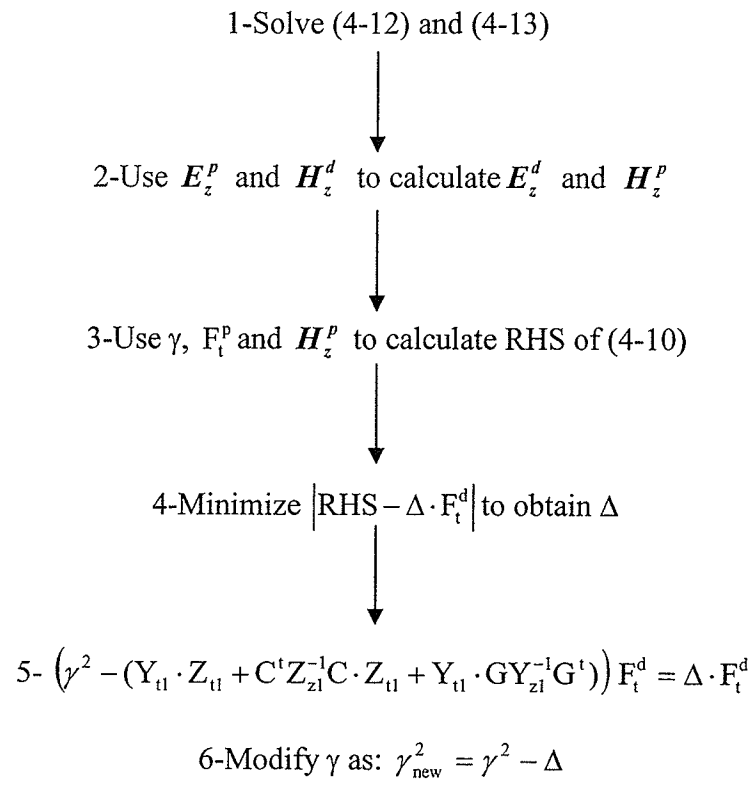

Figure 4-9: The proposed scheme to improve the accuracy of the zero-order solution of the uncoupled equations (4-12) and (4-13).

In the second step in the above diagram, interpolation functions are used as defined in Equation (4-17) and (4-18). In the third step F_t^p is obtained from the solution of (4-12) in the first step. This value is used to calculate the RHS of (4-10). The minimization used in step four can be the Least Squares Minimization (LSM) which results in Δ as a complex number, or the backslash operator (in Matlab) which results in Δ as a matrix with minimum non-zero elements minimizing $\left|RHS - \Delta \cdot V_t^p\right|$. When the size of the problem is large, this minimization takes a long time. If LSM is used, only γ can be modified. The result of applying this iterative procedure is reported in Chapter Six.

4.5 Series Impedance and Shunt Admittance

For a transmission line configuration and the Transverse Electric Magnetic (TEM) wave propagation, line voltage and line current are defined and definitions for series impedance , shunt admittance and characteristic impedance are given accordingly in different references (see [42, 49]). For a general waveguide structure, however, the line voltage and current are not uniquely defined. Other approaches (e.g. quasi-TEM approximations, loss calculation and energy approaches [49]) are then used to derive equivalent R, L, G, C, parameters for different modes in a waveguide structure.

In a quasi-TEM approximation, the characteristic impedance, Z_0 (Ω), p.u.l. series impedance, $z_{sr}(\Omega/m)$, and p.u.l. shunt admittance, $y_{sh}(\Omega m)^{-1}$, are related to each other and to the propagation constant, $\gamma(m^{-1})$, as [42]

$$\gamma = \sqrt{z_{sr} \cdot y_{sh}} \quad , \quad z_0 = \sqrt{\frac{z_{sr}}{y_{sh}}} \quad , \quad \begin{cases} z_{sr} = R + j\omega L \\ y_{sh} = G + j\omega C \end{cases} . \tag{4-23}$$

Matrix equations for a general waveguide structure in time-harmonic, (3-12) to (3-15), were given in section 3.2. The following matrix relations between transverse components of the electric and magnetic voltages can be derived from the above mentioned equations as

$$V_t^p = \frac{-1}{\gamma}(Z_t + GY_z^{-1}G^t) \cdot F_t^d \quad , \quad F_t^d = \frac{-1}{\gamma}(Y_t + C^t Z_z^{-1} C) \cdot V_t^p \tag{4-24}$$

To obtain expressions for series impedance and shunt admittance comparable with the differential expression, we rewrite (4-24) in terms of the transverse electric and magnetic fields as

$$E_t^p = \frac{-1}{\gamma} \cdot \underbrace{L_p^{-1} \cdot (Z_t + G Y_z^{-1} G^t)}_{Z_{sr}} \cdot L_d \cdot H_t^d \quad , \quad H_t^d = \frac{-1}{\gamma} \cdot \underbrace{L_d^{-1} \cdot (Y_t + C^t Z_z^{-1} C)}_{Y_{sh}} \cdot L_p \cdot E_t^p , \tag{4-25}$$

where $\boldsymbol{E}_t^p$, $\boldsymbol{H}_t^d$ are transverse electric and magnetic field vectors and L_p and L_d are diagonal matrices containing the length of primal and dual lines, respectively. Note that the field variables, $\boldsymbol{E}_t^p = L_p^{-1} V_t^p$, $\boldsymbol{H}_t^d = L_d^{-1} F_t^d$, are not directly dependent on the length of the primal and dual lines. Equations in (4-25) suggest a definition for the series impedance and shunt admittance for a general waveguide problem as

Series impedance$= z_{sr}$ which minimizes $\left| Z_{sr} \boldsymbol{H}_t^d - z_{sr} \boldsymbol{H}_t^d \right|$, (4-26)

Shunt admittance $= y_{sh}$ which minimizes $\left| Y_{sh} \boldsymbol{F}_t^p - y_{sh} \boldsymbol{F}_t^p \right|$, (4-27)

Equations (4-26) and (4-27) with a Least Square Minimization have been used to obtain p.u.l. R, L, G, C parameters for a CPW structure in Chapter Six, example 6-4.

The theoretical framework for the Incentric Cell Method is now completed and ready for realization and performance test. The Incentric scheme described in this chapter is expected to be computationally inexpensive, easy to implement, accurate and converging. The main advantage of this scheme is to provide with an eigenvalue system with diagonal (and therefore symmetric positive definite) constitutive matrices. These expectations will be examined in Chapter Six of this thesis.

Chapter 5- Boundary Conditions

Numerical techniques need to properly address the implementation of specific boundary conditions. Dirichlet boundary condition (where the value of the unknown function is known at the boundary) and Neumann (the derivative of the unknown function is known at the boundary) or combinations of these, are usually straightforward and efficiently implemented in most numerical techniques. Perfect Electric Conductor (PEC) and Perfect Magnetic Conductor (PMC) boundary condition are examples of Dirichlet and Neumann BCs, respectively, when the electric field is considered. A wide variety of applied electromagnetic phenomena (e.g. antenna and radiation, scattering, microstrip transmission lines, and overhead cables), however, occur in a physically unbounded region, usually free space. Possible approximate analytical solutions for this kind of problems include a condition on the behavior of the solution at infinity. This condition (e.g. Radiation Boundary Condition [50,51]) ensures the stability and well-posedness of the solution.

The term "open boundary" refers to the unbounded source-free region surrounding the "region of interest" including all EM structures, sources and excitations, as illustrated in Fig. 5-1.

When using numerical procedures, regardless of the category of the problem, the computational domain must be finite. An infinite open boundary therefore, should be truncated and its effect on the solution should be formulated in the form of an "Open Boundary Condition". The computational domain in this case is terminated by an artificial boundary with an open boundary condition.

Different approaches are available today for the truncation of open boundaries in EM area in both time and frequency domain analyses. Although most boundary truncation techniques were first introduced for Finite-Difference Time-Domain algorithms, generalized and hybrid versions became available later and could be utilized in other numerical techniques as well. Except for Integral Equation Boundary Condition which is a very accurate and computationally expensive approach based on uniqueness theorem [42], most other open boundary conditions are local discretization of the behavior of the approximate solution at infinity.

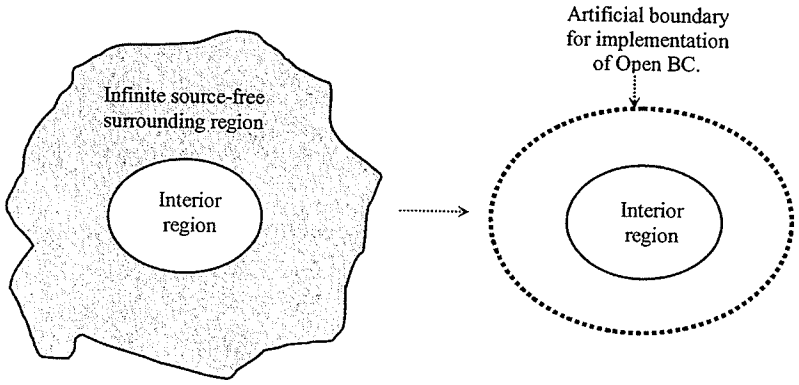

Figure 5-1: Unbounded open region surrounding the interior region is considered as an open boundary condition on an artificially boundary.

In this chapter we shall discuss the treatment of boundary conditions in the Incentric scheme. We also explain "the adaptive mesh open boundary" as our approach for the treatment of transverse open boundaries in waveguide structures. The theoretical basis for this approach is given and the reported results are justified in comparison with the results obtained from the implemented PML boundary condition in COMSOL.

5.2 PEC and PMC boundary conditions

Recalling the incentric dual formulations, (4-10) and (4-11), PEC and PMC boundary conditions are implemented in a dual manner. In V-formulation, electric voltage is defined on the primal lines. The PEC boundary condition is thus implemented as

$$\begin{aligned} &V_t^p(\alpha) = 0; \quad \text{for line } \alpha \in \text{PEC boundary} \\ &\boldsymbol{E}_z^p(\mathrm{i}) = 0; \quad \text{for point i} \in \text{PEC boundary} \end{aligned} \tag{5-1}$$

This implementation produces a reduced eigenvalue problem where the points and lines on the PEC boundary are removed from the original system of equations. The columns and rows corresponding to the removed lines and points are removed in all matrices in the LHS of (4-10).

In F-formulation, magnetic voltage is defined on the primal lines. In a very same manner, the PMC boundary condition is implemented as

$$\begin{aligned} &F_t^p(\alpha) = 0; \quad \text{for line } \alpha \in \text{PMC boundary} \\ &\boldsymbol{H}_z^p(\mathrm{i}) = 0; \quad \text{for point i} \in \text{PMC boundary} \end{aligned} \tag{5-2}$$

The implementation of a PEC boundary condition in F-formulation or a PMC boundary condition in V-formulation is also straightforward. Considering the half-surfaces on the PEC boundary as shown in Fig. 5-2, all the matrices in (4-10) and (4-11) remain unchanged. The same applies for the V-formulation and a PMC boundary condition. It is expected that PEC and PMC boundary conditions will be implemented more accurately within V- and F-formulations, respectively. This is because the primal point, P_i, does not represent the center for the dual half-surface on the boundary as it is assumed in the Cell Method formulation.

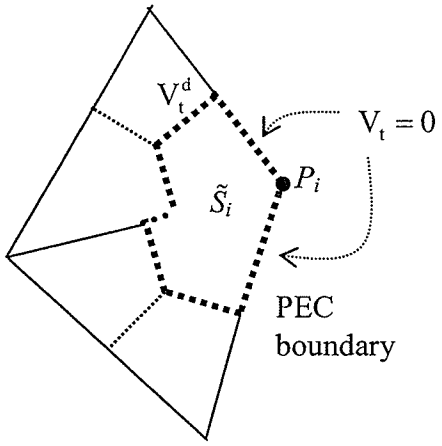

Figure 5-2 PEC boundary in F-formulation. The half-surface around P_i is considered as the dual surface and the electric voltage on the boundary lines is zero.

It is important to note that in general, the elements of CPL matrix are zero for all boundary lines. This implies that there is no additional consideration on the boundary conditions caused by the incentric scheme. General treatment of boundary conditions used in other numerical techniques, including the Cell Method and Finite Integration Technique with barycentric subdivision, can be utilized within the Incentric Cell Method as well.

5.2 Open boundary condition

Open boundary conditions are often considered and utilized in solving radiation, scattering and guided wave problems. In a guided wave problem, however, the open boundary condition can be applied in both the direction of propagation (which is the most common case) and the direction transverse to the structure's cross section. In a waveguide with PEC walls and invariant cross section, no boundary condition is applied in the propagation direction and an eigenvalue problem is solved to obtain the

propagation constant. If a material discontinuity (e.g. an air gap or a material change) occurs along the line, and we investigate the behavior of the fields close to discontinuity, we need to apply a proper open boundary condition to truncate the computational domain in the direction of propagation.

Berenger's Perfectly Matched Layer [52] has been the dominate approach in modeling open boundaries since 1994. This technique is based on inserting a layer of artificial lossy material around the region of interest to absorb an outward propagating electromagnetic wave without significant reflections. The technique was originally introduced for finite difference algorithms. Numerous references can be found on PML and its application in guided wave structure [see 53 and the references therein, 54]. We shall mention the following points about the performance of a PML especially in guided wave structure applications:

1- PML is very efficient in absorbing normally incident (to the boundary) propagating waves [52-55].

2- PML is less efficient in absorbing non-propagating (evanescent) waves [56].

3- PML introduces additional losses in a waveguide structure which is important when the losses are considered (e.g. parameter extraction, attenuation constant, finite conductivities...) [56,57].

4- PML's thickness, conductivity profile, cell size and number of cells are important and case-sensitive parameters which need to be determined by (performing many) numerical experiments [56,57].

Based on the above consideration, it can be concluded that PML is not an efficient choice to truncate the transverse boundaries in a waveguide structure.

The use of PML has been reported with the Cell Method formulation in scattering problems in the time-domain [25] and in the frequency domain [30].

Another interesting approach for modeling open boundaries is "squeezing open boundaries, [58]" which is based on transformation of coordinates and an inverse transformation for the material properties which keeps the Maxwell's equations invariant.

In the next section we consider a guided wave structure with transverse open boundaries (in x-y plane) and a cross section invariant with respect to z coordinate. An adaptive mesh open boundary is introduced and its performance is compared with the PML boundary condition implemented within COMSOL.

5.2.1 Adaptive mesh open boundary condition

The adaptive mesh open boundary is an approach similar to squeezing the open boundaries. We consider a PEC boundary far from the structure. The region between the structure and the PEC boundary is then coarsely meshed as depicted in Fig. 5-3. The coarseness of this mesh and the distance between the PEC boundary and the structure are important issues that shall be addressed.

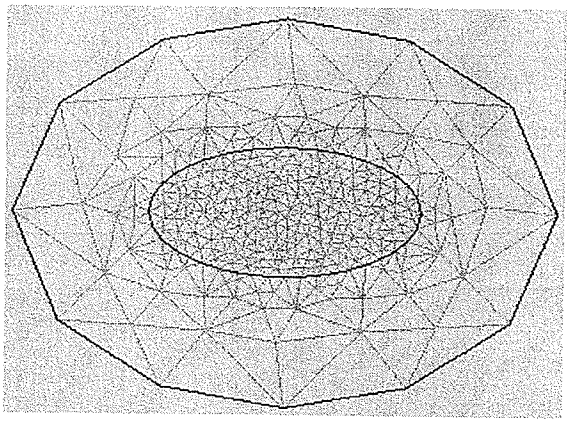

Figure 5-3: The adaptive mesh open boundary condition refers to a coarse mesh between the interior region of interest and a PEC boundary placed far from the structure

The behavior of the transverse field depends on the transverse wave number, k_t .The following characteristic equation define the relation between this number and the propagation constant:

$$k_t^2 + k_z^2 = k_0^2 \tag{5-3}$$

Where k_0 is the wave number of free space. If we consider a far circular boundary in free space, the behavior of the transverse wave can be estimated by the Hankel function of the second kind as [42]:

$$\sqrt{\frac{-2j}{\pi k_t r}} e^{-jk_t r} \quad , \quad k_t^2 = k_0{}^2 - k_z^2 \ . \tag{5-4}$$

The above wave vanishes at $k_t r \to \infty$. r is the radius of the artificial circular boundary.

It is clear from the above relation that for smaller values of k_t (lower frequencies) we need larger values for r to satisfy the "far enough condition in (5-4). In the common waveguide problems solved in this thesis, $k_z \approx \beta$ is about $2k_0$-$8k_0$. In the case of k_z=2.5 (as for the example in this chapter at f=10GHz) k_t= -2jk_0. This value with (5-4) implies a attenuating transverse wave which vanishes at approximately

$$k_t r \approx -j7,\ r \approx 7/k_t \approx 7/(2.5\, k_0) \approx 2 \text{ cm}.$$

The above approximate calculations can be used as a guide for choosing the boundary far enough to have an accurate solution.

The adaptive mesh open boundary condition is suitable for techniques which use irregular mesh. The adjustable cell size in an irregular mesh allows having a fine mesh in the interior region and a coarse mesh in the exterior region in order to save computational requirements. The performance of the adaptive mesh open boundary condition is investigated through an example described in the next section.

5.2.2 Example: Asymmetric CPW structure

The structure used to investigate the performance of the proposed adaptive mesh boundary condition is an asymmetric CPW studied in [57] where a PML is used as the open boundary condition. The geometry and the specification of the problem are depicted in Fig. 5-4. Details of the different study cases and the obtained results are given in Table 5-1.

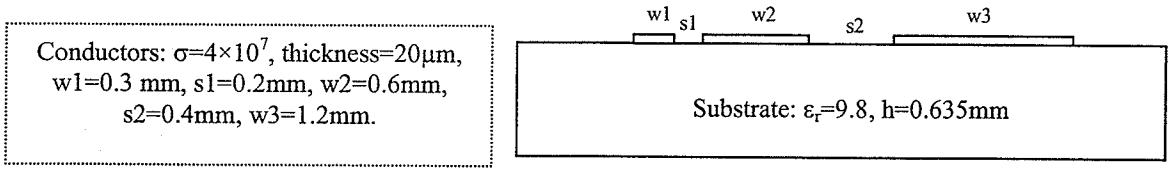

Figure 5-4: The geometry and description of the asymmetric coplanar waveguide being studied.

The quasi-TEM mode supported by this structure is the mode with the lowest propagation constant which is more sensitive to the boundary condition applied. Table 5-1 reports the value of the complex propagation constant for different cases when the PEC boundary surrounding the structure is moved further. The details about the mesh in each case is also given. Figs. 5-4 to 5-7 depict different meshes used in the cases reported in Table 5-1.

Table 5-1 Details about different cases studied to investigate the performance of the adaptive mesh open boundary condition.

Case No.	Dimension (x, mm)	Dimension (y, mm)	No. of elements	$\beta\ (m^{-1})$	$\alpha\ (m^{-1})$
1	-2 ↔ 2	-0.635 ↔1.5	10845	2.5723	0.00236
2	-2.5 ↔ 2.5	-0.635 ↔ 2.5	11040	2.6582	0.00225
3	-3 ↔ 3	-0.635 ↔ 2.5	10913	2.7060	0.00218
4	-4 ↔ 4	-0.635 ↔ 3.5	11150	2.7532	0.00215
5	-5 ↔ 5	-0.635 ↔ 5	11268	2.7738	0.00213
6	-7 ↔ 7	-0.635 ↔ 7	11601	2.785	0.0021
7	-10 ↔ 10	-0.635 ↔ 10	11741	2.788	0.0021
8	-15 ↔ 15	-0.635 ↔ 15	12570	2.789	0.0021
9 (reference)	**-30 ↔ 30**	**-0.635 ↔ 30**	**14860**	**2.789**	**0.0021**
PML(FEMLAB)	2 mm thickness	2 mm thickness	11378	2.954	0.026
Adaptive Mesh	-10 ↔ 10	-0.635 ↔ 10	6747	2.791	0.0022

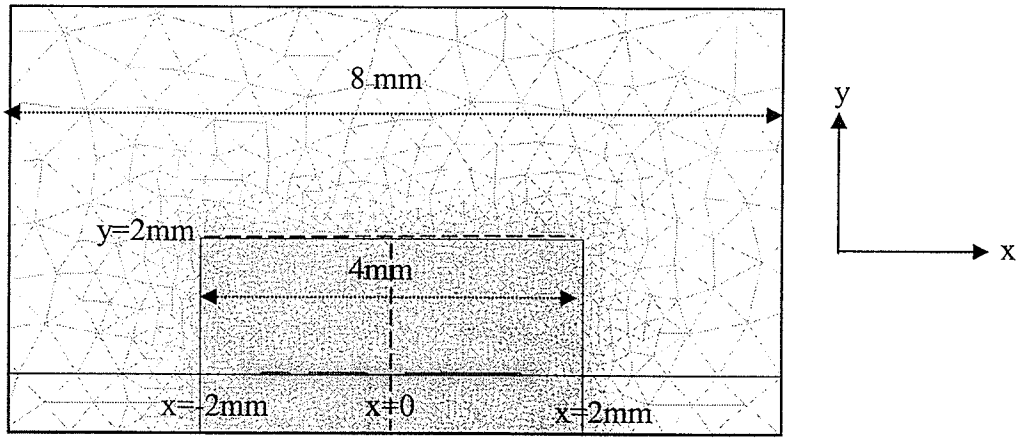

Figure 5-5: The mesh used in COMSOL simulation with an implemented PML.

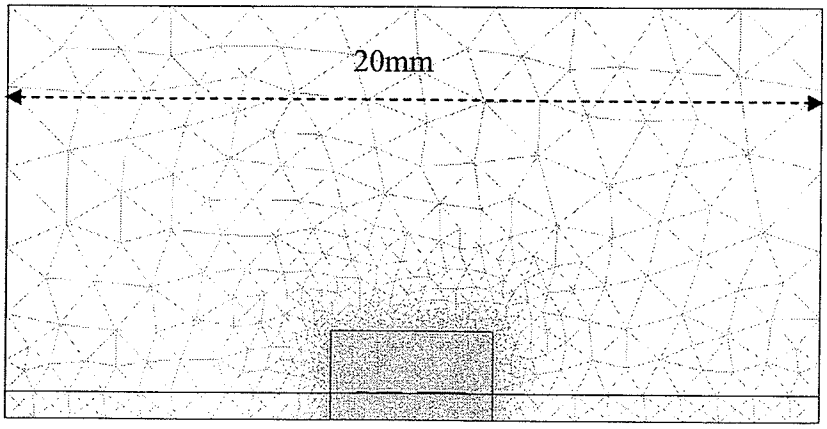

Figure 5-6: The mesh used as the adaptive mesh open boundary condition.

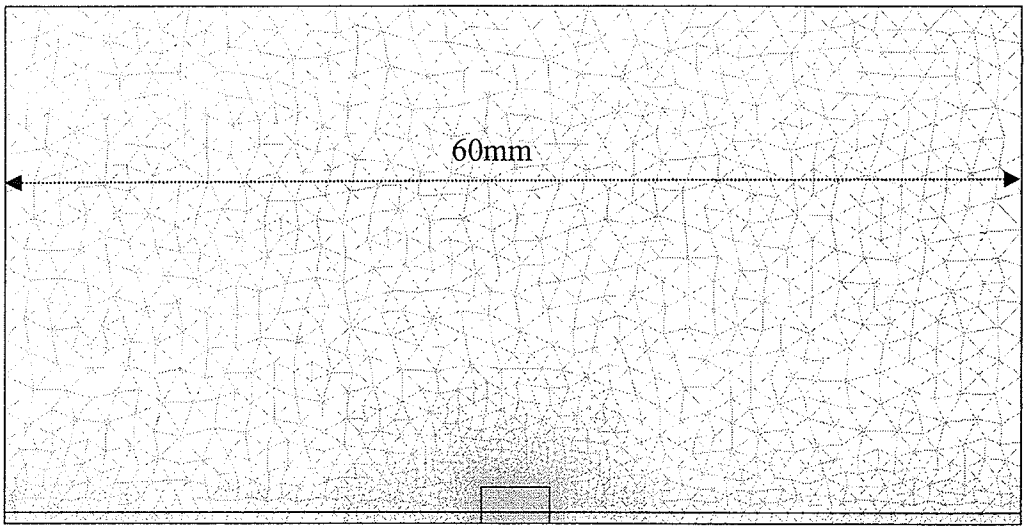

Figure 5-7: The mesh used in the reference case (case No. 9).

In table 5-1, cases 1-8 are the cases when we have increased the dimensions of PEC boundary from 4 mm to 30 mm. Case 9 is the reference case when a very far PEC boundary (60mm) and a fine mesh (15000 elements) is used. The propagation constant is reported for all 9 cases as well as the results of implemented PML in COMSOL and the proposed adaptive mesh. The PML feature implemented in COMSOL Multiphysics is an automatic feature which does not give user many options to choose the parameters. The thickness of the PML and the direction of the conductivity profile can be chosen by user. A thicker PML results in better absorption and less reflection at the interface. While the physical dimension of the problem being simulated is not an issue in a computer code, the computational dimension is important. As it is seen in Table 5-1, the computational size of the problem in the case of an adaptive mesh open boundary condition is almost the same as the size of the problem when a PML is used.

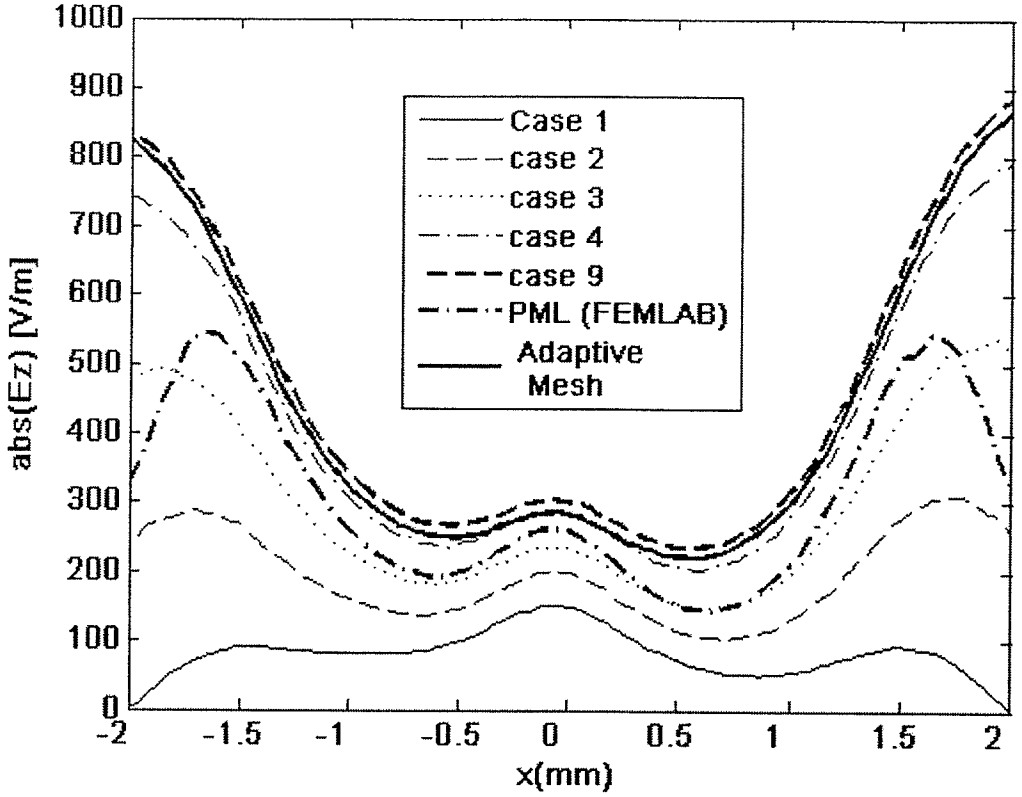

Figure 5-8: Magnitude of the electric field (z component) on the horizontal cross section (y=2mm) shown in Fig. 5-5.

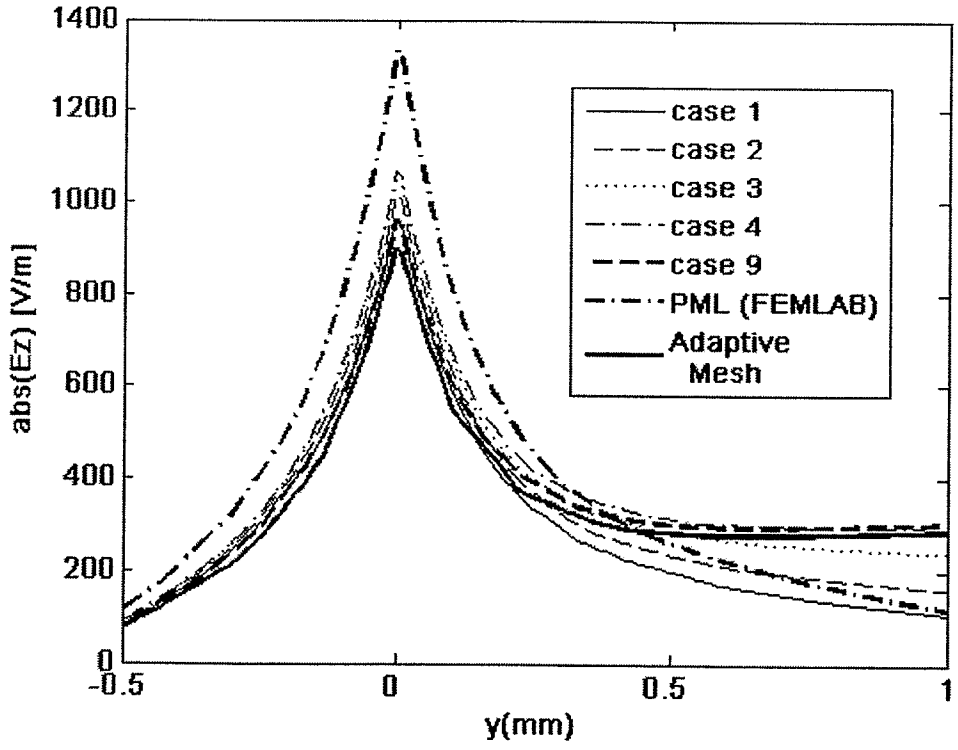

Figure 5-9: Magnitude of the electric field (z component) on the vertical cross section (x=0) shown in Fig. 5-5.

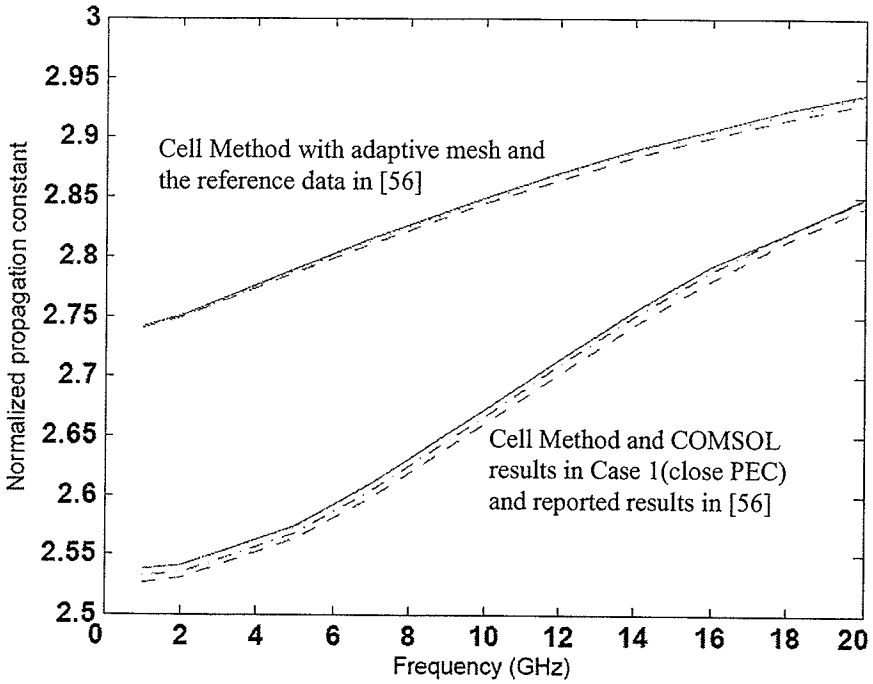

Figure 5-10: Normalized propagation constant ($\beta/\beta 0$) of the ACPW for close PEC boundary compared with the results of applying an adaptive mesh open boundary.

The example presented in this chapter and the reported results verify that for common waveguide structures a "far enough" PEC boundary with a coarse mesh between the structure and the PEC boundary (Adaptive mesh open boundary condition) works very well without the problems of choosing a proper PML absorbing boundary.

Chapter 6- Examples and Results

In the previous chapters of this thesis, we discussed Finite Formulation as a robust framework for expressing electromagnetic laws. Finite Formulation utilizes a primal-dual mesh complex and therefore requires a proper construction of the dual mesh. The most common choice for the construction of a dual mesh is the barycentric subdivision. A barycentirc dual mesh results in non-diagonal constitutive matrices which make the computational procedure more complicated in comparison with having diagonal constitutive matrices. A new scheme for the construction of the dual mesh, the Incentric Cell Method, was proposed as an alternative to the barycentric subdivision in Chapter Four. In order to validate the proposed Incentric Cell Method formulation and to understand the capability of this scheme in modeling complex structures, some common and practical waveguide structures were examined. The results are compared with those obtained from a commercial FEM solver, COMSOL. Analytical solutions were also presented when applicable. The reported parameter is a common expression of the propagation constant or the attenuation constant. Field distributions are also reported whenever it has been helpful in clarifying the comparisons.

The proposed Incentric Cell Method is expected to:

1- make the construction of the dual mesh possible for any primal triangulation

2- be computationally efficient by building diagonal constitutive matrices even when an orthogonal dual mesh cannot be built

3- efficiently produce a fast solution for any primal triangulation. This solution can be used as the first approximation in higher order schemes

4- improve the accuracy of first approximation

5- be able to model fairly complex electromagnetic structures (inhomogeneous, anisotropic and multi-scale structures)

In this chapter, a variety of examples are chosen to validate the above expectations and to examine convergence, accuracy and efficiency of the proposed scheme in comparison with well known numerical (or analytical) solutions.

In all examples, the mesh used for Cell Method simulations are imported from COMSOL program in order to have a fair comparison. In general the output of the common mesh generator program can be used as the primal mesh for Incentric Cell Method simulations. The largest mesh size used in the Inceteric simulations is 50000 primal triangles.

6.1 Rectangular Waveguide, TE modes

A rectangular waveguide with PEC walls and dimension of a=10cm and b=20 cm is considered. The empty waveguide geometry is chosen since it supports TE and TM propagation and therefore is suitable to confirm the simplified TE and TM equations, (4-19) and (4-20). In order to investigate the convergence of the scheme with respect to the cell size, and to validate the minimization process, V1-formulation (4-22), we analyzed the problem with 9 different meshes. The first mesh, the extremely coarse mesh, consists of only 26 elements and the last mesh, the extremely fine mesh, consists of 21258 elements. Fig. 6-1 depicts the waveguide cross section with the two mentioned meshes. The cell size in the first mesh (extremely coarse, Fig. 6-1.a) is about 5 cm, and in the last mesh (extremely fine, Fig 6-1.b) is about 1 mm. The results of this study for TE_{11} mode

are reported in Fig. 6-2. In Fig. 6-2 the percentage error is calculated relative to the analytical solution for the propagation constant (β_{th}= 22.8231 m^{-1}).The cut off frequency for TE_{11} mode is: f_c=1.67 GHz and the operating frequency is considered f=2GHz (k_0=41.8879 m^{-1}).

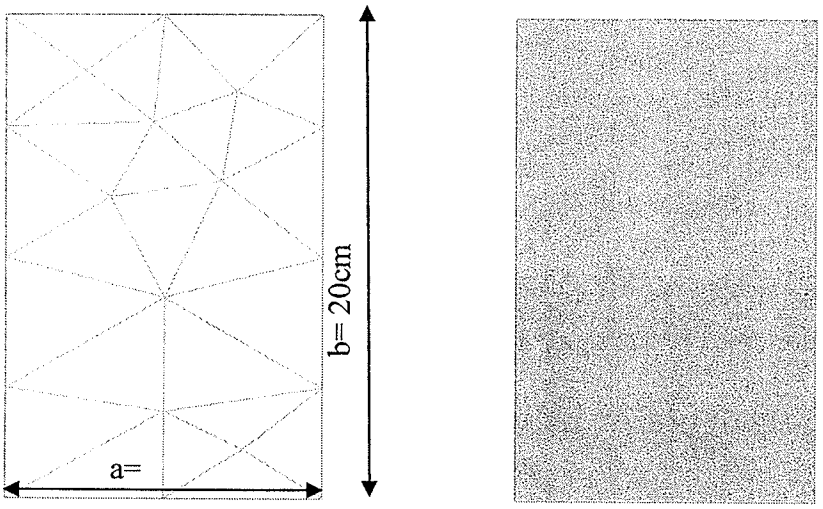

Figure 6-1: Transverse dimensions of the rectangular waveguide and a) extremely coarse mesh, b) extremely fine mesh.

The results reported in Fig 6-2 show that the minimization process for TE modes (V1-formulation, (4-22)) effectively improves the accuracy and convergence of the solution. It is also observed that for coarse meshes the Incentric Cell Method scheme results in more accurate solution compared with COMSOL solution. It is seen that V1- Formulation gives better results for very coarse meshes compared with COMSOL, however, the solution does not converge to a more accurate result by refining the mesh to extremely fine meshes. It is also the case with the COMSOL solution. Cell Method shows a greater error for fine meshes compared with COMSOL which is expected due to different order of accuracy for the two methods.

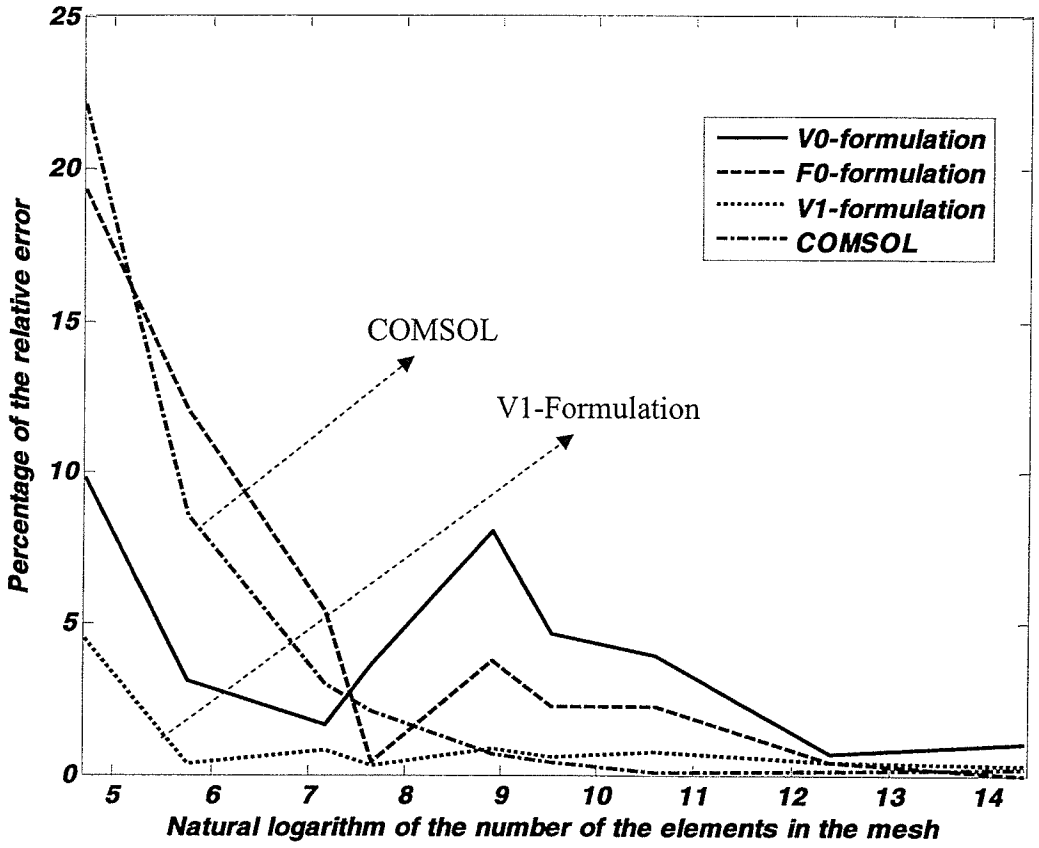

Figure 6-2: Relative error for zero-order solutions (V0- and F0-) and V1- formulation with respect to the number of the elements in the primal mesh for TE_{11} mode in a rectangular waveguide. The operating frequency is f=2 GHz.

6.2 Partially-filled Waveguide

This example is particularly chosen to compare the results of the Incentric Cell Method with the reported results in [38] for a barycentric dual mesh. The geometry and the specification of the problem are given in Fig. 6-3. We consider TE_{10} mode (with respect to z direction). In [38], the relative error is reported for the barycentric Cell Method, HFSS and a FEM solver in comparison with analytical solution. The reported

results show that HFSS produces the most accurate results and FEM works considerably more accurate than the barycentric Cell Method.

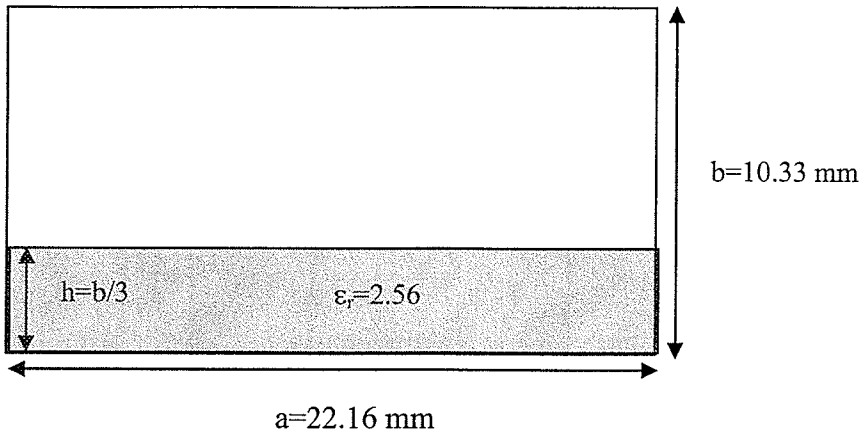

Figure 6-3: Dimensions and specifications of the partially filled waveguide chosen as a test case for barycentric Cell Method in [38].

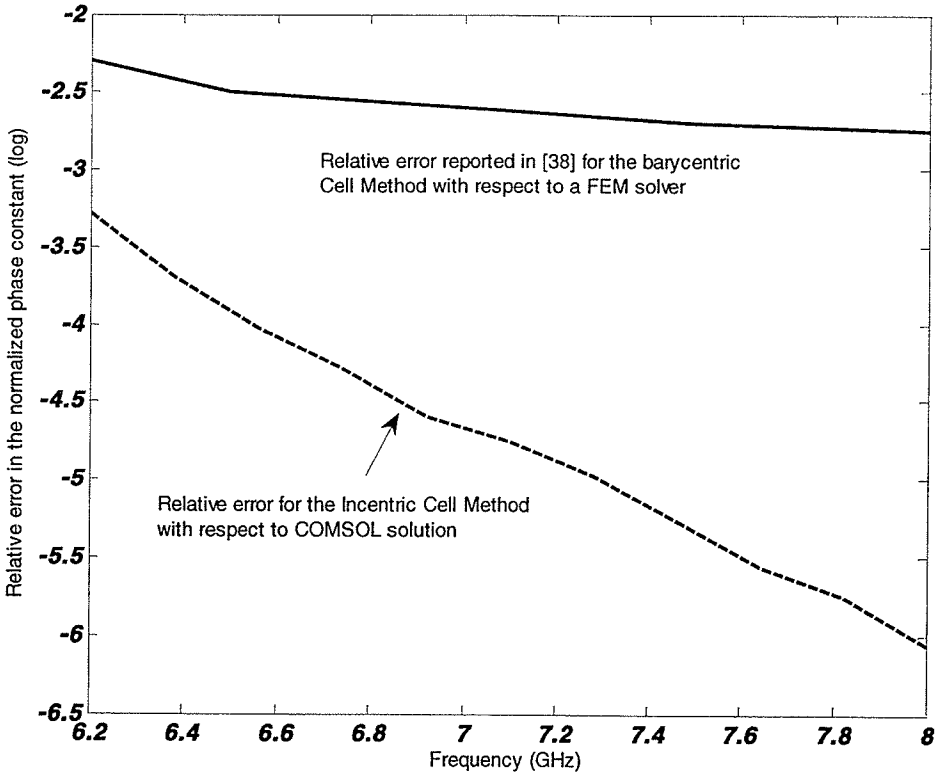

Figure 6-4: Relative error of the Incentric Cell Method solution (V1-formulation) with respect to the COMSOL solution. The approximate reported error for the barycentric Cell Method in [38] is also shown.

Fig. 6-4 shows that the Incentric Cell Method solution is considerably more accurate in comparison with the barycentric Cell Method solution. This problem is discussed and the analytical solution is driven in [42, p 158] .

6.3 Buried and Overhead Cable

The determination of the propagation constant and fields for systems of conductors located above or embedded in a lossy half-space is of interest for low frequency radio transmission and in the power engineering field for transmission line network analysis. It is important to accurately determine the effect of the air-earth interface on the dispersion and loss characteristics of a given geometry. Most studies still utilize Carson's quasi-TEM formulation for overhead lines at power frequencies [59], but this becomes inaccurate at high frequencies. Furthermore, unlike the overhead case, the behavior of a buried cable system is more strongly influenced by the electrical properties of the earth and approximate methods do not work as well. Exact analytical formulations for the overhead [60] and buried [61] cases are available for simple geometries and under special assumptions (cylindrical thin-wire approximation), but they cannot be used for general conductor geometries or when the conductor is near the interface.

In this example, the Incentric Cell Method formulation is used to solve for the propagation constant of the geometry shown in Fig. 6-5. A thin insulated wire located above earth interface is moved towards the interface, passes through the interface becoming an insulated cable and then moved to a depth of several skin-depths in the earth.

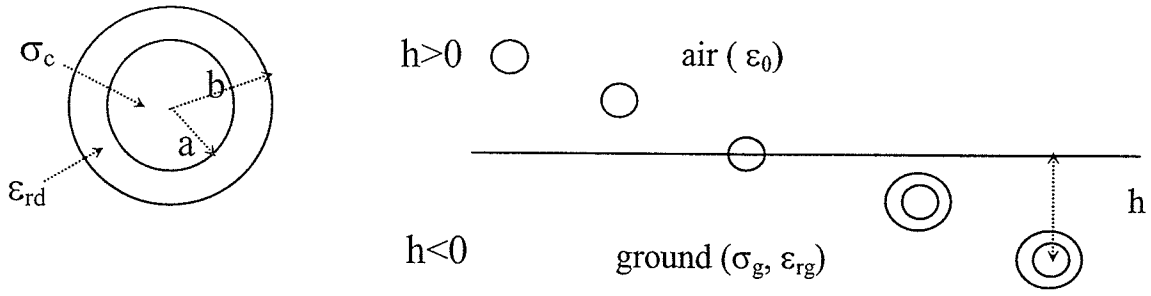

Figure 6-5: Cross section of a thin insulated and its location either over a lossy ground or buried in the lossy ground. The conductor can be partially buried.

We consider a thin insulated wire with inner conductivity, σ_c, and insulation dielectric constant, ε_d. To investigate the effect of the earth, we assume a perfect conductor ($\sigma_c \approx \infty$) and an air insulating region ($\varepsilon_{rd}=1$). The conductor and insulation radius are a=5 cm and b=6cm, respectively. The electrical parameters of the lossy ground are $\varepsilon_{rg}=10$ and $\sigma_g=0.05\ (\Omega.m)^{-1}$, typical of moist earth. The ground acts as a fairly good conductor in the frequency range below 9 MHz and we choose f=1MHz in our example. For this case the depth of penetration (skin-depth) is $\delta_g=5.033$m.

For the truncation of open boundary, the adaptive mesh is used (as described in Chapter Five) which consists of a fine mesh near the conductor and a progressively coarser mesh extending to a far (d=25m) PEC boundary, as shown in Fig. 6-6. The distance from the center of the conductor to the air-ground interface, h, is varied from h=10m (overhead wire) to h= -10m (buried cable). The behavior of $|E_z|$ for the case when the cable is at the interface, h=0, is depicted in Fig. 9. Although $|E_z|$ vanishes in the earth at a distance of d $\approx$ -10m from the interface, $|E_z|$ in the air region is still significant. This suggests that the distance to the PEC truncation boundary should be increased. Figs. 6-7 and 6-8 show that a PEC truncation boundary with d=25m is a good choice considering the convergence of

the calculated propagation constant with respect to the distance between the cable and the PEC truncation boundary.

The propagation constant ($\gamma = \alpha + j\beta$), was calculated using V0- and F0- formulations (4-12) and (4-13) as well as V1-Formulation and is reported in Figs. 6-9 and 6-10. for varying distance from the interface.

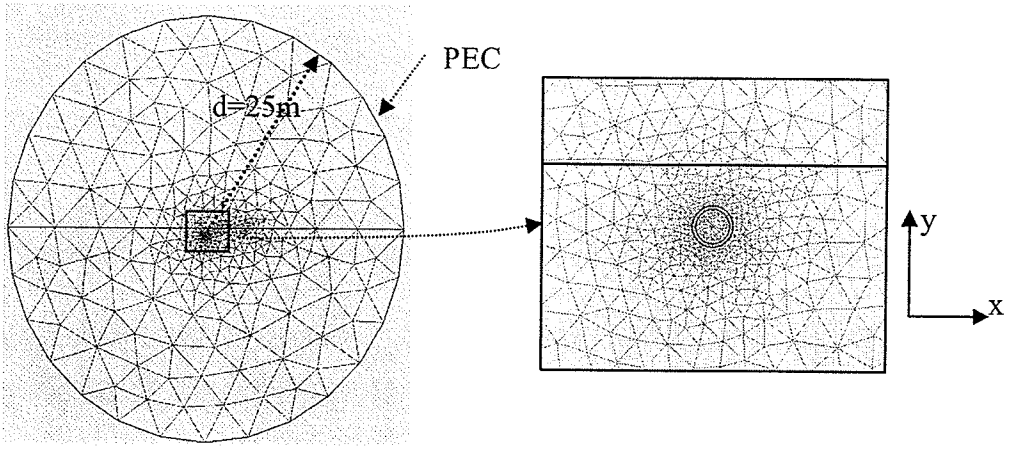

Figure 6-6: Geometry of the above-ground or buried cable and the adaptive mesh open boundary.

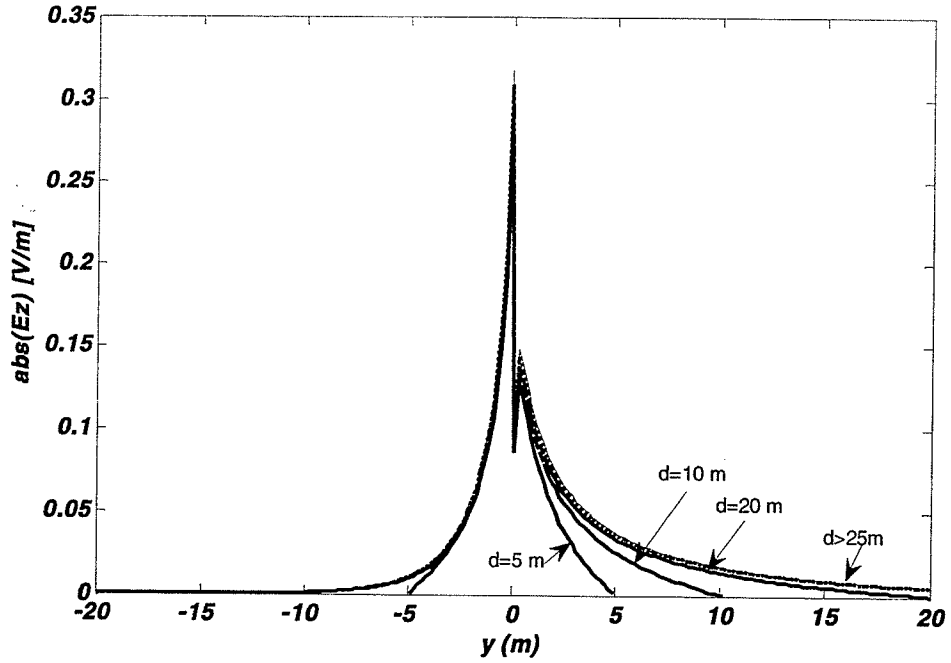

Figure 6-7: Magnitude of the z component of electric field for the vertical cross section (x=0) when the conductor is at the interface (h=0) for different distances between the cable and the PEC truncation boundary.

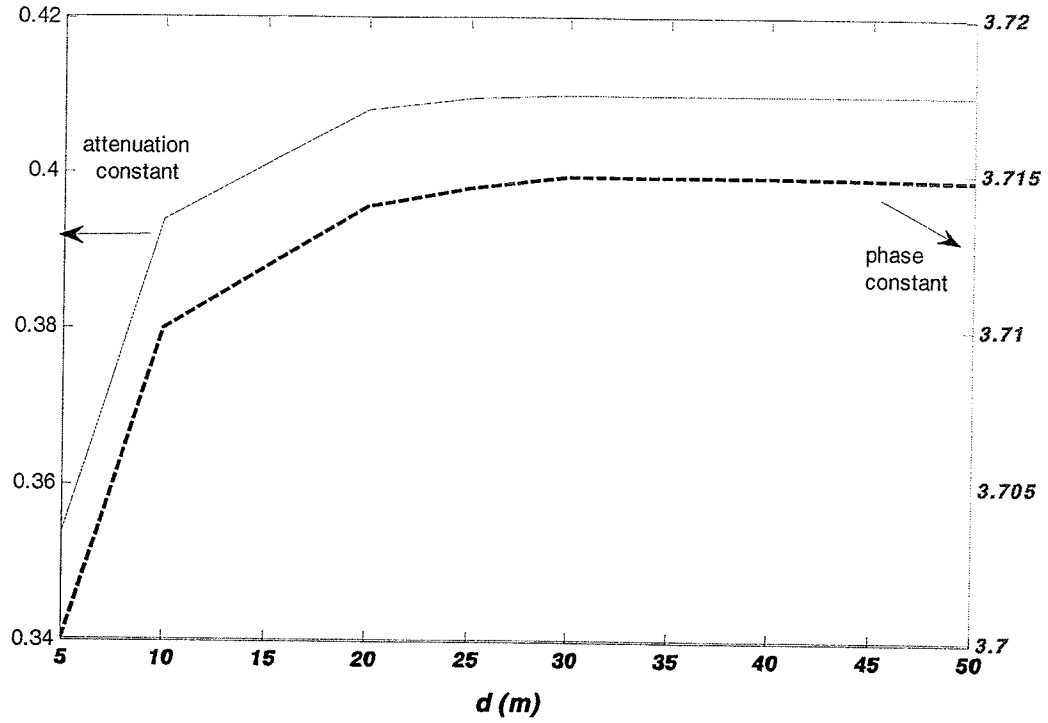

Figure 6-8: Convergence of the calculated propagation constant with respect to the distance between the cable and the PEC boundary.

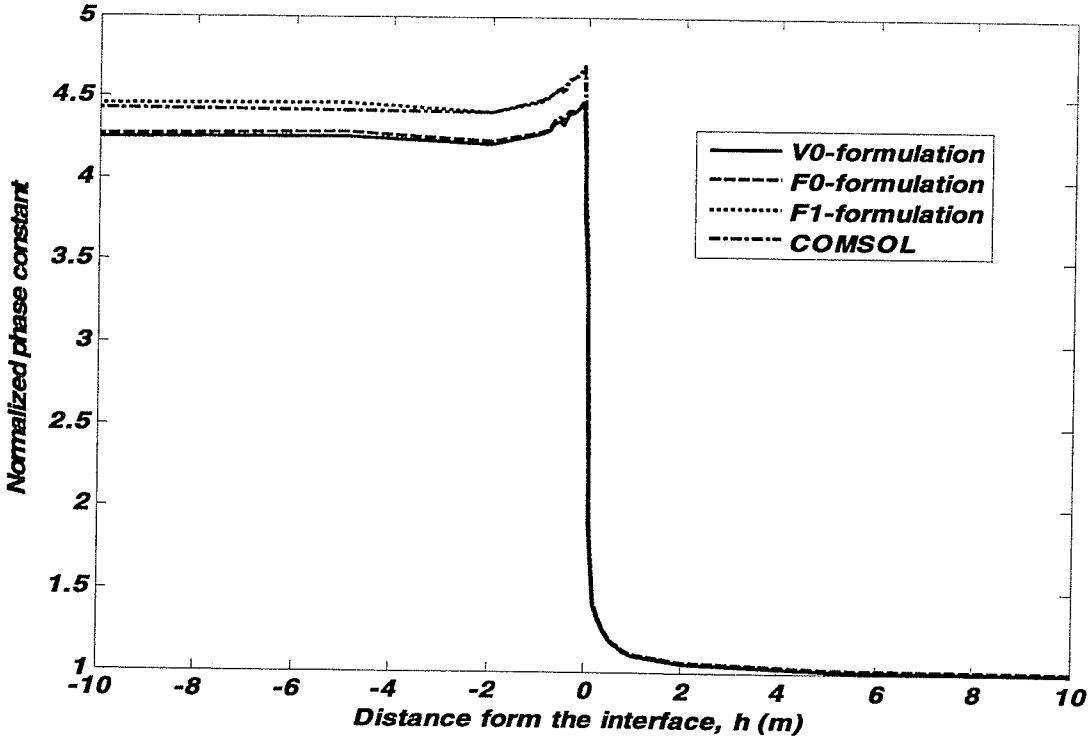

Figure 6-9: Normalized phase constant with respect to the distance of the conductor from the interface.

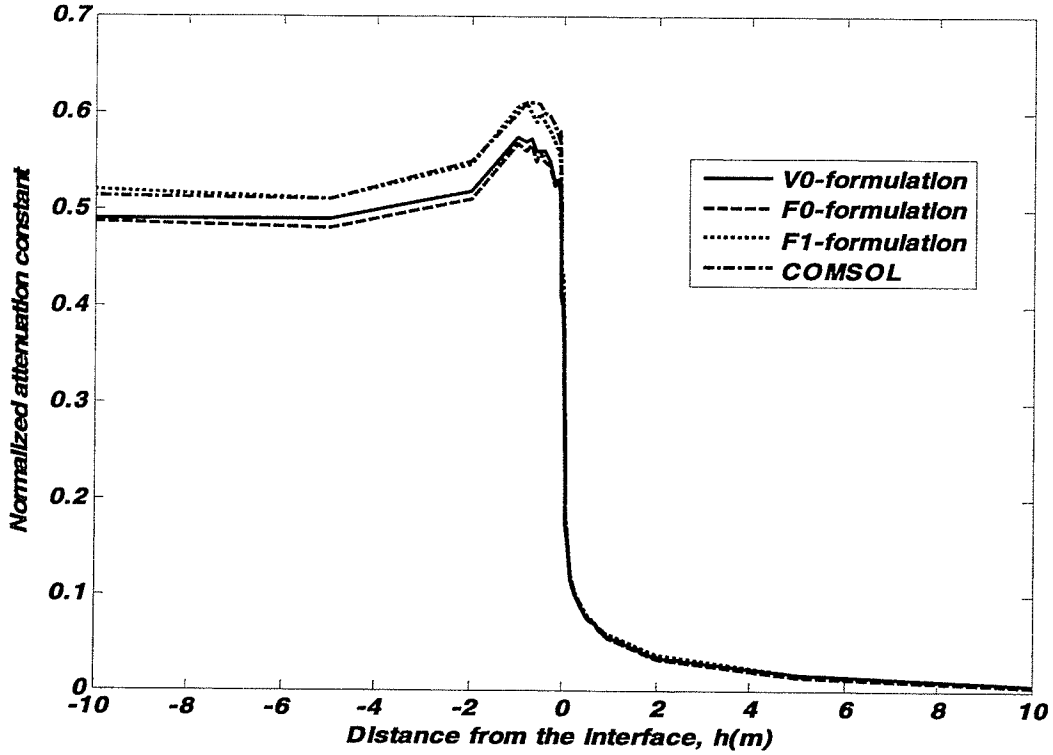

Figure 6-10: Normalized attenuation constant with respect to the distance of the conductor from the interface.

These results clearly confirm the effectiveness of F1-Formulation in improving the accuracy of the incentric solution. In this example COMSOL uses a full-wave analysis. It is shown that the rapid change in the propagation constant as the conductor is moved through the interface can be accurately calculated using this technique.

To investigate the range of validity for available analytical solutions, the behavior of these solutions as well as numerical solutions is illustrated when the conductor is very close to the interface (-0.5m<h<0.5m) . The results depicted in Figs.6-11 and 6-12 show that thin-wire based analytical approach fails when the conductor is very close to or at the interface. The Incentric Cell Method scheme proves effective and accurate in modeling the complex problem of overhead or buried cables close to the interface of a lossy medium.

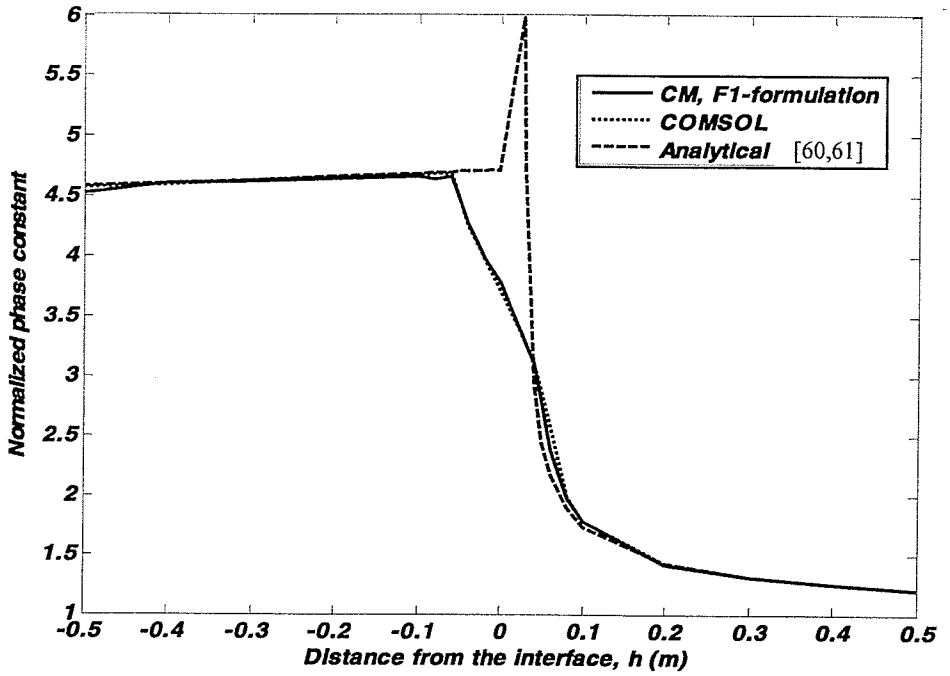

Figure 6-11: Normalized phase constant as the conductor is moved close to and passes through the interface.

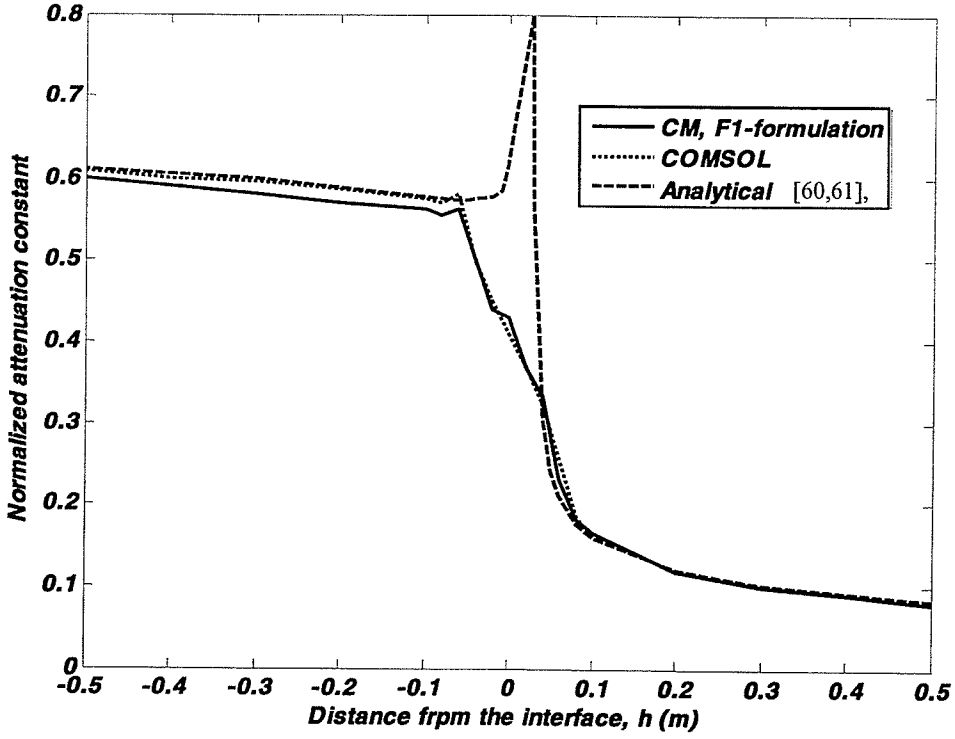

Figure 6-12: Normalized attenuation constant as the conductor is moved close to and passes through the interface.

6.4 CPW structure, RLGC parameters

As an example for application of the Cell Method, an inhomogeneous lossy CPW structure is chosen. The geometry and specifications of the problem are given in Fig. 6-13. Co-Planar Waveguide (CPW) structure is a common configuration in Integrated Circuits technology and simulation is useful for investigating the effect of different materials, geometries and etching profiles [62].

The propagation constant for the quasi-TEM mode is calculated and compared to those obtained from COMSOL for the exact same geometry. A PEC box, 500 μm by 300 μm, surrounds the structure. For the CPW geometry, three different propagating modes are distinguished. The quasi-TEM mode (lowest propagation constant) is studied where the fields are concentrated between the center and outer conductors.

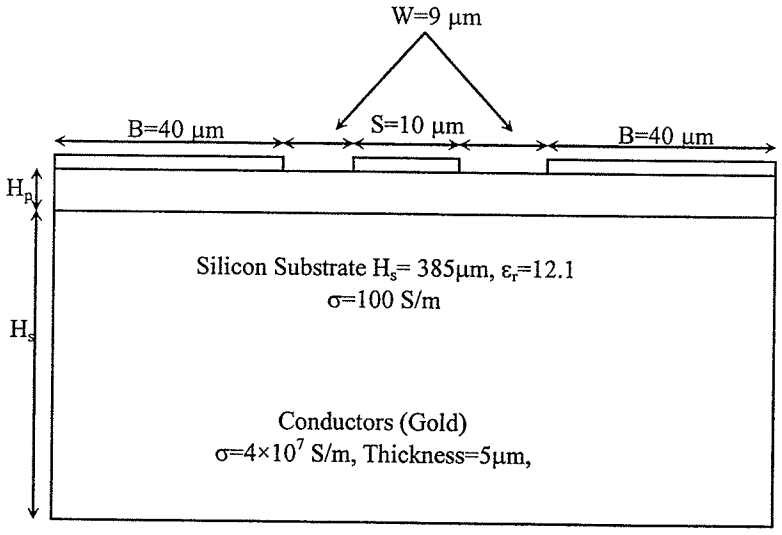

Figure 6-13: The geometry and specifications of the CPW structure.

The calculated complex propagation constant for the CPW geometry of Fig.6-13, obtained using Incentric Cell Method formulation (V0- and V1-formulations) is reported in Figs. 6-14 and 6-15. It should be mentioned that having an appropriately dense mesh,

especially in the conductor regions is necessary for the convergence and accuracy of both methods. The frequency range is from f= 15 GHz to f=50 GHz.

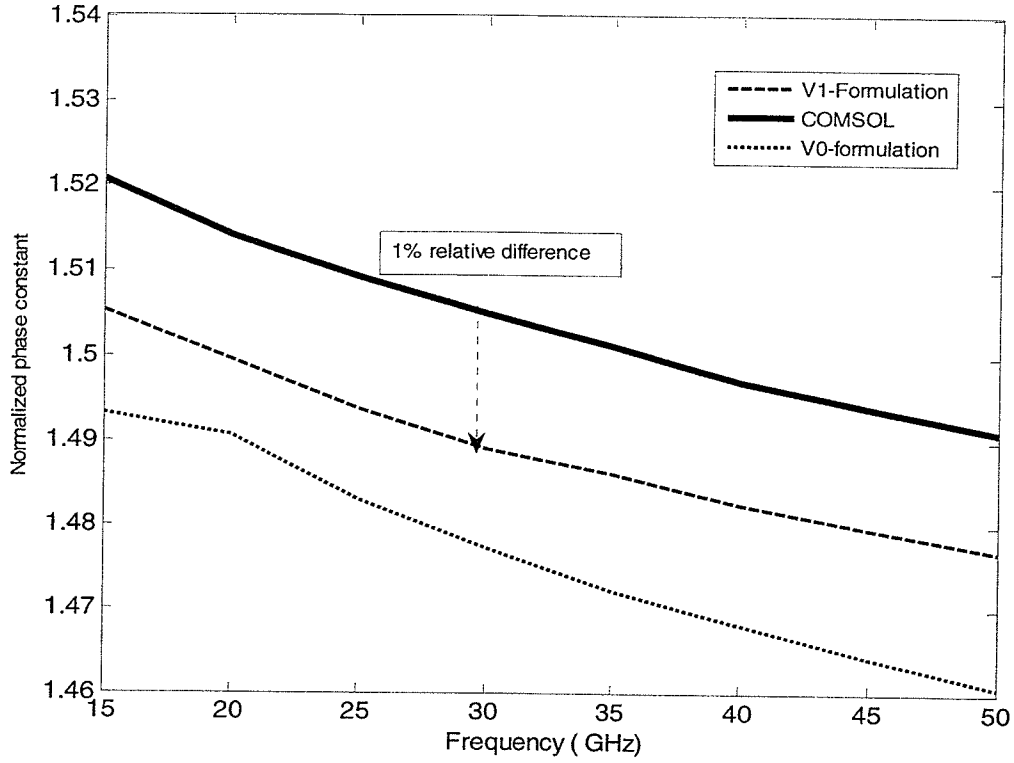

Figure 6-14: Normalized phase constant for the geometry of Fig. 6-13.

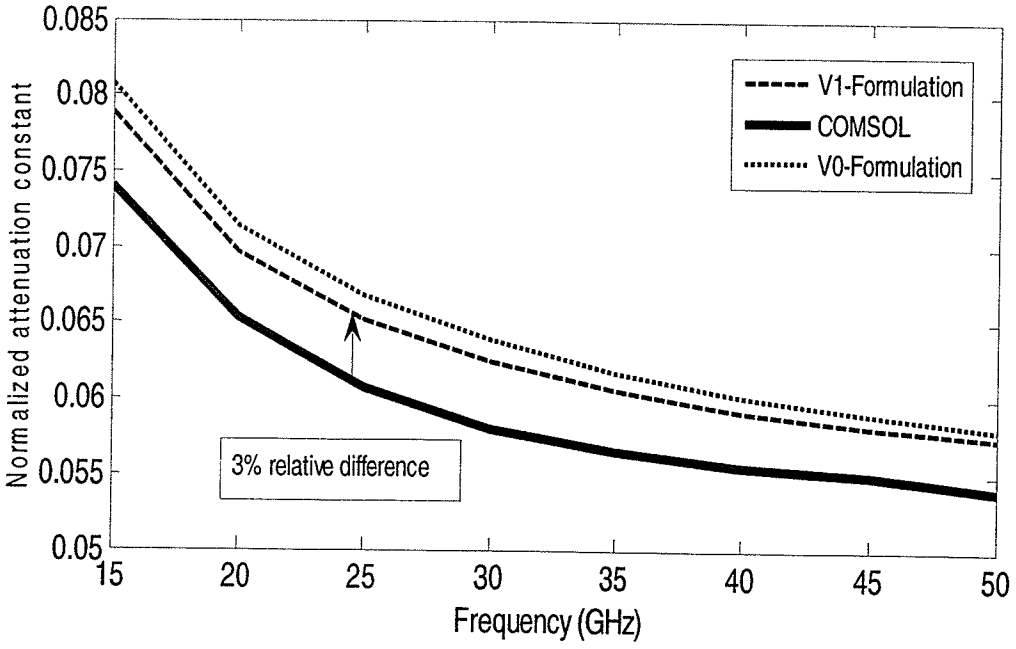

Figure 6-15: Normalized attenuation constant for the geometry of Fig 6-13.

It is seen from Figs. 6-14 and 6-15 that Incentric Cell Method is capable of accurately simulating the complicated structure of Fig. 6-13. It also shows the effect of the minimization procedure (4-22) and V1-Formulation. For this geometry, we have also applied equations (4-26) and (4-27) to calculate the series impedance and shunt admittance of the CPW geometry. Fig. 6-16 depicts the results of this application. The behavior of calculated series impedance and shunt admittance seems reasonable and in agreement with the results reported in [62].

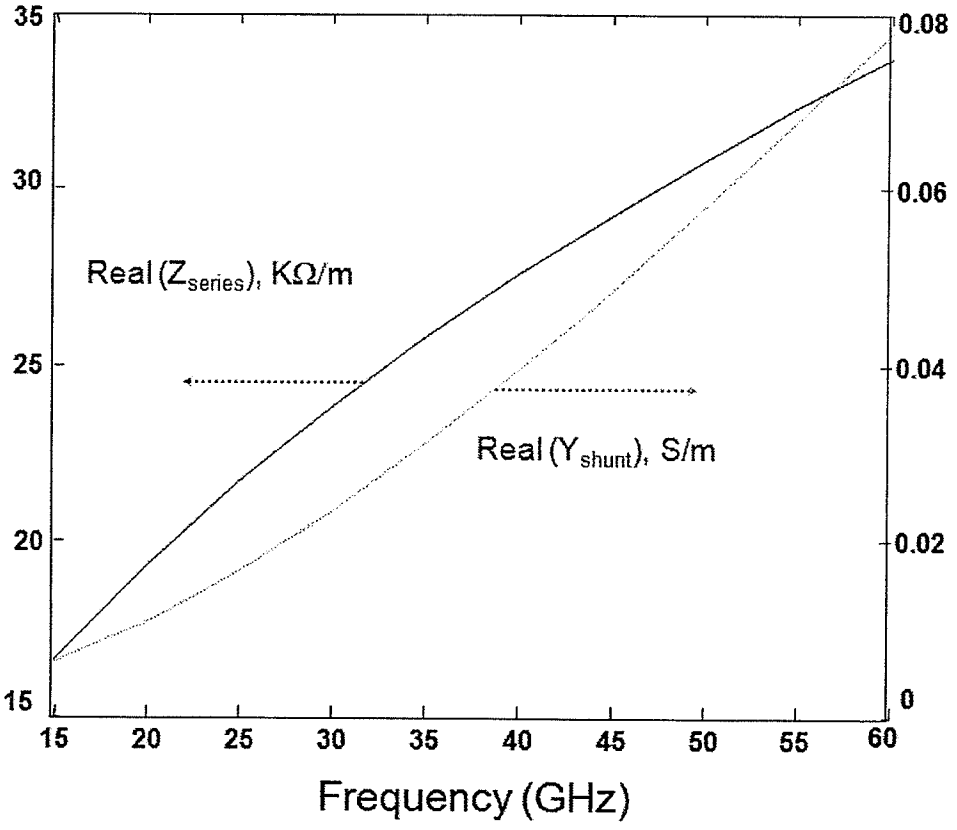

Figure 6-16: Extracted series impedance and shunt admittance for the CPW geometry. Equation (4-26) and (4-27) are used to calculate the parameters.

6.5 Microstrip structure with a magnetic conductor

Microstrip transmission line is a common and wildly used component in communication engineering and Integrated Circuits. In this section, we consider an interesting application of microstrip configuration. The use of a microstrip configuration to extract magnetic parameters of magnetic ribbons has been reported in the literature [63-65]. In [66], we used a microstrip configuration to measure and study Giant Magneto-Impedance, GMI, effect on Co-based magnetic ribbons in the high-frequency regime. GMI can be explained as huge changes in the permeability of the ribbon (resulting a change in the impedance of the ribbon) when a static magnetic field is applied and changed [63].The magnetic material, available in the form of a thin ribbon, acts as the center conductor of a terminated microstrip transmission line as shown in Fig. 6-18.

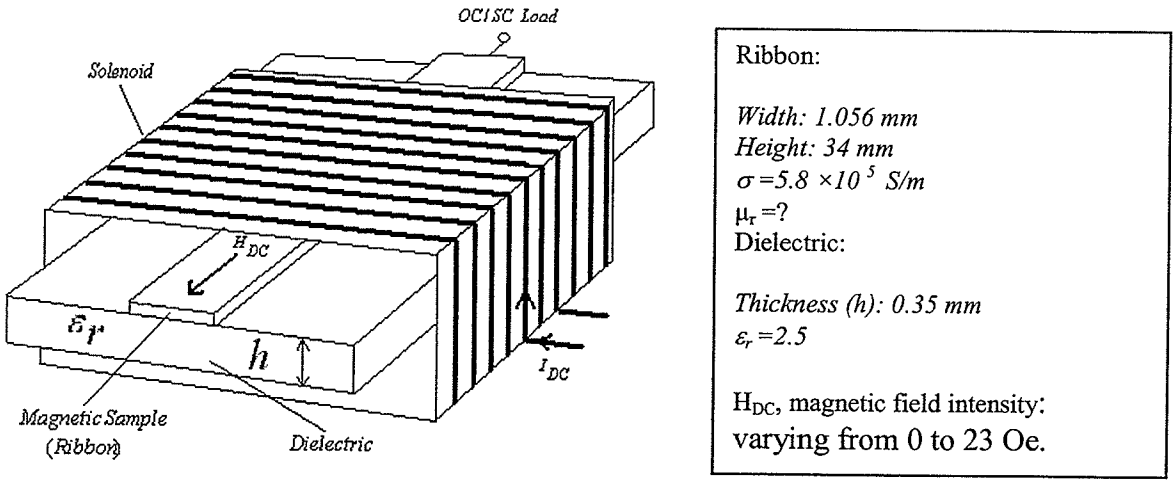

$$Z_C = \sqrt{Z_{SC} Z_{OC}} \quad , \gamma = [\tanh^{-1}(\sqrt{Z_{SC} / Z_{OC}})]$$

$$\gamma = \alpha + j\beta$$

Figure 6-17: A magnetic ribbon is used as the center conductor of a microstrip transmission line in order to extract the magnetic parameter of the ribbon. The complex propagation constant is calculated based on the given formulation using measured values for Z_{sc} and Z_{OC}.

Scattering parameters of the open-ended and/or short-ended line are measured using a Vector Network Analyzer, VNA. The measurement results are then used in an empirical-analytical model based on the skin effect [49] to extract the equivalent circuit parameters, R, L, G, C. The complex permeability of the lossy magnetic material is then extracted based on the skin effect and internal impedance of the center conductor. The calculated attenuation constant (based on measured data) for various H_{DC} values is reported in Fig. 6-19.

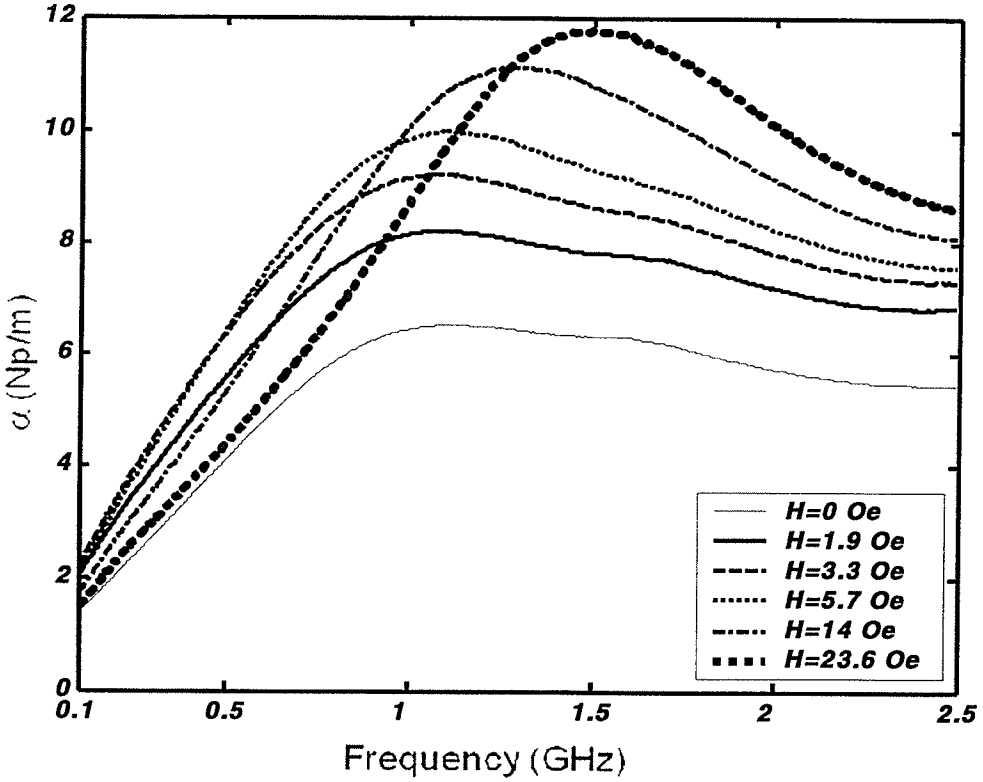

Figure 6-18: Measured attenuation constant of the transmission line shown in Fig.6-18, as the Dc magnetic field intensity changes from 0 to 23.6 Oe.

The behavior of the extracted complex permeability (real and imaginary parts)for the magnetic ribbon at H_{DC}=0 Oe is shown in Fig. 6-20.

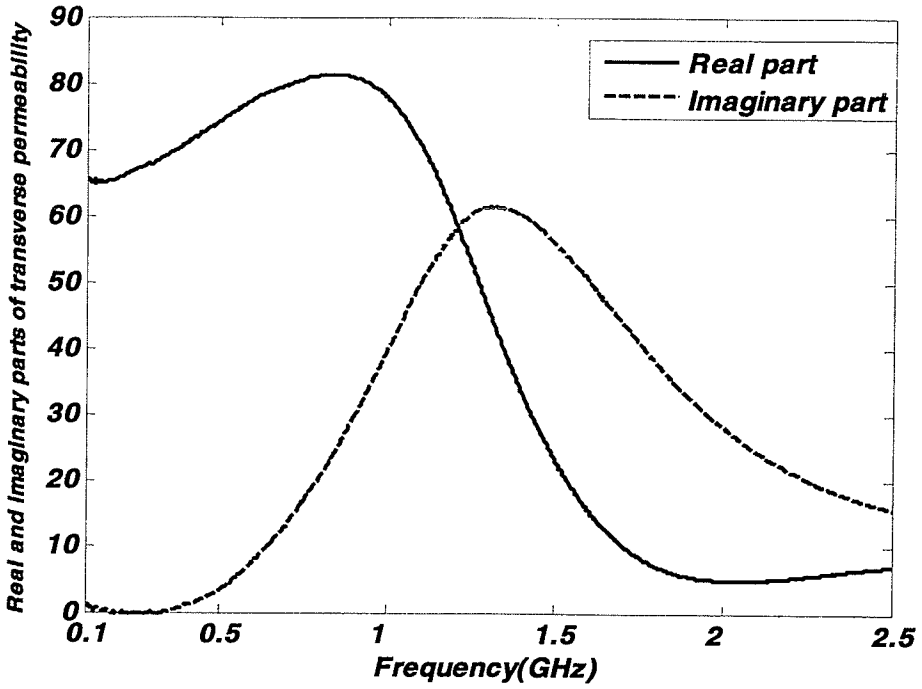

Figure 6-19: Real and imaginary parts of the extracted permeability for the magnetic ribbon.

In the next step, the circuit of Fig.6-18 is simulated with the proposed Incentric Cell Method. The specification of the mesh is reported in Fig. 6-21.

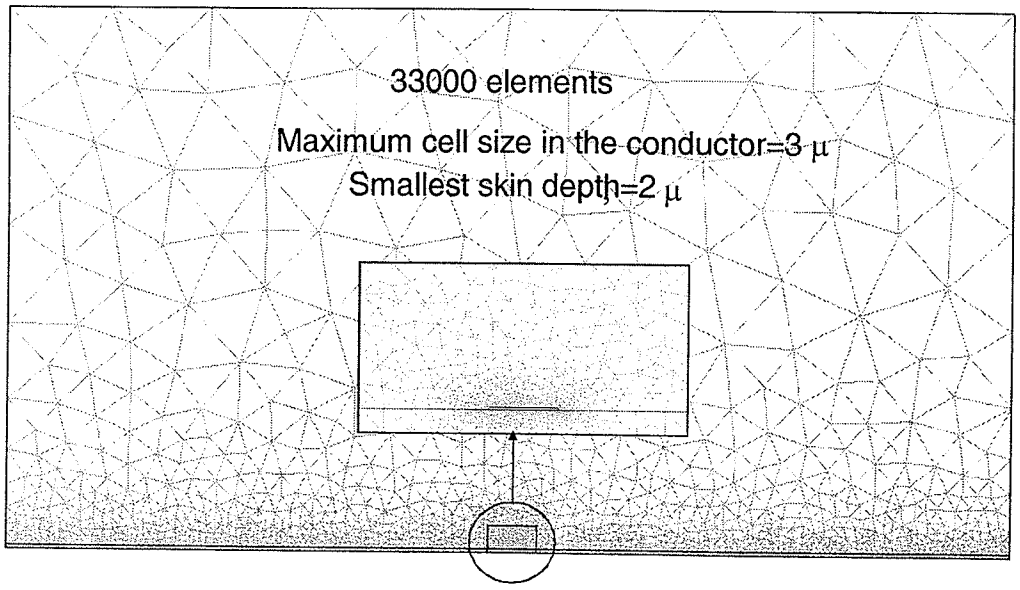

Figure 6-20: The primal triangulation used to simulate the circuit of Fig. 6-18. An adaptive mesh open boundary is used as described in Chapter Five.

The extracted magnetic parameters shown in Fig. 6-20 are then used in the simulation. The results of Cell Method simulation (V0-, F0-formulations) are reported in Fig. 6-21. The results obtained from COMSOL and measurements are also given for comparison.

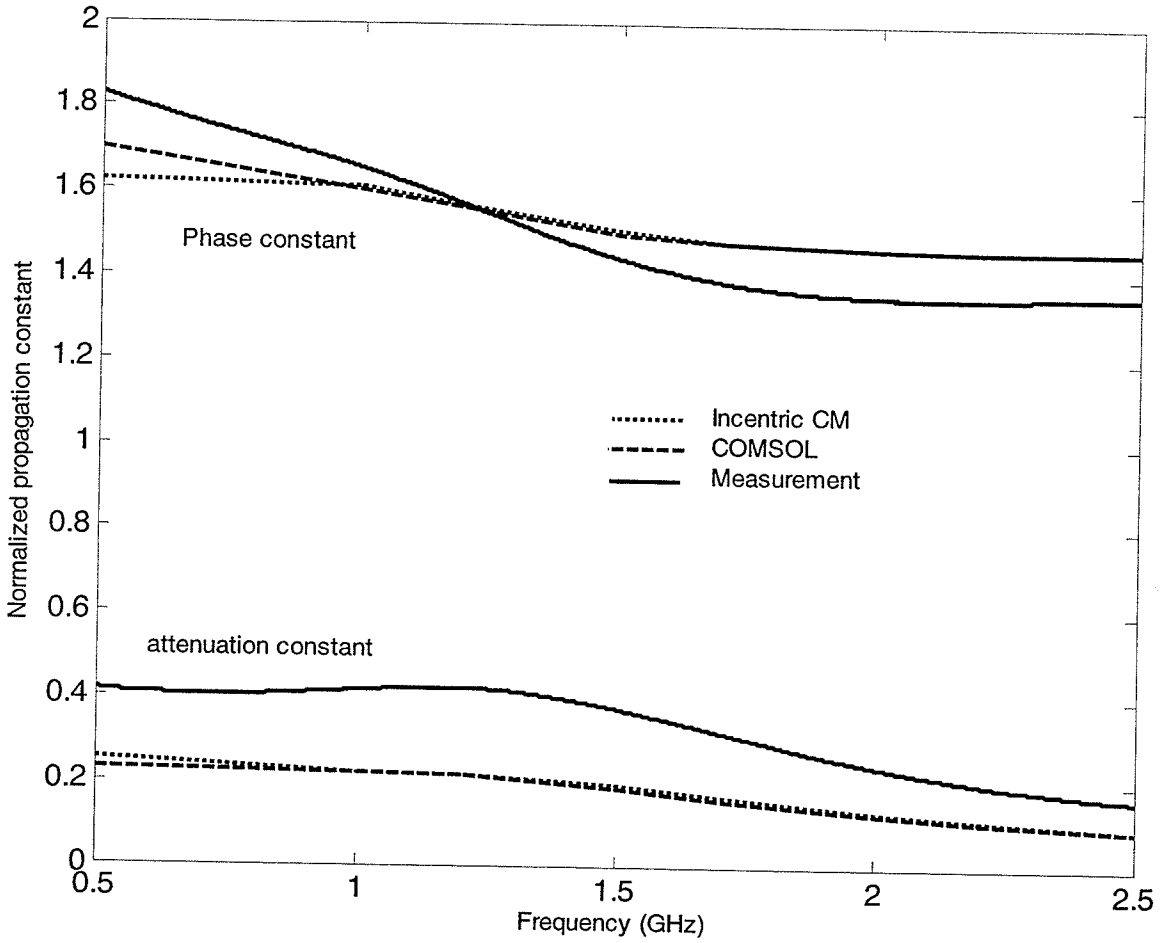

Figure 6-21: Complex propagation constant for the magnetic conductor in a microstrip configuration. The results of the Incentric Cell Method are compared to COMSOL solution and the measurement results.

The Incentric CM solution in Fig. 6-21 is simply obtained by taking the average of V0- and F0-formulation results. It is in a very good agreement with the results obtained

from COMSOL. The discrepancy between the measurement results and simulation results is expectable regarding the conditions of the experiment. The magnetic material was an unknown material and the electric parameters for that were measured for low frequencies. The complex and anisotropic permeability is another complexity in this experiment. The magnetic material was glued to the substrate which increases the inaccuracy of the results considering possible air gaps. This example is an interesting mixture of measurements, a proposed theoretical model for magnetic parameter extraction, application of a new finite formulation scheme and is considered successful based on the results presented in Fig. 6-21.

Different examples investigated in this chapter were meant to validate the Incentric Cell Method formulation, its capability in modeling complex geometries, inhomogeneous media, implementation of different boundary conditions, convergence and accuracy. The presented results are considered encouraging and positive, however, there is still a lot to be done. There is a possibility to construct an iterative scheme as V0- V1-V2-... to obtain better accuracy for the Incentric solution which we did not consider in this thesis. There were no comparisons about the time and memory use between the Cell Method and COMSOL. This is because the code in this thesis is written in Matlab and is not optimized for memory usage and time. The comparisons are only done regarding the type of the constitutive matrices involved as diagonal or non-diagonal constitutive matrices.

The next chapter of this thesis, Conclusion, closes this phase of the research on the Incentric Cell Method.

Chapter 7-Conclusion

The Incentric Cell Method was introduced in details in Chapter Four of this thesis. The results of applying this scheme for solving a variety of complex electromagnetic structures were given in Chapter Six. The major motivation behind proposing the Incentric scheme was "being able to construct diagonal constitutive matrices (therefore an eigenvalue system with symmetric positive definite matrices) and overcome the accuracy issue caused by the non-orthogonal dual mesh". The results of applying the Incentric scheme presented in Chapter Six show good agreement with those obtained using a FEM solver and available analytical solutions. This validates the correctness and effectiveness of the proposed scheme including the zero-order solutions and the minimization procedure to improve the accuracy of the solution.

Finite formulation benefits from a simple but robust framework which does not use any differential calculus or variational techniques. In Finite Formulation, we start from the physical law and express them directly for the discretized spatial domain. This procedure results in separate topological and constitutive relations where approximations and discretization only affect the constitutive relations. Since the matrices (topological and constitutive) are also built independently, changes in material properties or frequency does not change topological matrices. In fact, topological matrices remain unchanged even when the geometry is changed (scaled) as long as the topology of the connections between the points, lines and surfaces has not changed. From the computational point of view, there is no need to update all matrices when one of the changes mentioned above takes place in the problem under study.

Finite formulation does not require any special condition for the spatial domain (for example rectangular mesh as in the original FDTD). In general, it is applicable on multi-scale inhomogeneous and anisotropic problems. Another advantage of finite formulation is implementation of continuity boundary condition. Since global variables are continuous on their geometrical objects, this condition is always satisfied on the interface (lines or surfaces) between two different materials filling adjacent primal cells.

Finite formulation benefits from the existence of the dual mesh in many ways. A dual mesh is used to assign global variables on proper geometrical objects which is an asset as it is seen in other staggered grid schemes like FDTD. It also allows easier implementation of PEC or PMC boundary conditions. An explicit dual mesh provides with clear and more understandable interpolation schemes as discussed in Chapter Three. It was also discussed in Chapter Three that FEM formulations implicitly resembles a non-orthogonal dual mesh. It is interesting that using a simple framework as Finite Formulation results in the same final algebraic equations as a variational technique does after using a good amount of differential calculus and manipulations. A dual mesh is also beneficial when introducing higher order interpolation schemes as it provides with additional points and a geometrical projection of the interpolation scheme.

The advantage of having diagonal constitutive matrices was already discussed in Chapters Three and Four. Having diagonal constitutive matrices guarantees stability and convergence of the system. The time required to solve a symmetric positive definite system reduces considerably by using previously defined functions (e.g. in Matlab). In the Incentric Cell Method this point is considered as a great advantage for the computational procedure.

The dual mesh introduced for the Incentric Cell Method is not orthogonal. To take into account the non-orthogonal components of the dual lines, we have used the variables which are not defined in one set of formulation but in the other. Introducing two sets of formulations (V-formulation and F-formulation) provides the opportunity to choose the suitable formulation based on the boundary conditions or the existing field's components This allows us to use Maxwell's equations (defined in the other formulation) in a dual sense, as an interpolation tool. In a zero-order approximation the effect of the tangential components is ignored and a simple symmetric positive definite system is solved. In the next step, a minimization procedure (Least Squares) is used as an efficient (validated in Chapter Six) way to improve the accuracy of the zero-order solution. In fact, a symmetric positive definite system and an additional Least Squares Minimization are all we need to solve instead of solving a non-symmetric non-positive definite system. Even the zero-order solutions from V0- and F0-formulations agree well with COMSOL solutions and in some cases this zero-order solutions can be used as a starting point in iterative schemes.

Waveguide structures are very common and practical components in communication systems and electronic devices. Calculation of p.u.l. parameters for such a widely used structure is always advantageous. It is often important to investigate the effect of different parameters (e.g. losses in the ground for overhead cables, etching profile in CPW structures) on the p.u.l. parameters of the line. An interesting advantage of using Finite Formulation and having separate (topological and constitutive) matrices is the possibility to define series impedance and shunt admittance as presented in Chapter Four. This enables one to calculate p.u.l parameters for any given geometry by using the matrices and the proposed scheme in Chapter Four.

Although there is still a long way to go to improve and develop the proposed scheme, the results are encouraging and positive. The advantage of this scheme may be more appreciated when solving complicated large sized problems in 3 Dimensions and time-domain.

The simple basis of Finite Formulation is an attractive alternative to the conventional framework of differential equations which unnecessarily seems to be a part of any electromagnetic analysis. This feature can also illuminate the way electromagnetic is understood with a different light.

References

[1] E. Tonti, "Finite Formulation of the Electromagnetic Field", *PIER 32, pp. 1-44, 2001.*

[2] E. Tonti, "A Direct Discrete Formulation of filed Laws: The Cell Method", *Computer Modeling in Engineering and science (CMES), vol. 2. No. 2, pp. 237-258, 2001.*

[3] C. Mattiussi, "An analysis of Finite Volume, Finite Element and Finite Difference Methods using some concepts from algebraic topology", *Journal of Computational physics, 113, pp. 289-309, 1997.*

[4] A. Bossavit, "How weak is the "weak solution" in Finite Element Methods", *IEEE Transactions on Magnetics, vol. 34, no. 5, pp. 2429-2432,1998.*

[5] T. Tarhassari, L. Kettunen, A. Bossavit, "Some Realizations of a discrete Hodge operator: A reinterpretation of finite element techniques", *IEEE Transactions on Magnetics, vol. 35, no. 3, pp. 1494-1497, 1998.*

[6] T. Weiland, "A discretization method for the solution of the eigenwave problem of longitudinally homogeneous waveguides", *Electronics and Communication (AEÜ), vol. 31, pp. 308-314, 1977.*

[7] T. Weiland, "Time Domain Electromagnetic field computation with finite difference methods", *International Journal of Numerical Modeling: Electronic networks, devices and fields, vol. 9, pp. 295-319, 1996.*

[8] R. Schuhmann and T. Weiland, "FDTD on non-orthogonal grids with triangular fillings", *IEEE Transactions on Magnetics, vol. 35, no. 3, pp. 1470-1473, 1998.*

[9] R. Schuhmann and T. Weiland , " The Nonorthogonal Finite Integration Technique Applied to 2D- and 3D-Eigenvalue Problems", *IEEE Transactions on Magnetics, vol. 36, no. 4, pp. 897-901, 2000.*

[10] A. Bossavit and L. Kettunen, "Yee-like schemes on a tetrahedral mesh, with diagonal lumping", *International Journal of Numerical Modeling: Electronic networks, devices and fields, vol. 12, pp. 129-142, 1999.*

[11] A. Bossavit and L. Kettunen, "Yee-like schemes on Staggered Cellular Grids: ASyntheis between FIT and FEM Approaches", *IEEE Transactions on Magnetics, vol. 36, no. 4, pp. 861-867, 2000.*

[12] I. E. Lager, E. Tonti, A. T. de Hoop, G. Mur and M. Marrone, "Finite Formulation and Domain-Integrated Field Relations in Electromagnetics- A Synthesis", *IEEE Transactions on Magnetics, vol. 39, no. 3, pp. 1199-1202, 2003.*

[13] M. Repetto and F. Trevisan, "Global formulation of 2D magnetostatics using flux and gauged potentials", *International Journal for Numerical Methods in Engineering, vol. 60, no. 4, pp.755-772, 2004.*

[14] M. Marrone, "Computational Aspects of Cell Method in Electromagnetics", *PIER 32, pp. 317-356, 2001.*

[15] M. Heshmatzadeh and G. Bridges, "A Geometrical interpretation for equivalence between Cell Method and Finite Element Method in Electromagnetics", *CMES: Computer Modeling in Engineering and Sciences, vol. 18, no. 1, pp. 45-58 , 2007.*

[16] A. Okabe, B. Boots, K. Sogihara, *Spatial Tessellations: concepts and applications of Voronoi diagrams,* Chichester, England, Wiley, 1992.

[17] A. Bossavit, *Computational Electromagnetism*, Academic Press, 1998.

[18] R. Schuhmann and T. Weiland, "Conservation of discrete energy and related laws in the finite integration technique", *PIER Monograph Series, vol. 32, pp. 301-316, 2001.*

[19] M. Cinalli, F. Edelvik, R. Schuhmann and T. Weiland, "Consistent material operators for tetrahedral grids based on geometrical principles", *International Journal of Numerical Modeling: electronic networks, devices and fields, vol. 17, pp. 487-507, 2004.*

[20] M. Marrone, "A New Consistent Way to Build Symmetric Constitutive Matrices on General 2-D Grids", *IEEE Transactions on Magnetics, vol. 40, no.2, pp.1420-1423, 2004.*

[21] M. Marrone, "Properties of Constitutive Matrices for Electrostatic and Magnetostatic Problems", *IEEE transactions on Magnetics, vol. 40, no. 3, pp. 1516-1520, 2004.*

[22] M. Marrone, R. Mitra, "A Theoretical Study of the Stability Criteria for Generalized FDTD Algorithms for Multiscale Analysis", *IEEE transaction on Antennas and propagation, vol. 52, no. 8, pp. 2158-2167, 2004.*

[23] M. Marrone and R. Mitra, "A New Stable Hybrid Three-Dimensional Generalized Finite Difference Time Domain Algorithm for Analyzing Complex Structures.", *IEEE Transactions on Antenna and propagation, vol.53, no. 5,pp. 1729-1732, 2005.*

[24] M. Marrone, "Novel Numerical method for the analysis of 2D photonic crystals: The Cell Method", *Optic Express, vol. 10, no. 22, pp. 1299-1304, 2002.*

[25] R. Araneo, "Numerical Solution of Transient Electromagnetic Scattering Problems Using the Novel Time-Domain Cell Method", *IEEE International Symposium on Electromagnetic Compatibility,vol.1, pp. 291-296, 2002.*

[26] L. Codecasa, V. Minerva and M. Politi, "Use of Barycentric Dual Grids for the Solution of Frequency Domain Problems by FIT", *IEEE transactions on Magnetics, vol. 40,no. 2, pp. 1414-1419, 2004.*

[27] P. Alotto, I. Perugia, "Matrix Properties of a Vector Potential Cell Method for Magnetostatics", *IEEE transactions on Magnetics, vol. 40, no. 2, pp. 1045-1048, 2004.*

[28] F. Trevisan and L. Kettunen, "Geometric Interpretation of Discrete Approached to Solving Magnetostatic Problems", *IEEE Transactions on Magnetics, vol. 40, no.2, pp. 361-365 ,2004.*

[29] M. Cinalli and A. Schiavoni, "A Stable and Consistant Generalization of the FDTD Technique to Nonorthogonal Unstructured Grids", *IEEE Transactions on Magnetics, vol. 54, no.5, pp. 1503-1512, 2006.*

[30] P. Alotto, A. De Cian and G. Molinari, "A Time-Domain 3-D Full-Maxwell Solver Based on the Cell Method", *IEEE Transactions on Magnetics, vol. 42, no.4, pp. 799-802, 2006.*

[31] P. Bettini, S. Boscolo, R. Specogna and F. Trevisan, "A Geometric Approach for Wave Propagation in 2-D Photonic Crystals in the Frequency Domain", *IEEE Transactions on Magnetics, vol. 42, no.4, pp. 827-830, 2006.*

[32] P. Bettini, F. Trevisan, "Electrostatic Analysis for Plane Problems with Finite Formulation", *IEEE transactions on Magnetics, vol. 39, no.32, pp.1127-1130, 2003.*

[33] M. Bullo, F. Dughiero, M. Guarnieri and E. Tittonel, "Isotropic and Anisotropic Electrostatic Field Computation by Means of the Cell Method", *IEEE transactions on Magnetics, vol. 40, no. 2, pp.1013-1016, 2004.*

[34] M. Repetto and F. Trevisan, "3-D Magnetostatic with the Finite Formulation", *IEEE transactions on Magnetics, vol. 39, no.32, pp.1135-1138, 2003.*

[35] F. Bellina, P. Bettini, E. Tonti and F. Trevisan, "Finite Formulation for the Solution of a 2-D Eddy-Current Prooblem", *IEEE transactions on Magnetics, vol. 38, no. 2, pp.561-564, 2002.*

[36] F. Trevisan, "3-D Eddy Current Analysis With the Cell Method for NDE Problems", *IEEE transactions on Magnetics, vol. 40, no. 2, pp.1314-1317, 2004.*

[37] R. Specogna and F. Trevisan," Discrete Constitutive Equations in A-χ Geometric Eddy-Current Formulation", *IEEE Transactions on Magnetics, vol.41, no. 4, 2005.*

[38] M. Marrone, P. Grassi and R. Mitra, "A new technique based on the Cell Method for calculation the propagation constant of inhomogeneous filled

waveguide", *International Symposium on Antenna and propagation, IEEE, June 2004.*

[39] **Zovatto L., Nicolini M.,** "Improving the Convergence Order of the Meshless Approach for the Cell Method for Numerical Integration of Discrete Conservation Laws", *International Journal for Computational Methods in Engineering Science and Mechanics, Vol. 8, No. 5, pp. 273- 281, 2007.*

[40] P. Alotto, M. Guarnieri and F. Moro, "A Boundary Integral Formulation on Unstructured Dual Grids for Eddy Current Analysis in Thin Shields", *IEEE Transsctions on. Magnetics, vol. 43, no. 4, pp. 1173-1176, 2007.*

[41] P. Alotto, A. De Cian, G. Molinari and M. Rossi, "Implementation of Surface Impedance Boundary Conditions in the Cell Method via the Vector Fitting Technique", *COMPEL, vol. 26, no.3, pp. 859-872, 2007.*

[42] R. F. Harrington, *Time-Harmonic Electromagnetic Fields,* McGraw-Hill, 1961.

[43] L. Zovatto, M. Nicolini, "The Meshless Approach for the Cell Method: A New Way for the Numerical Solution of Discrete Conservation Laws", *International Journal of Computational Engineering Science, vol. 4, no. 4, 2003.*

[44] P. P. Silvester and R. L. Ferrari, *Finite Elements for electrical engineers,* Cambridge University Press, 1990.

[45] A. M. Winslow, "Magnetic field calculation in an irregular triangular mesh", *Lawrence Radiation Lab., Livermore, CA, UCRL-7784-T, Rev. 1, 1965.*

[46] V. Shankar, A. H. Mohammadian and W. F. Hall, "A time-domain finite-volume treatment for the Maxwell equations", *Electromagnetics, vol. 10, pp. 127-145, 1990.*

[47] D. Baumann, K. Krohne, C. Fumeaux and R. Vahldieck, "Progress of the Finite-Volume Method in Time Domain (FVTD) and in Frequency Domain (FVFD)", *In Proceedings on FACE2006 conference, Victoria, Canada, June 2006.*

[48] COMSOL Multiphysics, www.COMSOL.com.

[49] R. E. Collin, *Foundations for microwave engineering,* McGraw-Hill,1992.

[50] A. Bayliss, E. Turkel, "Radiation boundary condition for wave-like equations", *Comm. Pure. App. Math., 33(1980), pp. 707-725.*

[51] B. Engquist, A. Majda, "Radiation boundary condition for acoustic and elastic wave calculations", *Comm. Pure. App. Math. 32(1979), pp. 313-375.*

[52] Jean-Pierre Berenger, "A Perfectly Matched Layer for the Absorption of Electromagnetic Waves", *Journal of Computational Physics 114,185-200, 1994.*

[53] Z. Wu, J. Fang," Numerical Implementation and Performance of Perfectly Matched Layer Boundary Condition for Waveguide Structures", *IEEE Trans. On microwave theory and techniques, vol. 43, no. 12, pp. 2676-2683, 1995.*

[54] Sh. Luo, Z. Chen, "A FDTD-Based Modal PML", *IEEE microwave and wireless component letters, vol. 16, no. 10, pp. 528-530, 2006.*

[55] C.M. Rappaport, M. Kilmer, E. Miller, "Accuracy consideration in using PML ABC with FDTD Helmholtz equation computation", *International Journal of Numerical Modeling: Electronic networks Devices and fields, 13:471-482, 2000.*

[56] J. Fang, Z. Wu, " Generalized Perfectly Matched Layer-An Extension of Berenger's Perfectly Matched Layer Boundary Condition", *IEEE microwave and guided wave letters, vol. 5, no. 12, pp. 451-453, 1995.*

[57] Jiunn-Nan Hwang, "A Compact 2-D FDFD Method for Modeling Microstrip Structures With Non-uniform Grids and Perfectly Matched Layer", *IEEE Trans. On microwave theory and techniques, vol. 53, no. 2, pp. 653-659, 2005.*

[58] D. Shyroki, " Squeezing of Open Boundaries by Maxwell-Consistent Real Coordinate Transformation", *IEEE microwave and wireless component letters, vol. 16, no. 11, pp. 576-578, 2006.*

[59] J.R. Carson, "Wave Propagation in Overhead Wires with Ground Return", *Bell System Technical Journal, vol. 5, pp. 539-554, 1926.*

[60] G.E. Bridges and L. Shafai, "Plane Wave Coupling to Multiple Conductor Transmission Lines Above a Lossy Earth", *IEEE Trans. on Electromagnetic Compatibility, vol. EMC-31, pp. 21-33, 1989.*

[61] G.E. Bridges, "Fields Generated by Bare and Insulated Cables Buried in a Lossy Half-Space", *IEEE Trans. Geosciences and Remote Sensing, vol. 30, pp. 140-146, 1992.*

[62] B. Kordi, G. Bridges, J. LoVetri and A. Foroozesh, "Time-Domain Analysis of Lossy-Substrate Interconnects with Frequency-Dependent Parameters", *Proceeding of ANTEM, July 2005, France.*

[63] K. Mandel, S. Puetra, M. Vazqucz, A. Hernando, " The frequency and Stress Dependence of Giant Magnetoimpedance in Amorphous Microwires" *IEEE Trans. Magnetics*, vol. 36,pp. 3257-3259, 2000.

[64] L. Brunetti, P. Tiberto, F. Vinai, "A new Measurement method for magneto-impedance in soft amorphous ferromagnets at microwave frequency", *Sensors and Actuators A, vol. 67, pp. 84-88, 1998.*

[65] A. E. P. de Araujo, F. L.A. Machado, F. M. de Aguiar, S.M. Rezende, "GMI measurements in ribbons of CoFeSiB in a wide range of frequencies", *J. of Magnetism and Magnetic materials, vols.* 226-230 pp. 724-726, 2001.

[66] M. Heshmatzadeh, G. Bridges, X. Zhou, G. Williams, "High-Frequency GMI Measurements and complex permeability behavior of soft magnetic Co-based ribbons", *IEEE Trans. On Magnetics, Vol.41, No.8, 2005.*

[67] L. Codecasa and F. Trevisan, "Constitutive equations for discrete electromagnetic problems over polyhedral grids", *Journal of computational physics, vol. 225, no. 2, pp. 1894-1918, 2007.*

[68] Weiland, T. "On the numerical solution of Maxwell's equations and applications in the field of accelerator physics", *Particle Accelerators, 245-292, 1984.*

[69] J. A. Stratton, *Electromagnetic Theory*, McGraw-Hill, 1941.

[70] James R. Wait, *Electromagnetic wave theory*, HarperCollins Publishers, 1985.

Additional References

[1] M. Marrone," Convergence and stability of the Cell Method with Non Symmetric Constitutive Matrices", *13th Compumag Conference, 2001.*

[2] M. Marrone", A Novel Technique to build Constitutive Matrices for Generalized FDTD Algorithm.", *IEEE AP-S International Symposium on Antennas and Propagation, Columbus, Ohio, USA, 22-27 June 2003.*

[3] M. Marrone, A.M.F. Frasson, H.E.H. Figueroa,"A Novel Numerical approach for electromagnetic Scattering: The Cell Method", *On Proceeding, IEEE AP-URSI, 2002.*

[4] M. Guarnieri, F. Moro, R. Turri," An Integral Method for ELF Magnetic Shielding", CEFC1164.

[5] M. Marrone,"The equivalence between Cell Method, FDTD and FEM", *IEEE 4th International Conference on Computation in Electromagnetics,2002.*

[6] M. Repetto, F. Trevisan," Global Formulation of 3D Magnetostatics using Flux and Gauged Potentials", *International Journal for Numerical Methods in Engineering,vol. 60 issue 4,pp755-772,2004.*

[7] M. Bullo, F. Dughiero,M. Guarnieri,E. Tittonel," A 2-D Formulation for Eddy Currents Anisotropic Problems with the Cell Method", CEFC1421,2004.

[8] M. Heshmatzadeh and G. Bridges," Calculation of The Propagation Constant of a Lossy Integrated Transmission Line Using the Cell Method", *On Proceedings of Second IASTED Conference on Antennas, Radar and Propagation, July 19-21,2005, Banff*

[9] M.N.O. Sadiku, "A Simple Introduction to Finite Element Analysis of Electromagnetic problems:, *IEEE Transactions on Education, vol. 32, no. 2 , May1989.*

[10] Y. Tsuji, M. Koshiba, "Guided-Mode and Leaky-Mode Analysis by Imaginary Distance Beam Propagation Method Based on Finite Element Scheme", *Journal of lightwave technology, vol. 18, no. 4, pp. 618-623, 2000.*

[11] Gerrit Mur, "Absorbing Boundary Conditions for the Finite-Difference Approximation of the Time-Domain Electromagnetic-Field Equations", *IEEE Trans. on electromagnetic compatibility, vol.EMC-23, no. 4, pp. 377-382,1981.*

[12] J.S. Wang and Raj Mittra," Finite Element Analysis of MMIC Structures Using Absorbing Boundary Conditions", *Microwave Symposium Digest, 1993, IEEE MTT-S International, pp. 745-748.*

[13] M. D'Amore, M. Sabrina, "Simulation Models of a Dissipative Transmission Line above a Lossy Ground for a Wide-Frequency Range-Part I: Single Conductor Configuration", *IEEE Trans. On electromagnetic compatibility, vol. 38, no. 2, pp. 127-138, 1996.*

[14] O. M. Ramahi, "Frequency-Domain Complementary Operators for Finite-Elements simulation", *IEEE Trans. On Antennas ans propagation, vol. 48, no. 4, pp. 629-631, 2000.*